To the Graduate Council:

I am submitting herewith a dissertation written by Prinya Promprated entitled "Petrology and Geochemistry of Upper Mantle and Lower Crustal Xenoliths from Thailand." I have examined the final copy of this dissertation for form and content and recommend that it be accepted in partial fulfillment of the requirements for the degree of Doctor of Philosophy, with a major in Geology.

Lawrence A. Taylor, Major Professor

We have read this dissertation

and recommend its acceptance:

Accepted for the Council:

Interim Vice Provost and

Dean of the Graduate School

PETROLOGY AND GEOCHEMISTRY OF UPPER MANTLE AND LOWER CRUSTAL XENOLITHS FROM THAILAND

A Dissertation

Presented for the

Doctor of Philosophy

Degree

The University of Tennessee, Knoxville

Prinya Promprated

May 2001

This dissertation is dedicated to my mother

Chaluay Promprated

(ฉลวย พรหมประเทศ)

and my wife

Wassana Apichatachutapan

(วาสนา อภิชาตะจุฑาภัณฑ์)

for all their love and encouragement.

ACKNOWLEDGMENTS

In accomplishing the degree of doctor of philosophy, I am deeply indebted to a number of people. First and foremost, I would like to express my sincere gratitude to my advisor, Dr. Lawrence A. Taylor, for his invaluable guidance and encouragement throughout my graduate career at UT. I am thankful for the opportunities he provided that helped me grow professionally as a scientist. I am especially grateful to other committee members: Drs. Harry Y. McSween, Claudia I. Mora, and Mark D. Dadmun for providing me "first-class" education and valuable advice towards completion the degree.

I acknowledge insightful discussions with the past members of Planetary Geosciences Institute (PGI): Drs. Alex Ruzica, Randall Keller, Vladimir Sobolov, and Wuyi Wang. Dr. Gregory Snyder is especially thanked for assisting me improving my perception about the Earth's mantle, and for his effort in revising my first manuscript. I am indebted to Allan Patchen for his helpful assistance with microprobe analysis. I deeply appreciate Dr. Clive Neal for his critiques and valuable advice on various aspects of my research, particularly trace-element chemistry. The ICPMS facilities at the University of Notre Dame and the University of Tsukuba are acknowledged for help in obtaining trace-element data. Mr. Rak Hansawek, Dr. Punya Charusiri, and Dr. Chakkaphan Suthirat are greatly appreciated for logistic supports in Thailand.

I deeply appreciate the generous financial support from the Department of Geological Sciences, University of Tennessee, through a Teaching Assistantship. I am particularly thankful for additional fund provided by the National Science Foundation through L.A. Taylor research grants.

Over the years, a number of people has helped me surmount this Ph.D. ordeals. I profoundly appreciate Dr. Dong-Hwa (Dawn) Taylor for her generosity and continual support. I am indebt to Dr. Marvin Bennett for his friendship, valuable advice, and assistance in numerous occasions. Thanks to fellow graduate students: David Remley, B.J. Bonin, Rene Wiesly, John Collins, Joshua Cahill, Heather Gastineau, Dana Miller, Milo Cameron, and Zhenshen Chen, for their friendship and closely sharing my time at UT.

There would not be this day without the love, encouragement, and sacrifice from my mother, Chaluay Promprated. I only hope that my very endeavor would at least partially fulfill her never-reached dream of having high education. I owe my sisters immensely for their sacrifices and supports while I am so far away from home. Last, but certainly not least, I would like to wholeheartedly thank my wife and best friend, Dr. Wassana Apichatachutapan, for her unconditional love and inspiration. Her plentiful happiness and energy have always strengthened me through times of crisis and despair.

ABSTRACT

Rare spinel-lherzolite xenoliths from Thailand offer a unique opportunity to investigate the compositions and processes of the upper mantle beneath this SE-Asia region. These xenoliths occur in Cenozoic alkali basalts from two lithospheric fragments, namely the Shan-Thai (western side) and Indochina (eastern side), that were joined along the Nan-River suture. Major-element chemistry in whole rocks shows large variations (e.g., ~33-49 wt% MgO and 1-6 wt% Al_2O_3), similar to those observed in eastern China spinel-lherzolite xenoliths. The Indochina xenoliths appear to be more fertile (i.e., lower in mg#), when compared to those of Shan-Thai. Xenoliths from both sides of the suture, however, yield comparable estimated temperatures (~890-1170°C), and often show evidence of interaction with the host basalts (i.e., spongy rims). Such metasomatic reaction profoundly depletes Al_2O_3 and Na_2O in the clinopyroxene within the spongy rims, and in some cases, lead to the formation of K-Na rich, feldspathic glass.

Trace-element compositions of the xenoliths selected for detailed studies record variable extents of mantle processes, including basaltic-melt extraction and metasomatism. Using clinopyroxene trace-element modeling, it is demonstrated that the majority of lherzolite xenoliths experienced small degrees (<6%) of partial melting, although up to 16% melting is necessary for a depleted sample (5% modal Cpx). In a unique xenolith, clinopyroxenes are significantly LREE-depleted (La/Lu = 0.01), possibly reflecting their derivation from garnet breakdown. In addition, the modeling of LREE-enriched samples, with pronounced HFSE (Ti, Zr, Hf) depletion, suggests metasomatic modification by carbonate-rich fluids/melts, unrelated to the host basalts. This metasomatic enrichment was more intense in xenoliths from the eastern

microcontinent (up to 30%), compared to that occurred in samples of the western counterpart. It is possible that, initially, spinel-lherzolite xenoliths from both microcontinents possessed similar compositions, but experienced different degrees of partial melting and metasomatism. Perhaps this metasomatic enrichment was a consequence of subduction at the Mesozoic Nan-River suture, or occurred later during Cenozoic continental rifting.

In the Chantaburi-Trat basaltic field of Thailand, granulite-facies xenoliths were discovered. They represent the only known occurrence of lower crustal material in this region. These mafic xenoliths (43-49% SiO_2) can be classified into 3 groups: (1) olivine-garnet clinopyroxenite, (2) garnet-rich granulite, and (3) clinopyroxene-rich granulite. All possess similar geochemical features in the whole rocks, including high normative olivine, plagioclase, and diopside; low and generally flat REE abundances (~0.5-6.0 x C1 for HREE); and positive Eu anomalies. These characteristics indicate cumulate origins, possibly from underplating basaltic magmas. Mineralogical and chemical evidence suggests that the original cumulate mineralogy (Ol, Pl, and Cpx) was transformed to granulite-facies assemblages (Ol, Pl, Cpx, and Gt) at ~1100 to 1200° C and 15 to18 kbar. Corundum inclusions were also produced at the upper limit of this P-T range. Subsequently, extensive kelyphitization developed on garnets, possibly triggered by decompression. It is possible that lower crustal evolution in the Thai region closely relates to asthenospheric upwelling and magmatism in the Cenozoic.

TABLE OF CONTENTS

PAGE

PART 1: INTRODUCTION

Introduction 2

References 5

PART 2: PETROCHEMISTRY OF THE MANTLE BENEATH THAILAND— EVIDENCE FROM PERIDOTITE XENOLITHS

Abstract 7

Introduction 7

Tectonic evolution of Southeast Asia 8

Distribution of basalts and ultramafic xenoliths 10

Analytical technique 12

Petrography 13

Whole-rock chemistry 17

Mineral chemistry 18

Discussion 31

Conclusions 49

References 52

PART 3: TRACE-ELEMENT CHARACTERISTICS OF THE SPINEL-PERIDOTITE XENOLITHS FROM THAILAND— MELTING AND METASOMATISM OF MANTLE BENEATH A SUTURE ZONE

Abstract 58

Introduction 58

Sample preparation and analytical technique 61

Major-element chemistry and temperature estimates 64

Whole-rock trace-element chemistry 72

Trace-element chemistry of minerals 78

Discussion 84

Conclusions 93

References 95

Appendices 99

PART 4: NATURE OF THE LOWER CRUST BENEATH THAILAND—
A RECORD FROM GRANULITE XENOLITHS

Abstract 105

Introduction 105

Samples and petrography 106

Analytical technique 112

Whole-rock chemistry 115

Mineral chemistry 124

Discussion 136

Conclusions 144

References 146

VITA 151

LIST OF TABLES

TABLE PAGE

PART 2: PETROCHEMISTRY OF THE MANTLE BENEATH THAILAND— EVIDENCE FROM PERIDOTITE XENOLITHS

1. Ultramafic xenoliths from Thailand and their host rocks 11
2. Reconstructed primary modal abundances and whole-rock analysis of ultramafic xenoliths from Thailand 14
3. Average compositions of olivine 20
4. Average compositions of orthopyroxene 23
5. Average compositions of clinopyroxene 27
6. Average compositions of spinel 32
7. Selected analyses of spongy rim on clinopyroxene 40
8. Temperature estimates of mantle xenoliths beneath Thailand 43

PART 3: TRACE-ELEMENT CHARACTERISTICS OF THE SPINEL-PERIDOTITE XENOLITHS FROM THAILAND— MELTING AND METASOMATISM OF MANTLE BENEATH A SUTURE ZONE

1. Modal abundances and whole-rock compositions of peridotite xenoliths and host basalts from Thailand 65
2. Estimated temperatures of peridotite xenoliths from Thailand 71
3. Trace-element compositions of whole-rock peridotites and host basalts, analyzed by ICP-MS 73
4. Trace-element compositions of clinopyroxene in spinel-lherzolite xenoliths

from Thailand, analyzed by LA-ICP-MS 79

5. Trace-element compositions of orthopyroxene in spinel-lherzolite xenoliths from Thailand, analyzed by LA-ICP-MS 80

6. Trace-element compositions of olivine in spinel-lherzolite xenoliths from Thailand, analyzed by LA-ICP-MS 81

7. Trace-element compositions of spinel in spinel-lherzolite xenoliths from Thailand, analyzed by LA-ICP-MS 81

A-2. Major-element compositions of clinopyroxene in spinel-peridotite xenoliths from Thailand 100

A-3. Major-element compositions of orthopyroxene in spinel-peridotite xenoliths from Thailand 101

A-4. Major-element compositions of olivine in spinel-peridotite xenoliths from Thailand 102

A-5. Major-element compositions of spinel in spinel-peridotite xenoliths from Thailand 103

PART 4: NATURE OF THE LOWER CRUST BENEATH THAILAND—A RECORD FROM GRANULITE XENOLITHS

1. Reconstructed primary modal abundances of granulite xenoliths from Thailand 109

2. Whole-rock compositions and CIPW normative mineralogy of granulite xenoliths and host basalt 116

3. Trace-element analyses of whole-rock granulite xenoliths, analyzed by ICP-

MS 117

4. Representative compositions of clinopyroxene in granulite xenoliths from Thailand 125

5. Selected analyses of secondary minerals and interstitial glass 130

6. Representative compositions of plagioclase in granulite xenoliths 132

7. Average compositions of garnet in granulite xenoliths 135

8. Average compositions of kelyphite in granulite xenoliths 136

9. Average compositions of olivine and corundum 137

10. P-T estimates of granulite xenoliths from Thailand 140

LIST OF FIGURES

FIGURE PAGE

PART 2: PETROCHEMISTRY OF THE MANTLE BENEATH THAILAND—EVIDENCE FROM PERIDOTITE XENOLITHS

1. Schematic map of Thailand showing distributions of Cenozoic basalts and major tectonic features 9
2. Modal abundances of ultramafic xenoliths from Thailand 15
3. Photomicrographs of selected textural features of spinel-peridotite xenoliths from Thailand 16
4. Major-oxide plots as a function of MgO for whole-rock analyses of Type I ultramafic xenoliths 19
5. Concentrations of NiO in olivine and TiO_2 in clinopyroxene plotted against average Fo contents of olivine 21
6. Pyroxene quadrilateral showing compositions of orthopyroxene and clinopyroxene in Thai ultramafic xenoliths 25
7. Compositional variation along line X-Y on an orthopyroxene grain in sample BP35 26
8. Plots of mg#s versus selected major oxides in average core analyses of clinopyroxene 30
9. Compositions of spinel in Thai ultramafic xenoliths 33
10. Weight ratio of Ca/Al versus MgO for ultramafic xenoliths from Thailand ... 35
11. Fo content in olivine versus mg# in clinopyroxene and in orthopyroxene of

Thai ultramafic xenoliths 37

12. Representative compositional variations across clinopyroxenes 38

13. Al (vi) versus Na plot of average clinopyroxene compositions 41

14. Comparison of estimated temperatures from different thermometers 44

15. Plot of cr# versus f (O_2) of ultramafic xenoliths from Thailand 47

PART 3: TRACE-ELEMENT CHARACTERISTICS OF THE SPINEL-PERIDOTITE XENOLITHS FROM THAILAND— MELTING AND METASOMATISM OF MANTLE BENEATH A SUTURE ZONE

1. Major occurrences of peridotite xenoliths in Thailand 60

2. Plots of selected major-oxide concentrations versus MgO of whole-rock lherzolite xenoliths 67

3. Clinopyroxene major-element compositions of lherzolite xenoliths from Thailand compared with those from other world localities 69

4. Variation diagrams of MgO contents versus selected trace elements in whole rocks 75

5. REE concentrations of whole-rock lherzolite xenoliths compared with their clinopyroxene 76

6. Incompatible trace elements in clinopyroxene showing strong positive correlation with Ti contents 82

7. Trace-element patterns of clinopyroxene showing variable degrees of depletion and enrichment in these elements 83

8. REE abundances of whole-rock DC5 showing prominent negative Eu

anomaly similar to other surface materials 86

9. Clinopyroxene trace-element modeling showing variable degrees of partial melting experienced by spinel-peridotite xenoliths 89

10. Estimation of the degrees of metasomatic enrichment using two possible metasomatic agents and pre-metasomatized clinopyroxenes of samples DC3a and WB5 91

11. Calculated carbonate-rich fluids in equilibrium with clinopyroxenes of samples DC3a and WB5 92

PART 4: NATURE OF THE LOWER CRUST BENEATH THAILAND— A RECORD FROM GRANULITE XENOLITHS

1. Occurrences of granulite-xenolith locale in Thailand 107

2. Olivine-garnet clinopyroxenite showing "trains" of garnets 110

3. Corundum-bearing garnet granulite showing complete kelyphitization of garnets 113

4. Whole-rocks composition of Thai granulite xenoliths compared to those of Chudleigh and Mongolia 118

5. Selected trace-element plots as a function of MgO contents in whole-rock granulite xenoliths 120

6. Whole-rock REE profiles of three granulite xenolith groups showing general similarity with the Chudleigh granulite xenoliths and the Oman ophiolite cumulates 122

7. Major-element compositions of representative core and rim analyses of

clinopyroxenes in olivine-garnet clinopyroxenite, garnet granulite, and pyroxene-rich granulite 127

8. Characteristic zoning profiles of clinopyroxenes 129

9. Representative core and rim compositions of plagioclase 134

10. P-T estimates of granulite xenoliths from Thailand 142

PART 1

INTRODUCTION

Introduction

Much of our understanding about the deep part of the Earth, the mantle, has derived from studying ultramafic xenoliths entrained by rapidly-erupted magmas such as alkali basalts or kimberlites. These ultramafic xenoliths have been classified into two groups: (1) Cr-diopside group or Type I, and (2) Al-augite group or Type II (Wilshire and Shervais, 1975; Frey and Prinz, 1978). Commonly, xenoliths of Type I are believed to be accidental fragments of upper-mantle wall rocks, while those of Type II represent crystallized cumulates of basaltic magmas.

Such mantle-derived xenoliths have been observed in the Cenozoic alkali basalts of Thailand (e.g., Barr and McDonald, 1978; Vichit et al., 1979). However, they have received inadequate study, compared to their host basalts, despite their valuable information about mantle compositions and processes. Therefore, this investigation was initiated in an attempt to unlock petrogenetic information from these mantle materials.

Most of the reported occurrences of the mantle xenoliths in Thailand were visited and sampled. The xenolith localities are located on both sides of a Mesozoic suture, the Nan-River suture, that tectonically divides Thailand into two separate lithospheric blocks: the Shan-Thai on the west and the Indochina on the east (e.g., Bunopas and Vella, 1992). This scenario opens a unique opportunity to compare the nature of the mantle beneath these two lithospheric domains.

In addition to the ultramafic xenoliths, granulite-facies xenoliths of mafic compositions were discovered in this study. This type of xenoliths is commonly believed to have lower crustal origin (e.g., Pearson et al., 1991; Rudnick and Taylor, 1991; Rudnick, 1992). Although at the present time, granulite-facies xenoliths are known to

have existed in only one basaltic locality, the suite of samples investigated reveals important insights towards an understanding the nature of upper mantle and lower crust beneath the Thailand region.

The work presented in the following sections consists of three parts, divided as follows:

(1) Petrochemistry of the mantle beneath Thailand: Evidence from peridotite xenoliths (part 2),

(2) Trace-element characteristics of the spinel-peridotite xenoliths from Thailand: Melting and metasomatism of the mantle beneath a suture zone (part 3), and

(3) Nature of the lower crust beneath Thailand: A record from granulite xenoliths (part 4).

These three parts are relatively independent; however, part 3 represents an extended work from part 2, which has been published in the International Geology Review (v. 41, 1999, p. 506-530).

In part 2, we have used major-element chemistry in whole rocks and minerals to distinguish between the ultramafic xenoliths of Type I and Type II. We have also demonstrated that the xenoliths from the eastern lithospheric block (Indochina) are relatively more fertile (i.e., lower mg#) than those observed from the west (Shan-Thai). Temperature estimates of xenoliths from both lithospheric blocks, however, are within the same range (~1000 to 1130° C). These may reflect a regional heating event as a consequence of asthenospheric upwelling.

Results of the trace-element data presented in part 3 lead us to believe that the majority of xenoliths experienced small degrees of partial melting (up to ~6%), and noticeably higher (~16%) in one sample. In addition, some xenoliths were affected by metasomatic enrichment, most likely by carbonate-rich melts/fluids.

In part 4, we have utilized both major- and trace-element data to interpret the petrogenesis of granulite-facies xenoliths. We have found that these granulite-facies xenoliths were derived from basaltic cumulates, whose compositions are similar to troctolite and olivine gabbro. We have also discovered corundum inclusions in some samples, and deduced the conditions of their formation. This is particularly important in this area, where gem corundum has been commercially mined.

References

Barr, S.M., and MacDonald, A.S., 1978, Geochemistry and petrogenesis of Late Cenozoic alkaline basalts of Thailand: Geol. Soc. Malaysia Bull. v. 10, p. 25-52.

Bunopas, S., and Vella, P., 1992, Geotectonic and geologic evolution of Thailand, *in* Proc. Nat. Conf. Geol. Resources of Thailand: Potential for Future Development: Bangkok, Dept. Min. Resources, Thailand, p. 209-228.

Frey, F.A., and Prinz, M., 1978, Ultramafic inclusions from San Carlos, Arizona: petrologic and geochemical data bearing on their petrogenesis, Earth Planet Sci Lett, 38, p. 129-176.

Pearson, N.J., O'Reilly, S.Y., and Griffin, W.L., 1991, The granulite to eclogite transition beneath the eastern margin of the Australian craton, Eur. J. Mineral., v. 3., p. 293-322.

Rudnick, R.L., 1992, Xenoliths -- Samples of the lower continental crust, *in* Fountain, D.M, Arculus, R., and Kay, R.W., eds, Continental lower crust, Amsterdam, Elsvier, p. 269-316.

Rudnick, R.L., and Taylor, S.R., 1991, Petrology and geochemistry of lower crustal xenoliths from northern Queensland and inferences on lower crustal composition, *in* Drummond, B., ed, The Australian lithosphere, Geol. Soc. Australia, v. 17, p. 189-208.

Vichit, P., Vudhichativanich, S., and Hansawek, R., 1979, The distribution and some characetristics of corundum-bearing basalts in Thailand, Royal Thai Department of Mineral Resources Special Report, M4, p. 1-38.

Wilshire, H.G., and Shervais, J.W., 1975, Al-augite and Cr-diopside ultramafic xenoliths in basaltic rocks from Western United States, *in* Ahrens, L.H., Press, F., Runcorn, S.K., Urey, H.C. (eds), Phys Chem Earth, 9, p. 257-272.

PART 2

PETROCHEMISTRY OF THE MANTLE BENEATH THAILAND: EVIDENCE FROM PERIDOTITE XENOLITHS

Abstract

Spinel-peridotite xenoliths in late Cenozoic alkali basalts of Thailand were systematically investigated, for the first time, to evaluate the physico-chemical nature of the upper mantle of two separate lithospheric domains, the Shan-Thai and the Indochina microcontinents. Major-element chemistry of the xenoliths reveals a large variation in MgO contents (32.7-43.2 wt%), which form negative correlations with other major-oxide components. This suggests a fundamental control by partial melting and metasomatism. Subsolidus reequilibration is recognized by a decrease in Al_2O_3 contents at the margins of clino- and orthopyroxene. In addition, the xenoliths were compositionally modified by metasomatic partial melting, which was caused by interaction with the enclosing basalts. This resulted in the formation of a secondary assemblage on clinopyroxene known as "spongy rim", which is composed of a refractory clinopyroxene (i.e., low in Al_2O_3 and Na_2O) and often with K-Na rich, feldspathic glass.

Comparison between the xenoliths from the two microcontinents shows that xenoliths from the Shan-Thai commonly have higher mg# but lower oxidation states. Such differences may indicate the interaction of the Indochina xenoliths with influxes of oxidized fluids or melts. Nevertheless, the xenoliths from both microcontinents were equilibrated at a similar temperature range (~1000 to 1130° C), perhaps reflecting a regional heating event as a result of asthenospheric upwelling in the Cenozoic.

Introduction

Ultramafic xenoliths of mantle origin are common in many alkali basalts (e.g., Frey and Green, 1974; Frey and Prinz, 1978; Press et al., 1986; Qi et al., 1995). They

provide direct and valuable insights into processes controlling the geochemical evolution of the upper mantle. In Thailand, ultramafic xenoliths occur in late Cenozoic alkali basalts that were erupted onto two contrasting lithospheric blocks, namely the Shan-Thai and Indochina microcontinents (Fig. 1). Despite this rather unique tectonic setting, the Thai ultramafic xenoliths received inadequate investigation, until this study.

The work presented here represents the first attempt to reveal petrogenetic information from these ultramafic xenoliths. This was carried out by: (1) determination of the major-element compositions in both bulk rocks and minerals of the xenoliths, (2) deducing the petrogenesis of these xenoliths, and (3) comparison and contrasting the petrology and geochemistry of the xenoliths from the Shan-Thai and Indochina microcontinents. It is the purpose of this study to establish an understanding of the physico-chemical nature of the mantle beneath Thailand.

Tectonic Evolution of SE Asia

Tectonic interpretations of Thailand and neighboring SE-Asia region (Fig. 1) have recognized an assemblage of lithospheric fragments of various origins. The various models proposed for the tectonic evolution of this region (e.g., Bunopas, 1981; Mitchell, 1981; Barr and MacDonald, 1978, 1991; Stauffer, 1988; Tapponier et al., 1986; Hutchison, 1989; Bunopas and Vella; 1992), appear to agree upon the presence of two lithospheric fragments, i.e., Shan-Thai and Indochina microcontinents. According to Bunopas and Vella (1992), these two lithospheric blocks were rifted off a larger continent, presumably Gondwanaland, and drifted to the northern hemisphere in the late Paleozoic to early Mesozoic. By mid-Triassic, Shan-Thai was sutured to the Indochina,

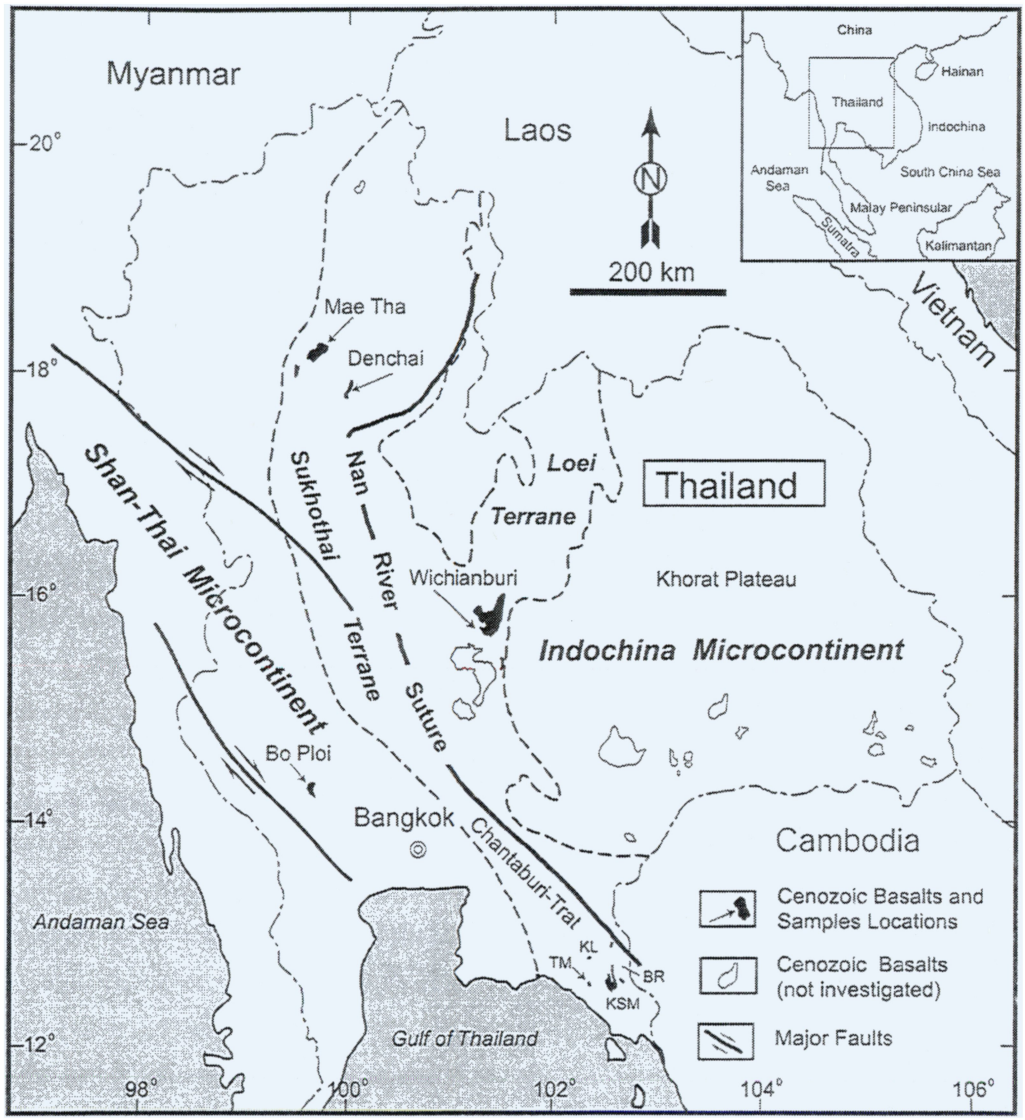


Figure 1. Schematic map of Thailand showing distributions of Cenozoic basalts and major tectonic features. Ultramafic xenoliths occur in at least 5 major localities, including the Bo Ploi, Mae Tha, Denchai, Wichianburi, and Chantaburi-Trat. Abbreviations for some towns mentioned in Table 1: KL = Klung, TM = Tha Mai, KSM = Kao Saming, BR = Bo Rai. Modified from the maps of Zhou and Mukasa (1997), Vichit et al. (1997), and the Royal Thai Department of Mineral Resources (Department, 1987).

producing a complex belt of folded Paleozoic and Mesozoic rocks, and the deformed ophiolite and melange assemblages, known as the Nan-River Suture. These two blocks were separated and partly overprinted by accretionary volcanic-arc complexes of the Sukhothai and Loei terranes. During the Cenozoic, extensional rifting and related lithospheric thinning resulted in numerous fault basins in central Thailand. This extensional regime probably triggered, or resulted from, asthenospheric upwelling that resulted in the volcanism of Late Cenozoic basalts (e.g., Smith, 1998).

Distributions of Basalts and Ultramafic Xenoliths

Upper Cenozoic volcanism in Thailand is dominated by the eruption of basaltic magmas, predominantly alkalic, with occurrences of tholeiitic types locally (Barr and MacDonald, 1981). Eruptive centers of basalts are small and scattered on the Shan-Thai microcontinents, but become more voluminous on the Indochina microcontinent (Fig. 1). Ultramafic xenoliths are commonly found in basaltic fields of the Shan-Thai block, whereas only a small proportion of xenoliths occurs in the Wichianburi basalts of the Indochina block. The eight locations from which samples were collected for this study are shown in Figure 1. The variety of xenolith types and ages of basaltic host-rocks are presented in Table 1.

The majority of ultramafic xenoliths obtained from Thai basalts are spinel lherzolites, with lesser harzburgite, and rare websterite, dunite, and pyroxenite. They are accompanied by a variety of mantle- and crustal-derived megacrysts, including pyroxene, spinel, olivine, garnet, zircon, magnetite, nepheline, ilmenite, feldspar, quartz, biotite, and corundum (Vichit et al., 1979; Barr and Dostal, 1986). Some diabasic and gneissic

Table 1. Ultramafic xenoliths from Thailand and their host rocks.

Location	Host rock	Age of host rock (Ma)	Xenolith*
Bo Ploi	Basanite, Ne-hawaiite[1]	3.14 - 4.17[2,3]	Sp-lherzolite (97)[†], Wehrlite (1)
Denchai	Hawaiite[1]	5.62 - 6.06[4]	Sp-lherzolite (22), Dunite (1), Harzburgite (14)
Mae Tha	Hawaiite, Basanite[3]	0.59 - 0.95[3,5,6]	Sp-lherzolite (17), Clinopyroxenite (1)
Wichianburi	Alkali basalt[7]	9.08[7]	Sp-lherzolite (14)
Tha Mai (Khao Wua)	Nephelinite[5]	3.0[3]	Sp-Ol websterite (2), Sp-lherzolite (18), Harzburgite (4)
Bo Rai (Nong Bon)	Nephelinite, Basanite[5]	1.13 - 2.38[3,5]	Harzburgite (1)
Kao Saming (Ban Na Wong)	n.a.	n.a.	Sp-lherzolite (1), Harzburgite (5)
Klung (Ban Bo Welu)	n.a.	n.a.	Sp-lherzolite (1), Crustal xenolith (11)[‡]

[1]Barr and Dostal (1986); [2] Barr and James (1990); [3] Suthirat et al. (1994); [4] Barr and MacDonald (1979); [5] Barr and MacDonald (1981); [6] Sasada et al. (1987); [7] Intasopa (1992); n.a. : not available.
*Based on megascopic study.
[†]Number of xenoliths whose sizes are greater than 1.5 cm.
[‡]Crustal xenoliths are studied separately.

fragments are also reported in the Bo Ploi area (Barr and Dostal, 1986). Based on mineral and whole-rock compositions (e.g., mg# and Cr_2O_3), these xenoliths can be classified as Type I (Cr-Diopside group) and Type II (Al-augite group) (Wilshire and Shervais, 1975; Frey and Prinz, 1978). Type I xenoliths are considered to be accidental fragments of upper-mantle wall rocks, whereas Type II xenoliths are basaltic cumulates formed under high pressures. Our study emphasizes the xenoliths of the Type I, with some comparison to samples of the Type II.

Analytical Technique

Chemical analyses were performed on polished thin-sections, using a fully automated CAMECA SX-50 electron microprobe (EMP) at the University of Tennessee. Bulk-rock glass beads were prepared following a procedure similar to that of Jezek et al. (1978); the rock powder was fused on a molybdenum strip-heater under a nitrogen atmosphere. EMP analytical conditions employed an accelerating voltage of 15 kV, a beam current of 30 nA at 5 μm beam size for minerals and 20 nA with a 10 μm beam size for glass samples, and full ZAF theoretical correction. The counting time was 20 seconds for each element. Loss on ignition (LOI) was determined by subtracting the oven-dried weight (heated overnight at 110°C) from the sample weight after heating in a muffle furnace at 1000° C for 2 hours. The weight increase due to the oxidation of Fe from Fe^{2+} to Fe^{3+} was added to the above LOI value to get the true LOI.

Petrography

Ultramafic xenoliths in our collection consist of 198 xenoliths that range in size from 1 to 9 cm, but most are about 2 to 5 cm. They constitute 170 spinel lherzolites (86%), 24 harzburgites (12%), with small amounts of wehrlite, dunite, olivine websterite, and clinopyroxenite. The xenoliths from the Bo Ploi and Denchai locales are most abundant and make up ~68% of our samples. Most xenoliths are angular with few deformational features, some with indistinct foliation owing to parallel orientation of tabular olivines and interstitial spinels. Although most samples are invariably weathered and oxidized on the surface, fresh samples can be obtained from cut surfaces. A pyroxene megacryst from the Bo Ploi area was also investigated for comparative study. Up to three representative samples from each of the locales were selected for this study. Modal analyses of the xenoliths were obtained using a point-counter, usually ~1500 points per thin section (Table 2). Classification of the ultramafic xenoliths studied is shown in Figure 2.

Most xenoliths display protogranular to porphyroclastic textures, indicating varying degrees of deformation. Triple-junctions between minerals, especially olivines are common (Fig. 3a). All the primary phases are in contact with each other, suggesting attainment of equilibrium. Olivines (Ol) in the majority of samples range in size from 1 to 3 mm, and up to 8 mm in some samples. They invariably display weak kink bands (Fig. 3b) and undulatory extinction. Small (0.3 to 0.5 mm), round olivines also occur as inclusions in orthopyroxenes and clinopyroxenes. Primary clinopyroxenes (Cpx; 0.5 to 3 mm) are emerald green and occur as anhedral crystals. In some samples, Cpx grains have spongy-textured rinds (Fig. 3c) that consist of secondary Cpx and high K-Na glass of

Table 2. Reconstructed primary modal abundances and whole-rock analysis of ultramafic xenoliths from Thailand.

Sample:	BP35	BP6[2]	BP15	DC5	DC3a[2]	DC14b	MT1[2]	MT7[2]	MT12[2]	WB3a	WB5	WB6	TM13[2]
Rock Type:[1]	LZ	LZ	WL	LZ	HB	DN	LZ	LZ	CP	LZ	LZ	LZ	WT
Modal abundances (vol%)[3]													
Ol	62.5	55.4	58.2	51.8	67.8	95.2	50.5	45.7	-	46.7	41.1	42.2	23.3
Opx	23.9	26.6	-	28.8	26.4	-	31.2	29.2	-	32.4	39.6	38.0	54.1
Cpx	11.9	15.3	41.0	16.2	5.1	3.7	16.2	22.4	98.4	17.4	15.7	17.6	19.7
Sp	2.2	2.7	0.8	3.2	0.7	1.1	2.1	2.7	1.6	3.5	3.6	2.2	2.9
Whole-rock compositions (wt%)[4]													
SiO_2	42.5	44.4	41.5	44.4	44.7	44.6	45.6	45.7	43.2	44.9	45.0	44.1	48.5
TiO_2	0.10	0.13	0.30	0.12	<0.03	0.08	0.15	0.16	2.03	0.13	0.16	0.11	0.13
Al_2O_3	2.94	4.31	3.40	4.50	0.92	2.26	4.12	4.55	14.9	4.85	4.94	3.90	5.80
Cr_2O_3	0.32	0.50	0.14	0.38	0.57	0.39	0.45	0.53	0.02	0.39	0.42	0.40	0.38
MgO	41.2	38.6	38.3	37.6	43.2	40.5	37.5	35.7	10.3	36.9	34.1	37.0	32.7
CaO	2.35	3.28	4.93	3.01	1.44	2.12	3.47	4.74	21.2	3.71	3.62	3.60	4.53
MnO	0.13	0.13	0.14	0.11	0.14	0.15	0.14	0.13	0.10	0.11	0.17	0.13	0.13
FeO[5]	7.77	8.50	9.19	7.69	8.66	8.45	7.92	7.43	7.19	7.89	9.69	8.30	7.25
NiO	0.05	0.22	0.04	0.06	0.28	0.03	0.19	0.17	<0.03	0.07	0.08	0.06	0.11
Na_2O	0.05	0.27	0.09	0.15	0.04	0.06	0.34	0.44	1.27	0.18	0.21	0.16	0.29
K_2O	<0.03	<0.03	<0.03	<0.03	<0.03	0.03	<0.03	<0.03	<0.03	<0.03	0.04	<0.03	<0.03
SO_3	0.04	n.a.[8]	0.03	<0.03	n.a.	0.03	n.a.	n.a.	n.a.	<0.03	0.03	0.03	n.a.
P_2O_5	0.03	n.a.	0.03	<0.03	n.a.	0.03	n.a.	n.a.	n.a.	0.04	0.06	0.04	n.a.
LOI[6]	2.10	n.a.	1.84	2.14	n.a.	1.72	n.a.	n.a.	n.a.	1.44	1.59	2.58	n.a.
Total	99.57	100.32	99.94	100.14	99.92	100.48	99.88	99.59	100.23	100.58	100.14	100.38	99.80
mg#[7]	90.4	89.0	88.1	89.7	89.9	89.5	89.4	87.9	71.8	89.3	86.3	88.8	88.9

[1]LZ = Sp-lherzolite, WL = Wehrlite, HB = Harzburgite, DN = Dunite, CP = Clinopyroxenite, WT = Olivine websterite.
[2]Whole-rock compositions were calculated from modal abundances and mineral analyses.
[3]Determined by point counting, up to 1500 points per thin section.
[4]Average from 10 analyses.
[5]Iron was analyzed as FeO.
[6]Loss on Ignition.
[7]100Mg/Mg+Fe.
[8]Not analyzed.

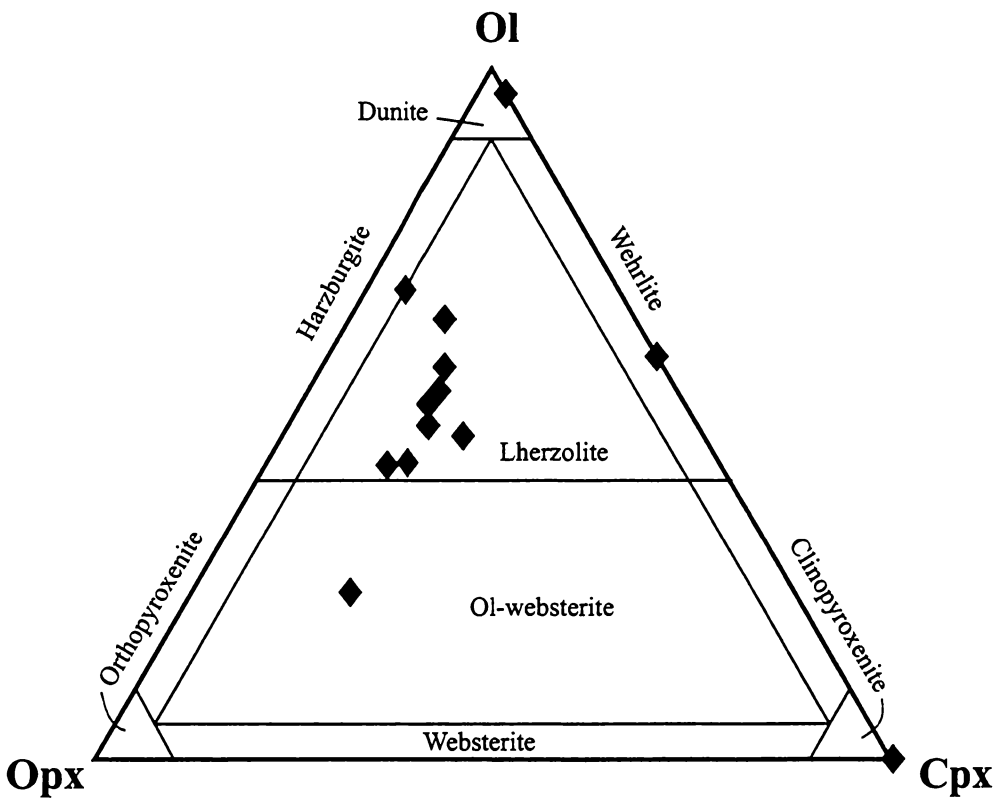


Figure 2. Modal abundances of ultramafic xenoliths from Thailand.

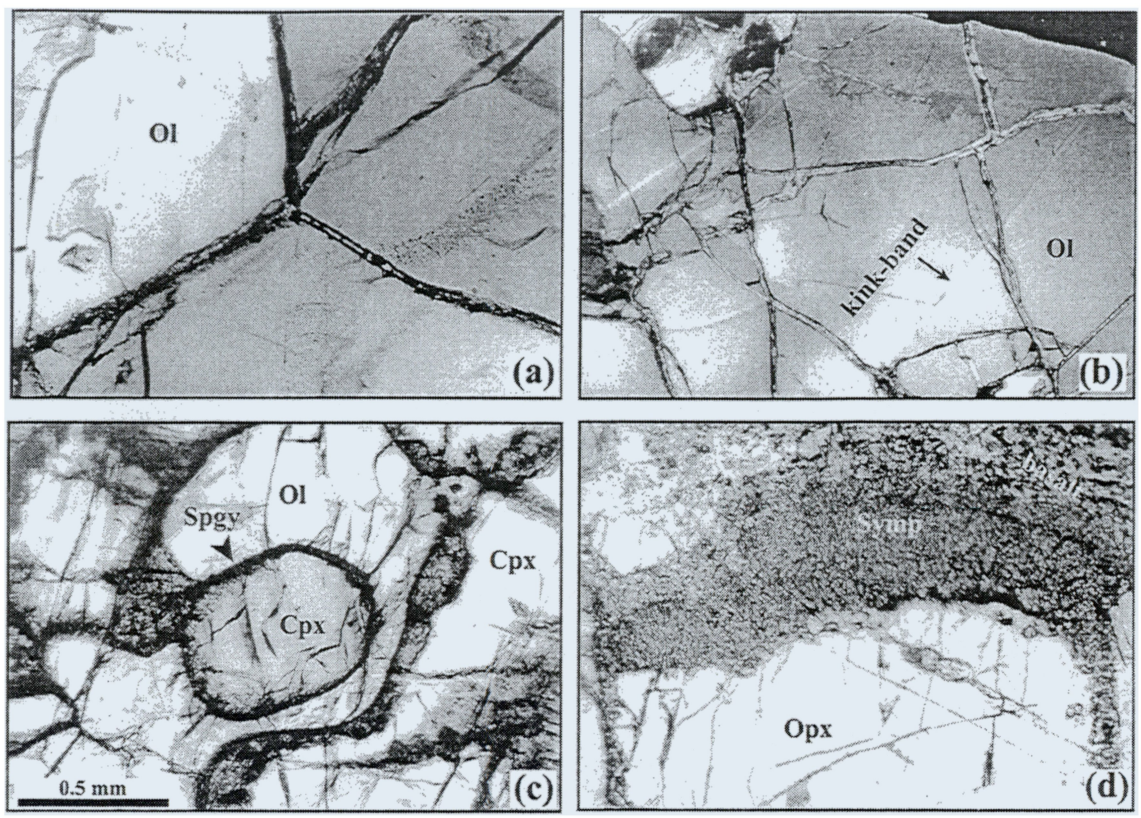


Figure 3. Photomicrograph of selected textural features of spinel-peridotite xenoliths from Thailand. All photos are under cross-nicols, and have the same magnification [scale bar in (c)]. (a) Large olivine grains (Ol) exhibit triple-junction grain boundaries. (b) Kink-band observed in a large olivine grain. (c) Spongy rims (Spgy) developed at the edges of clinopyroxene. (d) Symplectite textures (Symp) formed on orthopyroxene (Opx) at contact with host basalt. The symplectite consists of fine-grained secondary clinopyroxene and olivine.

varying compositions. Orthopyroxenes (Opx) are dark brown in hand samples, but pale brown in thin sections. They occur as subhedral grains, with the average grain sizes ~2 to 4 mm, some of which exhibit weak kink bands. Fine exsolution lamellae of clinopyroxene are observed in some large Opx grains. In some samples, orthopyroxenes at the contact with host basalts show metasomatic effects by forming corona of fine-grained, secondary clinopyroxene and olivine, commonly known as symplectite texture (Fig. 3d). Spinels (Sp) occur as a brown interstitial phase with grain sizes ranging from ~0.1 to 2.0 mm.

Several samples display distinct textures and mineralogy. Sample TM13 is unique inasmuch as it contains large (8 to 10 mm) Opx grains, surrounded by smaller (1 to 2 mm), interstitial Opx, Ol, Cpx, and Sp. Sample DC14b contains equigranular olivine and clinopyroxene (~0.5 mm). Some xenoliths from the Wichianburi (WB) locale contain serpentine stringers. Sample MT12 is a clinopyroxenite, with euhedral to subhedral clinopyroxenes that commonly display triple-junction grain boundaries. The clinopyroxene megacryst selected for comparative study (BPm1) is approximately 2.3 x 1.3 in size, with curved edges probably due to resorption. Based upon mineralogy and texture, three samples (MT12, BP15, and BPm1) can be classified as Type II xenoliths; the rest are Type I.

Whole-rock Chemistry

Whole-rock compositions were analyzed on seven ultramafic xenoliths; those of the rest were reconstructed from mineral chemistry and modal abundances. This was necessary due to the small sizes of the xenoliths that made it difficult to separate fresh,

representative portions of the samples for analysis. The major-element chemistry of the whole rocks is presented in Table 2.

Type I ultramafic xenoliths from Thailand show substantial ranges in major-element contents (Fig. 4). With increasing MgO contents, SiO_2, CaO, Al_2O_3, Na_2O, and TiO_2 concentrations systematically decrease, whereas Cr_2O_3 increases subtly. These compositional trends are consistent with other peridotite xenoliths worldwide (e.g., Frey and Prinz, 1978; Frey et al., 1985; Press et al., 1986, Qi et al., 1995), and commonly interpreted as the result of partial melting of the upper mantle (Frey et al., 1985). Sample DC5 has a composition similar to models estimated by Sun (1982) and Nickel and Green (1984). Therefore, it will be considered as representative of the most "primitive" sample in this study. In addition, the trends in MgO versus SiO_2, CaO, and TiO_2 plots are in agreement with the average spinel lherzolite compositions from continental basalts throughout the world (McDonough, 1990).

Mineral Chemistry

Mineral compositions were investigated to evaluate the possibility of inter- and intragranular variations. In each sample, several grains of each mineral were analyzed, with particular attention to compositional changes in cores and rims.

Olivines in peridotite xenoliths are relatively homogeneous, except where the grain is in contact with basalt; then FeO increases, while MgO and NiO decrease. Compositionally, olivines are magnesian-rich with a narrow range of Fo contents from 87.6 to 90.4 (Table 3). Sample BP15 (wehrlite) contains the lowest Fo and NiO contents in olivines but the highest TiO_2 contents in clinopyroxenes (Fig. 5). Based on the

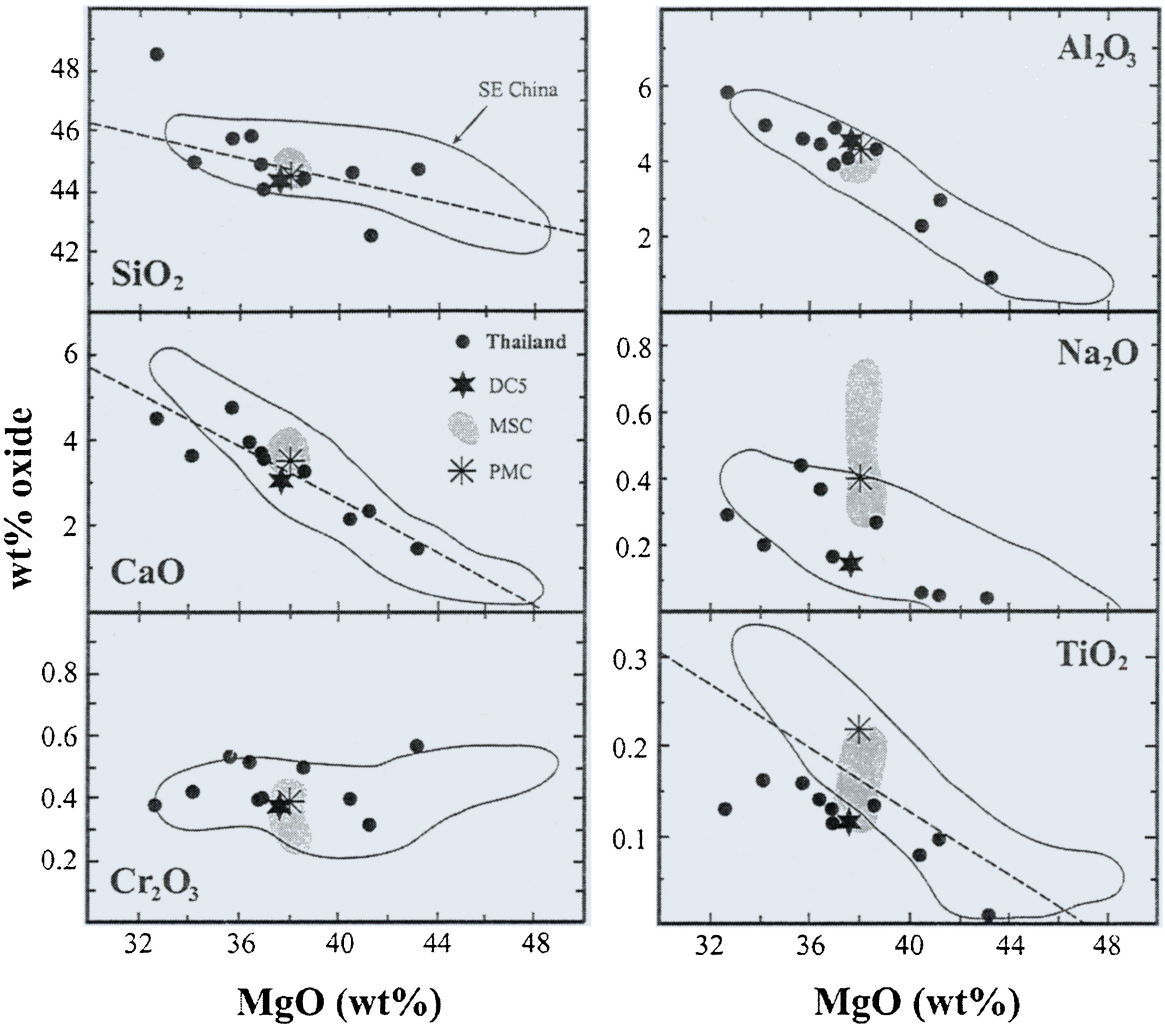


Figure 4. Major-oxide plots as a function of MgO for whole-rock analyses of Type I ultramafic xenoliths. The envelopes of mantle xenoliths from SE China are from Qi et al. (1995). Abbreviations: MSC = Mantle Source Composition (Nickel and Green, 1984); PMC = Primitive Mantle Composition (Sun, 1982). Dashed lines represent the average values of worldwide spinel lherzolite and harzburgite from continental basalts (McDonough, 1990). Sample DC5 lies closest to the MSC, and is considered representative of the most primitive Thai mantle composition.

Table 3. Average compositions of olivine.

Sample:	BP35	BP6	BP15	DC5	DC3a	DC14b	MT1	MT7	TM13	WB3a	WB5	WB6
n:[1]	12	12	13	16	12	21	13	11	12	18	17	7
SiO_2	40.5 (3)[2]	40.3 (5)	40.1 (2)	40.8 (3)	40.1 (5)	40.4 (3)	40.4 (1)	40.3 (3)	40.0 (2)	40.2 (2)	40.3 (3)	40.6 (3)
Cr_2O_3	<0.03	0.03 (1)	<0.03	<0.03	0.03 (2)	0.04 (4)	0.06 (4)	0.04 (4)	<0.03	0.04 (3)	0.04 (4)	<0.03)
MgO	48.5 (4)	48.8 (6)	47.6 (4)	48.6 (4)	49.8 (4)	49.0 (8)	48.7 (5)	48.7 (2)	48.7 (2)	48.9 (2)	48.3 (3)	49.2 (4)
CaO	0.07 (4)	0.11 (2)	0.13 (3)	0.07 (2)	0.12 (3)	0.11 (2)	0.10 (3)	0.09 (4)	0.04 (1)	0.07 (2)	0.07 (2)	0.08 (3)
MnO	0.14 (2)	0.14 (4)	0.18 (2)	0.14 (3)	0.13 (2)	0.16 (2)	0.16 (3)	0.15 (2)	0.15 (2)	0.15 (2)	0.17 (2)	0.15 (2)
FeO[3]	10.1 (1)	10.8 (6)	11.8 (2)	10.2 (3)	0.25 (1)	10.1 (2)	10.3 (3)	10.2 (1)	10.9 (1)	10.2 (2)	11.3 (2)	9.87 (2)
NiO	0.37 (2)	0.38 (4)	0.29 (2)	0.38 (2)	0.38 (2)	0.37 (2)	0.35 (6)	0.35 (6)	0.40 (3)	0.41 (3)	0.36 (3)	0.35 (5)
Total	99.73	100.56	100.08	100.18	99.78	100.21	99.99	99.77	100.18	99.94	100.58	100.26
Cations based on 4 oxygens												
Si	0.999	0.990	0.992	1.000	0.986	0.993	0.994	0.994	0.987	0.990	0.992	0.994
Cr	0.000	0.001	0.000	0.000	0.001	0.001	0.001	0.001	0.000	0.001	0.001	0.000
Mg	1.781	1.786	1.758	1.778	1.824	1.792	1.785	1.789	1.789	1.796	1.769	1.796
Ca	0.002	0.003	0.004	0.002	0.003	0.003	0.003	0.002	0.001	0.002	0.002	0.002
Mn	0.003	0.003	0.004	0.003	0.003	0.003	0.003	0.003	0.003	0.003	0.004	0.003
Fe	0.207	0.221	0.244	0.209	0.190	0.208	0.212	0.211	0.225	0.211	0.233	0.202
Ni	0.007	0.008	0.006	0.007	0.007	0.007	0.007	0.007	0.008	0.008	0.007	0.007
Σ	3.000	3.010	3.008	2.999	3.013	3.007	3.005	3.006	3.013	3.010	3.007	3.006
Fo	89.4	88.8	87.6	89.4	90.4	89.4	89.2	89.3	88.7	89.4	88.4	89.9

[1]Number of analyses used in average.
[2]Units in parenthesis represent 1 σ of replicate analyses in terms of last unit cited.
[3]Iron was analyzed as FeO.

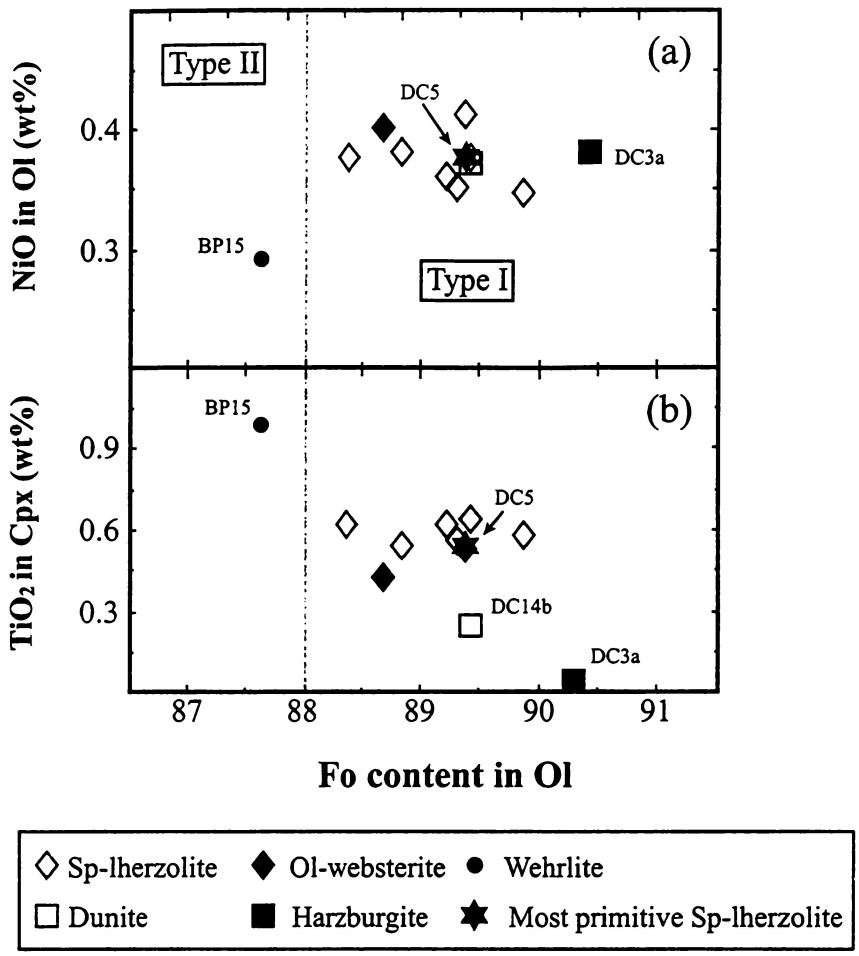


Figure 5. Concentrations of NiO in olivine (a) and TiO_2 in clinopyroxene (b) plotted against average Fo contents of olivine. The dashed line at Fo_{88}, which separates Type I from Type II xenoliths, is from Wass (1980). Note that the Type II xenolith (BP15), representing a solidified basaltic cumulate, contains the lowest Fo and NiO contents, but highest TiO_2 content. Harzburgite (DC3a), a depleted residue, has the lowest TiO_2 but highest Fo contents.

classification suggested by Wass (1980), BP15 is placed in Al-augite group (Type II); all other xenoliths studied, except pyroxenite MT12 and clinopyroxene megacryst BPm1, are in the Cr-diopside group (Type I).

Orthopyroxenes display minor, inter- and intragrain variation in terms of MgO, FeO, CaO, and TiO_2. However, Al_2O_3 contents exhibit large intergrain variation, from 2.17 to 5.89 wt% (Table 4), with systematically decreases in Al_2O_3 concentrations from core to rim (up to 0.66 wt%). A similar core-to-rim decrease, although to a lesser extent, is observed in Cr_2O_3 and CaO contents in most samples. In the pyroxene quadrilateral (Fig. 6), the orthopyroxenes from different samples occupy a rather restricted area ($Wo_{1.1\text{-}3.0}$ $En_{87.0\text{-}89.4}$ $Fs_{8.5\text{-}11.3}$). A traverse across a typical Opx grain shows a decreasing trend of Al_2O_3 towards the rim, whereas the CaO content is relatively constant (Fig. 7). Similar zoning patterns observed in xenoliths from central Asia are interpreted as the result of subsolidus cooling (Press et al., 1986; Witt-Eickschen and Seck, 1991).

Clinopyroxenes display only small intra- and intergrain compositional variations in terms of MgO, FeO, CaO, and TiO_2, within a single sample, but large variations among xenoliths with contrasting lithologies (Table 5). Figure 8 shows that mg#s vary positively with SiO_2, CaO, and Cr_2O_3, but negatively with Al_2O_3 and TiO_2. Rather weak correlation is observed in Na_2O-mg# plot. The largest compositional range is observed in the Al_2O_3 contents (2.66 to 7.71 wt%) of Type I xenoliths; Type II xenoliths have higher Al_2O_3 contents (7.75 to 13.4 wt%). In the pyroxene quadrilateral plot (Fig. 6), the Type I Cpx plots in the diopside field ($Wo_{42.9\text{-}48.5}$ $En_{46.5\text{-}50.9}$ $Fs_{4.3\text{-}7.1}$); Type II Cpx extends towards higher Fe content ($Wo_{42.5\text{-}53.9}$ $En_{34.2\text{-}50.3}$ $Fs_{6.9\text{-}12.8}$.). The excess Wo component

Table 4. Average compositions of orthopyroxene.

Sample:	BP35		BP6		DC5		DC3a		MT1	
	core [11][†]	rim [10]	core [9]	rim [10]	core [9]	rim [11]	core [8]	rim [10]	core [9]	rim [11]
SiO_2	54.4 (5)[‡]	55.0 (6)	53.6 (2)	53.5 (4)	54.4 (3)	54.6 (5)	55.5 (7)	55.9 (7)	54.1 (3)	54.3 (3)
TiO_2	0.14 (2)	0.12 (1)	0.16 (3)	0.15 (2)	0.13 (2)	0.11 (2)	0.02 (2)	0.03 (4)	0.16 (1)	0.14 (2)
Al_2O_3	4.75 (30)	4.09 (40)	5.89 (7)	5.80 (10)	4.88 (11)	4.60 (13)	2.29 (3)	2.17 (23)	5.29 (10)	5.07 (14)
Cr_2O_3	0.42 (3)	0.34 (7)	0.45 (5)	0.44 (4)	0.38 (4)	0.34 (3)	0.69 (3)	0.68 (4)	0.37 (2)	0.37 (3)
MgO	32.6 (6)	33.0 (6)	32.1 (2)	31.8 (14)	32.7 (4)	33.0 (3)	34.0 (2)	34.1 (3)	32.4 (2)	32.6 (2)
CaO	0.79 (21)	0.56 (7)	1.20 (4)	1.49 (87)	0.81 (4)	0.74 (1)	1.14 (3)	1.21 (15)	0.91 (5)	0.86 (2)
MnO	0.15 (3)	0.15 (3)	0.14 (3)	0.13 (1)	0.13 (2)	0.14 (2)	0.12 (2)	0.13 (3)	0.14 (1)	0.14 (3)
FeO*	6.57 (13)	6.56 (10)	6.55 (8)	6.44 (30)	6.43 (12)	6.44 (12)	5.65 (10)	5.72 (8)	6.47 (14)	6.44 (10)
Na_2O	0.06 (2)	0.05 (1)	0.16 (1)	0.27 (34)	0.11 (1)	0.10 (1)	0.05 (1)	0.06 (1)	0.13 (1)	0.13 (2)
Total	99.88	99.86	100.18	100.13	99.98	100.05	99.50	99.98	99.99	100.08
Cations based on 6 oxygens										
Si	1.866	1.905	1.856	1.856	1.885	1.888	1.927	1.933	1.875	1.880
Ti	0.004	0.003	0.004	0.004	0.003	0.003	0.001	0.001	0.004	0.004
Al^{iv}	0.114	0.095	0.144	0.144	0.115	0.112	0.073	0.067	0.125	0.120
Al^{vi}	0.080	0.072	0.097	0.094	0.084	0.075	0.021	0.021	0.091	0.086
Cr	0.012	0.009	0.013	0.012	0.010	0.009	0.019	0.018	0.010	0.010
Mg	1.686	1.703	1.655	1.646	1.686	1.702	1.763	1.756	1.673	1.682
Ca	0.029	0.021	0.044	0.056	0.030	0.027	0.042	0.045	0.034	0.032
Mn	0.004	0.004	0.004	0.004	0.004	0.004	0.004	0.004	0.004	0.004
Fe	0.191	0.190	0.190	0.187	0.186	0.186	0.164	0.165	0.188	0.186
Na	0.004	0.003	0.011	0.019	0.008	0.007	0.003	0.004	0.009	0.009
Σ	4.010	4.006	4.019	4.028	4.011	4.014	4.018	4.015	4.013	4.013
Wo	1.5	1.1	2.4	3.0	1.6	1.4	2.1	2.3	1.8	1.7
En	88.3	88.8	87.4	87.0	88.5	88.7	89.4	89.1	88.1	88.3
Fs	10.2	10.1	10.2	10.0	9.9	9.9	8.5	8.6	10.1	10.0
mg#[§]	89.8	90.0	89.7	89.8	90.1	90.1	91.5	91.4	89.9	90.0

(continues)

Table 4. (continued)

Sample:	MT7		TM13		WB3a		WB5		WB6	
	core [9]	rim [10]	core [12]	rim [8]	core [10]	rim [12]	core [4]	rim [4]	core [12]	rim [8]
SiO_2	54.4 (2)	54.8 (2)	53.6 (3)	54.2 (7)	54.0 (2)	54.2 (4)	54.6 (2)	55.0 (2)	53.6 (3)	54.2 (7)
TiO_2	0.12 (2)	0.08 (2)	0.10 (2)	0.08 (2)	0.12 (2)	0.10 (2)	0.12 (1)	0.11 (1)	0.10 (2)	0.08 (2)
Al_2O_3	4.65 (8)	4.11 (15)	5.38 (32)	4.72 (45)	4.73 (12)	4.52 (12)	4.58 (11)	4.33 (6)	5.38 (32)	4.72 (45)
Cr_2O_3	0.32 (3)	0.29 (4)	0.29 (7)	0.21 (9)	0.32 (4)	0.31 (3)	0.42 (5)	0.33 (2)	0.29 (7)	0.21 (9)
MgO	32.8 (3)	33.2 (1)	32.5 (3)	32.9 (2)	32.7 (2)	32.8 (1)	32.9 (1)	33.0 (1)	32.5 (3)	32.9 (2)
CaO	0.67 (4)	0.60 (2)	0.81 (23)	0.64 (2)	0.77 (5)	0.74 (3)	0.79 (1)	0.74 (3)	0.81 (23)	0.64 (2)
MnO	0.14 (2)	0.15 (3)	0.147 (3)	0.14 (3)	0.14 (2)	0.14 (2)	0.17 (2)	0.16 (2)	0.147 (3)	0.14 (3)
FeO	6.47 (6)	6.43 (11)	6.95 (15)	6.98 (13)	6.80 (9)	6.78 (9)	6.67 (57)	6.56 (67)	6.95 (15)	6.98 (13)
Na_2O	0.08 (1)	0.06 (1)	0.07 (1)	0.07 (1)	0.09 (0)	0.09 (2)	0.10 (1)	0.09 (1)	0.07 (1)	0.07 (1)
Total	99.65	99.74	99.83	99.95	99.62	99.75	100.37	100.36	99.83	99.95
Cations based on 6 oxygens										
Si	1.888	1.901	1.864	1.881	1.880	1.885	1.873	1.884	1.887	1.898
Ti	0.003	0.002	0.003	0.002	0.003	0.003	0.004	0.003	0.003	0.003
Al^{iv}	0.112	0.099	0.136	0.119	0.120	0.115	0.127	0.116	0.113	0.102
Al^{vi}	0.078	0.068	0.085	0.074	0.074	0.070	0.074	0.070	0.074	0.074
Cr	0.009	0.008	0.008	0.006	0.009	0.009	0.009	0.008	0.012	0.009
Mg	1.699	1.715	1.685	1.702	1.695	1.702	1.677	1.683	1.694	1.699
Ca	0.026	0.022	0.030	0.024	0.029	0.027	0.029	0.028	0.029	0.028
Mn	0.004	0.004	0.004	0.004	0.004	0.004	0.005	0.005	0.005	0.005
Fe	0.188	0.187	0.202	0.202	0.198	0.197	0.217	0.217	0.193	0.189
Na	0.005	0.004	0.005	0.004	0.006	0.006	0.006	0.006	0.006	0.006
Σ	4.012	4.012	4.022	4.019	4.019	4.019	4.021	4.019	4.014	4.011
Wo	1.3	1.1	1.6	1.2	1.5	1.4	1.5	1.4	1.6	1.2
En	88.7	88.9	87.7	88.1	88.0	88.2	88.4	88.7	87.7	88.1
Fs	10.0	10.0	10.7	10.7	10.5	10.4	10.1	9.9	10.7	10.7
mg#	90.0	90.2	89.3	89.4	89.5	89.6	89.8	90.0	89.3	89.4

Note: †Number of analyses used in the average; ‡1 σ of replicate analyses in terms of last unit cited; *Analyzed as FeO; §100Mg/(Mg+Fe).

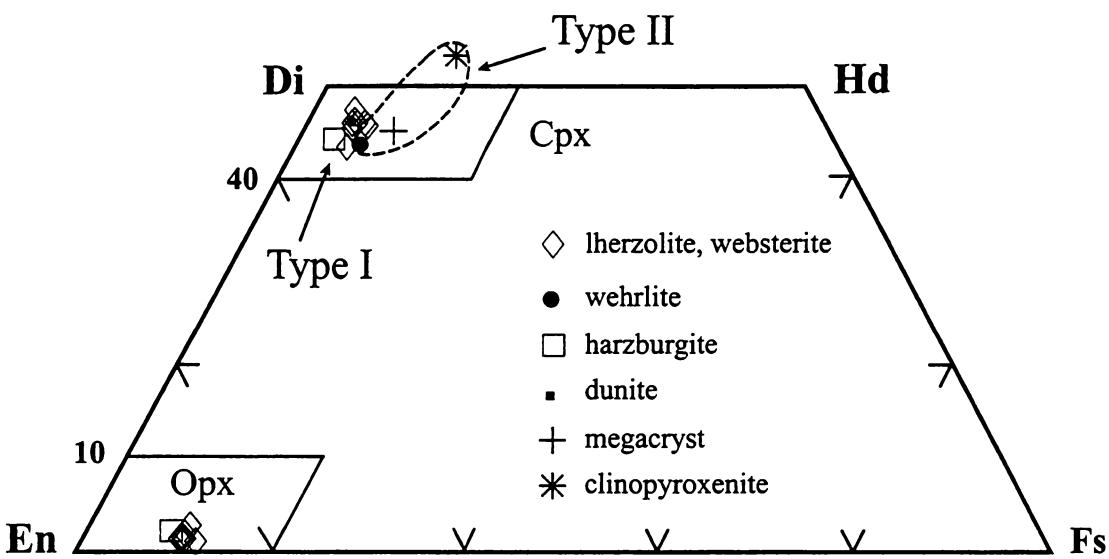


Figure 6. Pyroxene quadilateral showing compositions of orthopyroxene (Opx) and clinopyroxene (Cpx) in Thai ultramafic xenoliths. The excess Wo content shown in the Cpx from clinopyroxenite is due to the abundant non-quadrilateral component, such as Al_2O_3 and TiO_2.

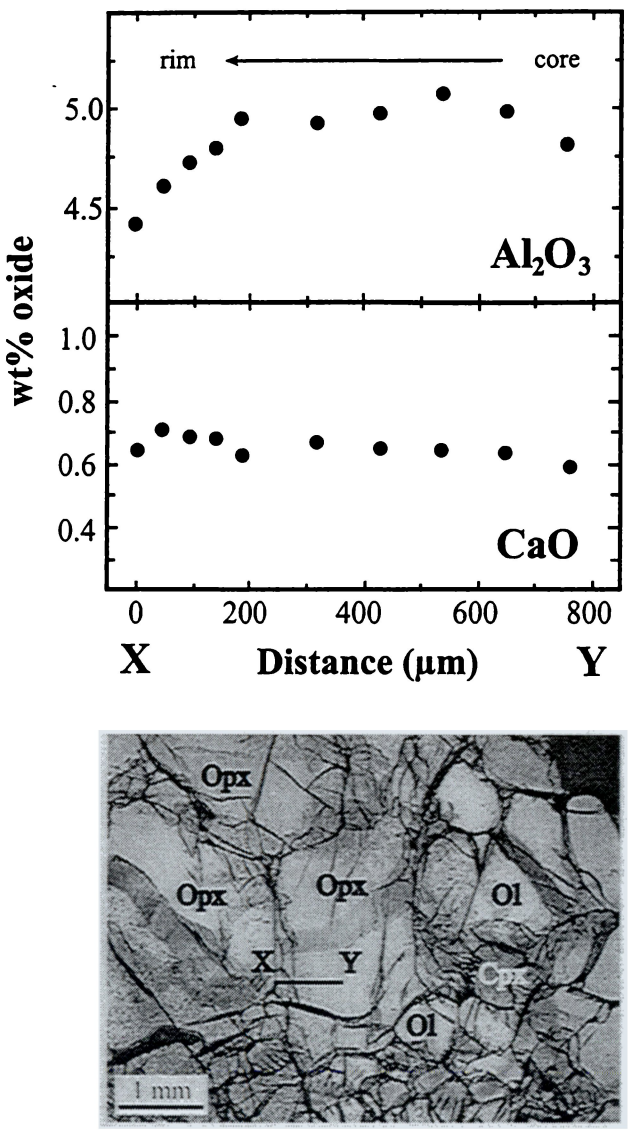


Figure 7. Compositional variation along line X-Y on an orthopyroxene grain in sample BP35. The decreasing Al_2O_3 at relatively constant CaO is due to the different diffusivities between Al and Ca. Photomicrograph is under plane-polarlized light. Abbreviations: Opx = orthopyroxene; Ol = olivine; Cpx = clinopyroxene.

Table 5. Average compositions of clinopyroxene.

Sample:	BP35		BP6		BP15		BPm1		DC5	
	core [12][†]	rim [8]	core [7]	rim [8]	core [7]	rim [8]	core [5]	rim [3]	core [8]	rim [8]
SiO_2	51.1 (2)[‡]	51.7 (4)	50.8 (2)	51.1 (7)	50.0 (1)	49.9 (4)	48.8 (3)	48.4 (9)	51.7 (2)	51.8 (3)
TiO_2	0.56 (4)	0.59 (3)	0.52 (2)	0.55 (6)	0.97 (5)	0.99 (9)	1.10 (2)	1.33 (32)	0.55 (2)	0.53 (2)
Al_2O_3	6.82 (23)	5.78 (43)	7.71 (18)	7.25 (58)	8.36 (13)	7.75 (76)	8.45 (4)	7.86 (81)	7.27 (8)	6.95 (6)
Cr_2O_3	0.90 (7)	0.72 (10)	0.75 (5)	0.73 (10)	0.41 (7)	0.38 (7)	0.11 (3)	0.11 (5)	0.77 (4)	0.71 (7)
MgO	14.7 (1)	15.3 (2)	16.0 (2)	16.0 (4)	15.7 (9)	15.5 (4)	14.4 (2)	13.5 (12)	14.9 (1)	15.0 (2)
CaO	21.3 (2)	21.7 (2)	18.8 (2)	19.3 (7)	18.5 (1)	19.8 (15)	19.4 (2)	20.0 (8)	19.6 (1)	19.7 (1)
MnO	0.09 (2)	0.07 (2)	0.10 (2)	0.09 (2)	0.12 (2)	0.12 (2)	0.11 (3)	0.19 (8)	0.08 (2)	0.07 (3)
FeO*	2.76 (6)	2.77 (4)	3.38 (8)	3.33 (20)	3.98 (3)	3.83 (34)	5.34 (4)	5.77 (75)	2.79 (5)	2.83 (5)
Na_2O	1.33 (7)	1.20 (4)	1.53 (2)	1.38 (23)	1.37 (3)	1.16 (29)	1.15 (1)	1.53 (64)	1.77 (3)	1.72 (3)
Total	99.52	99.86	99.58	99.84	99.49	99.43	98.90	98.82	99.37	99.30
Cations based on 6 oxygens										
Si	1.862	1.881	1.843	1.853	1.821	1.822	1.805	1.804	1.878	1.882
Ti	0.015	0.016	0.014	0.015	0.027	0.027	0.031	0.037	0.015	0.015
Al^{iv}	0.138	0.119	0.157	0.147	0.179	0.178	0.195	0.196	0.123	0.118
Al^{vi}	0.156	0.129	0.173	0.162	0.180	0.156	0.174	0.149	0.189	0.180
Cr	0.026	0.021	0.021	0.021	0.012	0.011	0.003	0.003	0.022	0.020
Mg	0.798	0.830	0.866	0.865	0.854	0.846	0.791	0.750	0.804	0.812
Ca	0.833	0.844	0.73	0.751	0.723	0.776	0.770	0.800	0.761	0.769
Mn	0.003	0.002	0.003	0.003	0.004	0.004	0.003	0.006	0.003	0.002
Fe	0.084	0.084	0.103	0.101	0.121	0.117	0.165	0.180	0.085	0.086
Na	0.094	0.085	0.108	0.097	0.096	0.082	0.082	0.111	0.124	0.121
Σ	4.010	4.012	4.022	4.017	4.016	4.020	4.020	4.043	4.003	4.005
Wo	48.5	48.0	42.9	43.7	42.5	44.5	44.5	46.1	46.1	46.0
En	46.5	47.1	50.9	50.3	50.2	48.6	45.8	43.2	48.6	48.7
Fs	5.0	4.9	6.2	6.0	7.3	6.9	9.7	10.7	5.3	5.3
mg#[§]	90.4	90.8	89.4	89.5	87.6	87.9	82.7	80.5	90.5	90.4

(continues)

Table 5. (continued)

Sample:	DC3a		DC14b		MT1		MT7		MT12	
	core [8]	rim [8]	core [2]	rim [2]	core [6]	rim [6]	core [4]	rim [5]	core [8]	rim [6]
SiO_2	53.0 (3)	53.1 (2)	52.8 (7)	53.4 (7)	51.1 (3)	51.3 (2)	51.1 (1)	51.4 (2)	43.9 (12)	44.5 (8)
TiO_2	0.04 (1)	0.05 (1)	0.28 (21)	0.22 (16)	0.63 (2)	0.61 (2)	0.55 (2)	0.57 (4)	2.06 (12)	1.95 (13)
Al_2O_3	2.66 (8)	2.75 (4)	5.15 (54)	4.80 (47)	7.69 (9)	7.08 (80)	7.16 (8)	6.78 (28)	13.4 (12)	11.8 (7)
Cr_2O_3	1.17 (7)	1.27 (12)	1.24 (3)	1.22 (4)	0.79 (5)	0.75 (4)	0.73 (4)	0.74 (7)	0.02 (2)	0.02 (3)
MgO	17.9 (1)	17.9 (1)	15.4 (1)	15.5 (2)	15.1 (1)	15.4 (4)	14.8 (1)	15.1 (2)	10.0 (6)	10.5 (3)
CaO	21.5 (2)	21.3 (1)	20.4 (3)	20.6 (1)	19.4 (1)	20.0 (12)	20.1 (1)	20.9 (4)	21.6 (20)	23.1 (1)
MnO	0.07 (1)	0.09 (2)	0.06 (0)	0.09 (2)	0.10 (3)	0.10 (4)	0.10 (1)	0.08 (2)	0.09 (3)	0.11 (2)
FeO	2.58 (7)	2.62 (8)	2.78 (9)	2.70 (14)	2.95 (11)	3.03 (6)	2.77 (4)	2.48 (18)	6.55 (57)	6.37 (10)
Na_2O	0.62 (4)	0.65 (3)	1.85 (3)	1.87 (8)	1.83 (4)	1.56 (55)	1.88 (3)	1.61 (18)	1.29 (59)	0.88 (3)
Total	99.60	99.68	99.89	100.43	99.49	99.86	99.20	99.55	98.93	99.17
Cations based on 6 oxygens										
Si	1.931	1.931	1.913	1.925	1.856	1.860	1.866	1.869	1.653	1.673
Ti	0.001	0.001	0.008	0.006	0.017	0.017	0.015	0.015	0.058	0.055
Al^{iv}	0.069	0.069	0.087	0.075	0.144	0.140	0.135	0.131	0.347	0.327
Al^{vi}	0.045	0.049	0.134	0.129	0.185	0.163	0.174	0.160	0.245	0.196
Cr	0.034	0.037	0.036	0.035	0.023	0.022	0.021	0.021	0.001	0.001
Mg	0.973	0.970	0.831	0.835	0.815	0.835	0.805	0.816	0.563	0.591
Ca	0.837	0.828	0.793	0.795	0.753	0.777	0.786	0.813	0.870	0.930
Mn	0.002	0.003	0.002	0.003	0.003	0.003	0.003	0.003	0.003	0.004
Fe	0.079	0.080	0.084	0.082	0.090	0.092	0.085	0.075	0.206	0.201
Na	0.044	0.046	0.130	0.131	0.129	0.110	0.133	0.114	0.094	0.065
Σ	4.016	4.014	4.017	4.015	4.015	4.017	4.021	4.016	4.041	4.042
Wo	44.3	44.0	46.4	46.4	45.3	45.5	46.8	47.6	52.9	53.9
En	51.4	51.6	48.6	48.7	49.1	48.9	48.0	47.8	34.3	34.2
Fs	4.3	4.4	5.0	4.9	5.6	5.6	5.2	4.6	12.8	11.8
mg#	92.5	92.4	90.8	91.1	90.1	90.1	90.5	91.5	73.2	74.6

(continues)

Table 5. (continued)

Sample:	TM13		WB3a		WB5		WB6	
	core [6]	rim [7]	core [7]	rim [6]	core [7]	rim [8]	core [4]	rim [4]
SiO_2	51.0 (1)	50.9 (4)	50.6 (1)	50.8 (2)	50.6 (4)	50.9 (3)	51.0 (2)	51.4 (6)
TiO_2	0.42 (3)	0.41 (3)	0.56 (2)	0.50 (4)	0.65 (3)	0.59 (3)	0.56 (4)	0.59 (4)
Al_2O_3	6.47 (16)	6.33 (23)	6.78 (13)	6.51 (7)	6.96 (13)	6.64 (7)	6.48 (3)	5.61 (147)
Cr_2O_3	0.44 (5)	0.42 (8)	0.66 (4)	0.63 (3)	0.66 (4)	0.64 (7)	0.84 (2)	0.79 (12)
MgO	15.5 (1)	15.7 (4)	15.0 (1)	15.1 (1)	14.8 (5)	14.9 (2)	15.1 (1)	15.6 (9)
CaO	20.9 (2)	20.9 (5)	20.2 (2)	20.4 (1)	19.8 (1)	20.0 (1)	20.2 (1)	20.5 (9)
MnO	0.10 (2)	0.09 (3)	0.09 (3)	0.09 (1)	0.11 (2)	0.11 (3)	0.09 (3)	0.08 (1)
FeO^3	3.13 (7)	3.07 (4)	3.60 (3)	3.65 (7)	4.00 (73)	3.99 (144)	3.43 (41)	3.28 (177)
Na_2O	1.31 (2)	1.27 (6)	1.55 (2)	1.52 (4)	1.57 (3)	1.50 (4)	1.62 (7)	1.40 (56)
Total	99.26	99.11	99.05	99.21	99.15	99.36	99.19	99.26
Cations based on 6 oxygens								
Si	1.865	1.865	1.857	1.863	1.856	1.864	1.867	1.880
Ti	0.012	0.011	0.015	0.014	0.018	0.016	0.015	0.016
Al^{iv}	0.135	0.135	0.143	0.137	0.144	0.136	0.133	0.120
Al^{vi}	0.144	0.138	0.150	0.144	0.157	0.151	0.146	0.121
Cr	0.013	0.012	0.019	0.018	0.019	0.019	0.024	0.023
Mg	0.846	0.859	0.822	0.826	0.808	0.815	0.824	0.853
Ca	0.820	0.818	0.796	0.802	0.780	0.786	0.791	0.805
Mn	0.003	0.003	0.003	0.003	0.003	0.003	0.003	0.002
Fe	0.096	0.094	0.110	0.112	0.123	0.122	0.105	0.101
Na	0.093	0.090	0.111	0.108	0.112	0.107	0.115	0.099
Σ	4.025	4.026	4.027	4.028	4.022	4.020	4.023	4.021
Wo	46.5	46.1	46.0	46.0	45.6	45.6	46.0	45.8
En	47.9	48.4	47.5	47.4	47.2	47.3	47.9	48.5
Fs	5.6	5.5	6.5	6.6	7.2	7.1	6.1	5.7
mg#	89.8	90.1	88.2	88.1	86.8	86.9	88.7	89.5

Note: †Number of analyses used in the average; ‡1 σ of replicate analyses in terms of last unit cited; •Analyzed as FeO; §100Mg/(Mg+Fe).

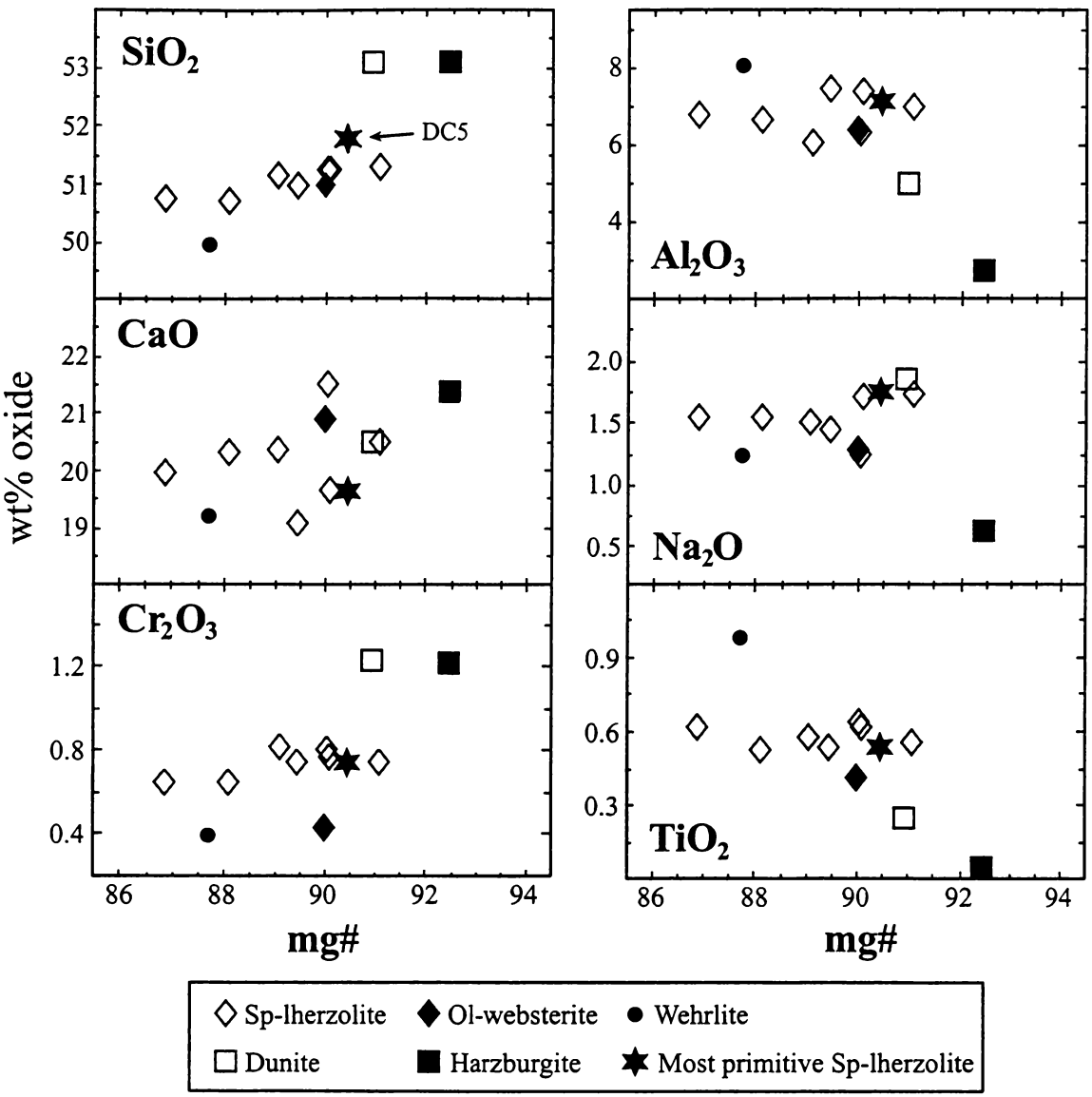


Figure 8. Plots of mg#s (100Mg/Mg+Fe) versus selected major oxides in average core analyses of clinopyroxene. The mg#s are positively correlated with SiO_2, CaO, and Cr_2O_3, while negatively correlated with Al_2O_3 and TiO_2, suggesting a control by partial melting and metasomatic enrichment.

observed in clinopyroxenite MT12 is due to abundant non-quadrilateral components, such as Al_2O_3 and TiO_2.

Spinels are relatively homogeneous within a sample, but they do show significant variations among samples, especially in Al_2O_3 and Cr_2O_3 contents (Table 6). Spinels in most samples are aluminum-rich (55.1 to 61.0 wt% Al_2O_3), as demonstrated in Figure 9a. Two samples, DC14b and DC3a, contain the highest in Cr_2O_3 contents (31.0 and 43.7 wt%, respectively), but lowest in Al_2O_3 and MgO, with strong correlation between cr# (100Cr/Cr+Al) and mg# (100Mg/Mg+Fe^{2+}) (Fig. 9b).

Discussion

Chemical variations of whole-rock compositions

The generally negative correlations of MgO with other major-oxide components in the whole rocks are typical for mantle xenoliths that experienced varying degrees of partial melting (e.g., Frey and Prinz, 1978; Frey et al., 1985; Press et al., 1986; McDonough, 1990; Qi et al., 1995). Besides melting, metasomatic and/or deformational enrichment could result in similarly negative trends. Often, it is difficult to distinguish between metamorphic and metasomatic enrichment in the absence of mineralogical (e.g., amphibole) and trace-element data. To further evaluate the possibility of enrichment processes that may occur to the xenoliths, two distinctive features of the major-element chemistry need to be discussed.

First, in MgO variation diagrams (Fig. 4), a number of peridotite xenoliths are more fertile than primitive mantle compositions, i.e., lower in MgO but higher in SiO_2, CaO, and Al_2O_3. One possible explanation of this extra-fertile mantle is that these

Table 6. Average compositions of spinel.

Sample:	BP35	BP6	BP15	DC5	DC3a	DC14b	MT1	MT7	MT12	TM13	WB3a	WB5	WB6
n:[†]	8	23	13	30	8	4	17	18	10	19	18	16	8
SiO_2	<0.03	0.09 (2)	0.08 (3)	0.04 (1)	0.04 (1)	0.04 (2)	0.05 (1)	0.03 (1)	0.02 (1)	0.05 (1)	0.04 (1)	0.04 (1)	0.06 (1)
TiO_2	0.10 (1)[‡]	0.19 (3)	0.31 (5)	0.10 (2)	0.09 (2)	0.22 (27)	0.13 (1)	0.05 (3)	0.20 (2)	0.08 (2)	0.07 (1)	0.11 (2)	0.16 (7)
Al_2O_3	56.8 (7)	57.6 (5)	60.0 (4)	58.3 (4)	25.5 (4)	36.7 (63)	58.7 (4)	58.8 (6)	59.8 (3)	61.0 (4)	55.1 (6)	55.2 (9)	53.8 (6)
V_2O_3	0.08 (2)	0.07 (3)	0.08 (2)	0.05 (3)	0.18 (3)	0.15 (11)	0.06 (3)	0.05 (3)	0.06 (3)	0.07 (3)	0.08 (2)	0.07 (2)	0.08 (1)
Cr_2O_3	10.1 (3)	8.93 (18)	4.98 (26)	9.01 (15)	42.7 (3)	31.0 (56)	8.59 (26)	9.46 (25)	0.14 (2)	5.34 (30)	9.54(18)	9.15 (17)	11.9 (3)
MgO	20.1 (3)	21.0 (3)	21.0 (2)	20.8 (2)	15.4 (3)	17.2 (16)	20.8 (2)	20.7 (3)	13.38 (1)	21.1 (2)	20.0 (3)	19.7 (3)	20.0 (3)
MnO	0.08 (4)	0.07 (2)	0.09 (2)	0.06 (2)	0.10 (2)	0.08 (1)	0.07 (1)	0.07 (2)	0.21 (3)	0.08 (3)	0.08 (2)	0.12 (3)	0.09 (3)
FeO*	11.2 (4)	10.7 (2)	12.3 (2)	10.3 (2)	14.7 (3)	13.6 (14)	10.2 (3)	9.37 (22)	25.2 (2)	11.3 (1)	13.2 (3)	14.4 (3)	12.8 (4)
NiO	0.37 (5)	0.36 (3)	0.33 (2)	0.40 (3)	0.18 (3)	0.22 (3)	0.38 (4)	0.37 (3)	0.08 (2)	0.45 (2)	0.44 (2)	0.42 (4)	0.34 (5)
ZnO	0.16 (3)	0.09 (5)	0.08 (6)	0.10 (5)	0.08 (4)	0.10 (6)	0.10 (4)	0.11 (7)	0.16 (4)	0.10 (4)	0.11 (6)	0.14 (5)	0.08 (4)
Total	99.01	99.14	99.07	99.05	98.84	99.36	99.11	99.05	99.33	99.50	98.64	99.41	99.35
Cations based on 4 oxygens													
Si	0.000	0.002	0.002	0.001	0.001	0.001	0.000	0.001	0.000	0.001	0.001	0.001	0.002
Ti	0.002	0.004	0.004	0.002	0.002	0.005	0.003	0.001	0.004	0.001	0.001	0.002	0.003
Al	1.756	1.768	1.830	1.785	0.913	1.240	1.792	1.794	1.909	1.845	1.727	1.726	1.684
V	0.002	0.001	0.002	0.001	0.004	0.004	0.001	0.001	0.001	0.001	0.002	0.001	0.002
Cr	0.209	0.184	0.102	0.185	1.027	0.703	0.176	0.194	0.003	0.108	0.201	0.192	0.251
Mg	0.787	0.815	0.809	0.803	0.696	0.733	0.805	0.799	0.540	0.806	0.793	0.780	0.791
Mn	0.002	0.002	0.002	0.001	0.002	0.002	0.002	0.002	0.005	0.002	0.002	0.003	0.002
Fe	0.245	0.233	0.263	0.223	0.373	0.327	0.222	0.203	0.571	0.243	0.294	0.320	0.284
Ni	0.008	0.008	0.007	0.008	0.004	0.005	0.008	0.008	0.002	0.009	0.009	0.009	0.007
Zn	0.003	0.003	0.002	0.002	0.002	0.002	0.002	0.002	0.003	0.002	0.002	0.003	0.002
Σ	3.014	3.017	3.025	3.012	3.025	3.021	3.012	3.004	3.039	3.020	3.032	3.037	3.027
mg#	79.2	81.4	80.4	80.7	69.4	73.0	80.8	80.7	53.6	80.9	79.3	78.2	79.30
cr#	10.6	9.4	5.3	9.4	52.9	36.5	8.9	9.8	0.2	5.6	10.4	10.0	13.0

Note: [†]Number of analyses used in the average; [‡]Represents 1 σ of replicate analyses in term of last unit cited; *Iron was analyzed as FeO; 100Mg/(Mg+Fe^{2+}), Fe^{2+} calculated based on stoichiometry; 100Cr/(Cr+Al).

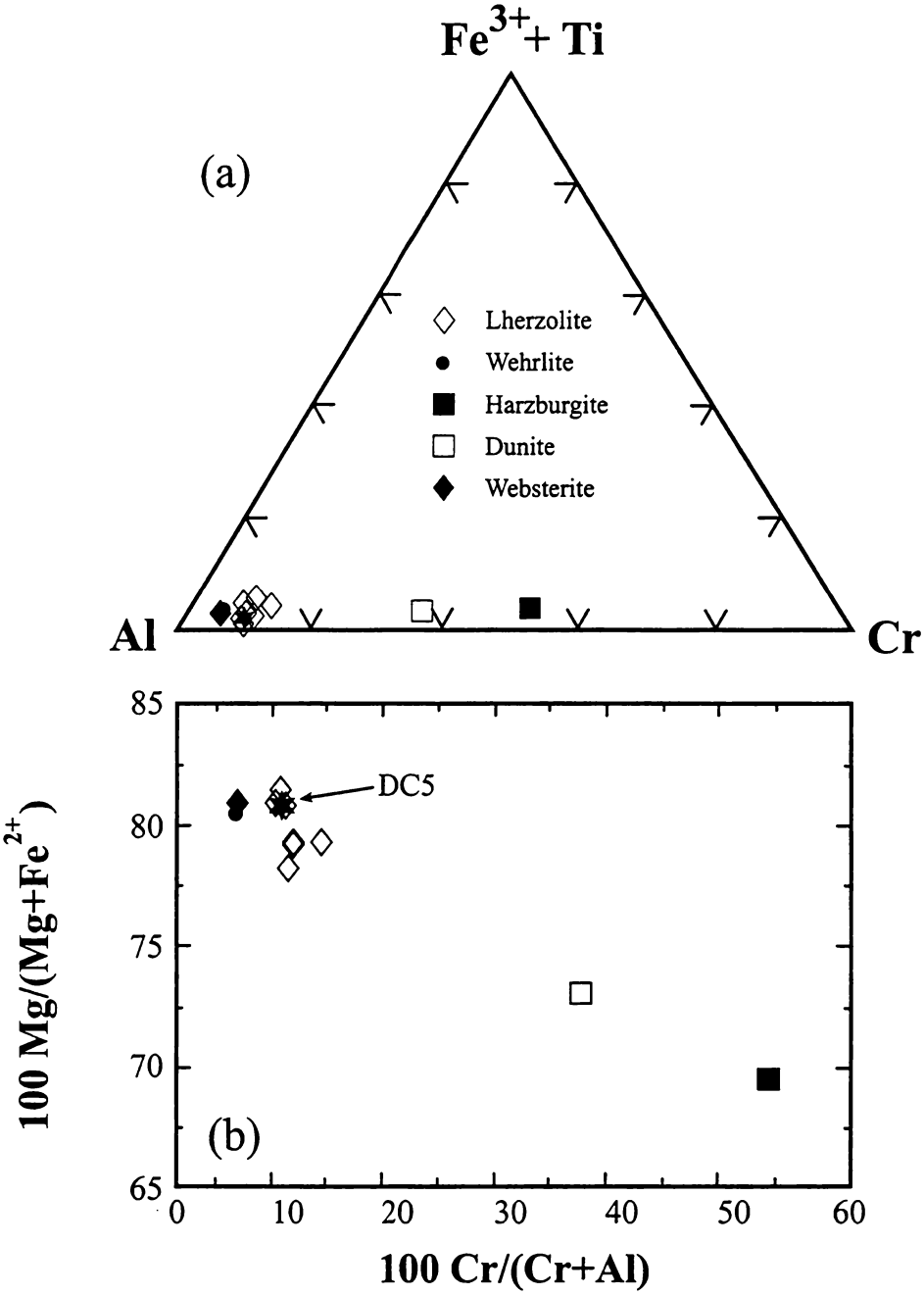


Figure 9. Compositions of spinel in Thai ultramafic xenoliths. (a) Most samples are Al-rich, except two depleted samples being significantly Cr-rich. (b) Strong correlation between cr# (100Cr/Cr+Al) and mg# (100Mg/Mg+Fe^{2+}) is the consequence of variable degrees of partial melting.

samples contain 'excess' modal Cpx, caused by metamorphic differentiation as observed in alpine peridotites (Dick and Sinton, 1979). However, Sun (1982) and Hart and Zindler (1986) argued that this metamorphic enrichment was not common on a large scale.

Plot of whole-rock weight ratios of Ca/Al against wt% MgO has been used to discriminate between metamorphic and metasomatic enrichment processes (Fig. 10). In general, the ratios of these two lithophile refractory elements in a 'primitive' mantle are within or slightly higher than the average chondritic ratio (~1.1). Adding a high-Ca, low-Al phase (i.e., clinopyroxene) into this mantle will increase the Ca/Al ratios, but with decreasing MgO contents. As observed in this study, most Thai mantle xenoliths contain Ca/Al ratios comparable to those of chondritic values. Therefore, metamorphic enrichment is probably *not* a dominant process affecting the Thai mantle xenoliths. This is supported by similar observation in mantle xenoliths from SE China (Qi et al., 1995). The high Ca/Al ratio in wehrlite (BP15), however, could be explained by the high modal Cpx of this Type-II cumulate xenolith. In contrast, the high Ca/Al ratio of harzburgite (DC3a) suggests partial-melt extraction that depletes Al more favorably than Ca (e.g., Hofmann, 1988).

Secondly, the olivine websterite (TM13) contains high modal abundance of orthopyroxene (~54%), resulting in its high SiO_2 in whole rock (Fig. 4). Kelemen (1990) and Kelemen et al. (1990, 1992) suggested that ascending melts or fluids could dissolve Cpx from the mantle wall rock, while depositing Opx and Ol. The presence of large Opx porphyroclasts, with some interstitial Opx, Ol, and Sp in this sample, may be an evidence for such metasomatic enrichment.

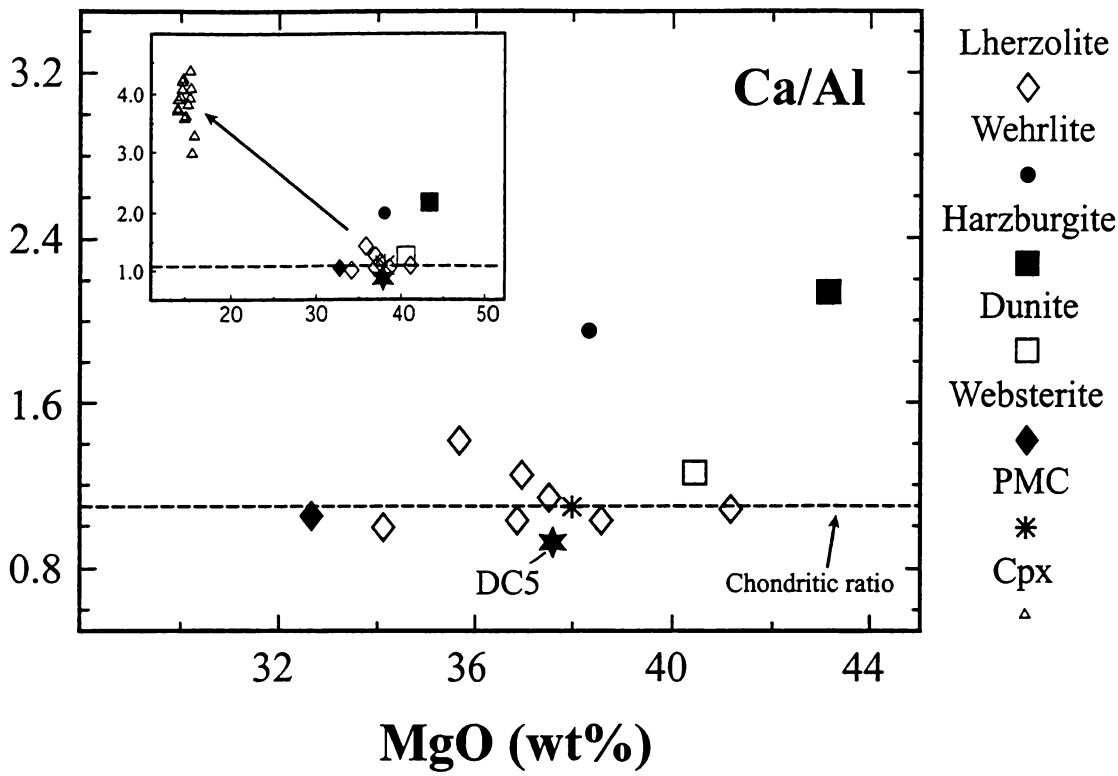


Figure 10. Weight ratio of Ca/Al versus MgO for ultramafic xenoliths from Thailand. Dash line is the average chondritic (C1) ratio from Palme and Nickel (1985); asterisk represents the Primary Mantle Composition (PMC) of Sun (1982). Inset is the same Ca/Al versus MgO plot that includes the average core-compositions of selected clinopyroxenes (open triangles). Thai mantle xenoliths plot close to the chondritic ratio, suggesting that local modal heterogenity (i.e., xenoliths with extra abundances of Cpx) is not significant, since mechanically adding Cpx to the peridotite xenoliths will increase the Ca/Al ratio in the peridotites (along the arrow in the inset).

Variations in mineral compositions

Coexisting minerals in the Thai mantle xenoliths exhibit evidence of equilibrium conditions such as the contact of all four phases, and the well-defined trends of mg# among coexisting phases (Fig. 11). However, some chemical variations in mineral phases, particularly clinopyroxene, deserve further detailed discussion.

Most clinopyroxenes show spongy-textured rinds (or spongy rims). A representative compositional profile across a clinopyroxene with spongy texture (Fig. 12a) shows substantial chemical variations within these rims. Most noticeably, the Al_2O_3 and Na_2O decrease with increasing CaO and MgO, and in some samples, with glass compositionally similar to alkali feldspar (Table 7). The presence of high-K_2O feldspathic glass (BP31a) suggests that the spongy rims cannot be produced by isochemical partial melting accompanying decompression (e.g., Donaldson, 1978). Snyder et al. (1997) suggested that spongy rims on clinopyroxenes are the result of metasomatic interaction between the xenoliths and the K-rich basaltic magma. This reaction produces secondary Cpxs with lower jadeite content, alkali feldspar, and possibly some oxide minerals.

Metasomatic effects resulting in the spongy rinds are also illustrated in the crystal chemistry of the clinopyroxene (Fig. 13). Negro et al. (1984) described clinopyroxene crystal structures formed in response to melting that are primarily achieved by progressive depletion in Al^{vi}, Ti^{4+}, Fe^{2+} in M1 and concomitant enrichment in Mg^{2+}, Cr^{3+}, Fe^{3+} in the M2 site. This results in the increase in mg# of spongy clinopyroxene. In addition, the stability of the Cpx during melting at high pressure is ultimately dependent on the charge balance ensured by Na^+ in the M2 site. This explains the depletion of Al^{vi}

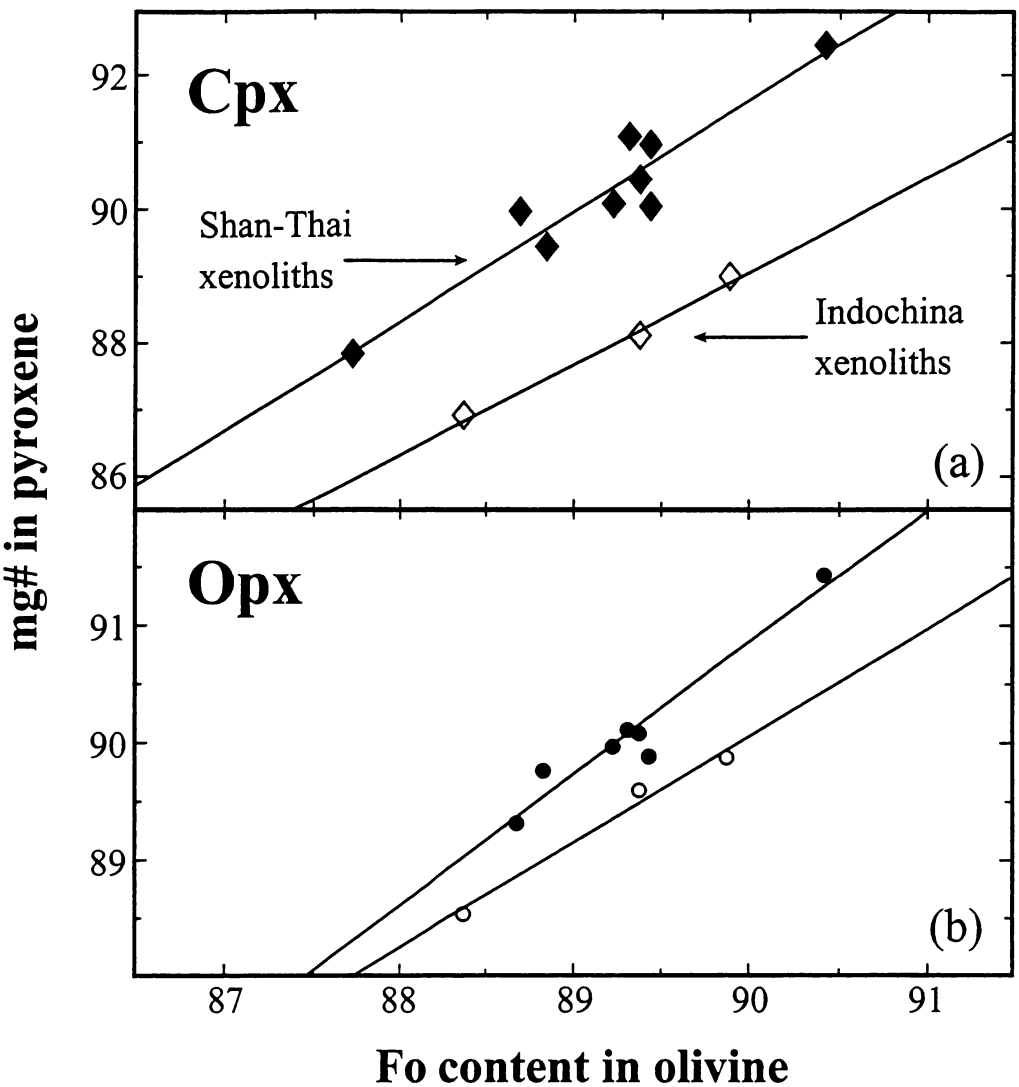


Figure 11. Fo content in olivine versus mg# in clinopyroxene (a) and in orthopyroxene (b) of Thai ultramafic xenoliths. Filled symbols represent pyroxenes of ultramafic xenoliths from the Shan-Thai microcontinent; open symbols are from the Indochina microcontinent. The strong correlation of the two parameters suggests that the xenoliths have attained equilibration before being entrained in the host basalts. The lower mg#s of pyroxenes in xenoliths from the Indochina microcontinents, compared to those from Shan-Thai, possibly reflect the influx of oxidized fluids beneath the Indochina mantle.

Figure 12. Representative compositional variations across clinopyroxenes. (a) clinopyroxene (Cpx) in sample MT1 with spongy-textured rinds (Spgy). These rinds are produced by interaction between the Cpx grain and K-rich basaltic melt. The photomicrograph below (a), taken under plane-polarized light (PPL), shows the analyzed rim-to-core traverse X-Y. (b) Cpx with no spongy texture in sample BP35. The Al_2O_3 gradient, developed during subsolidus cooling, is the result of slower diffusivity of Al compared to other cations. Below (b) is the photomicrograph (PPL) showing the analyzed traverse X-Y. Abbreviations: Ol = olivine; Sp = spinel; Opx = orthopyroxene.

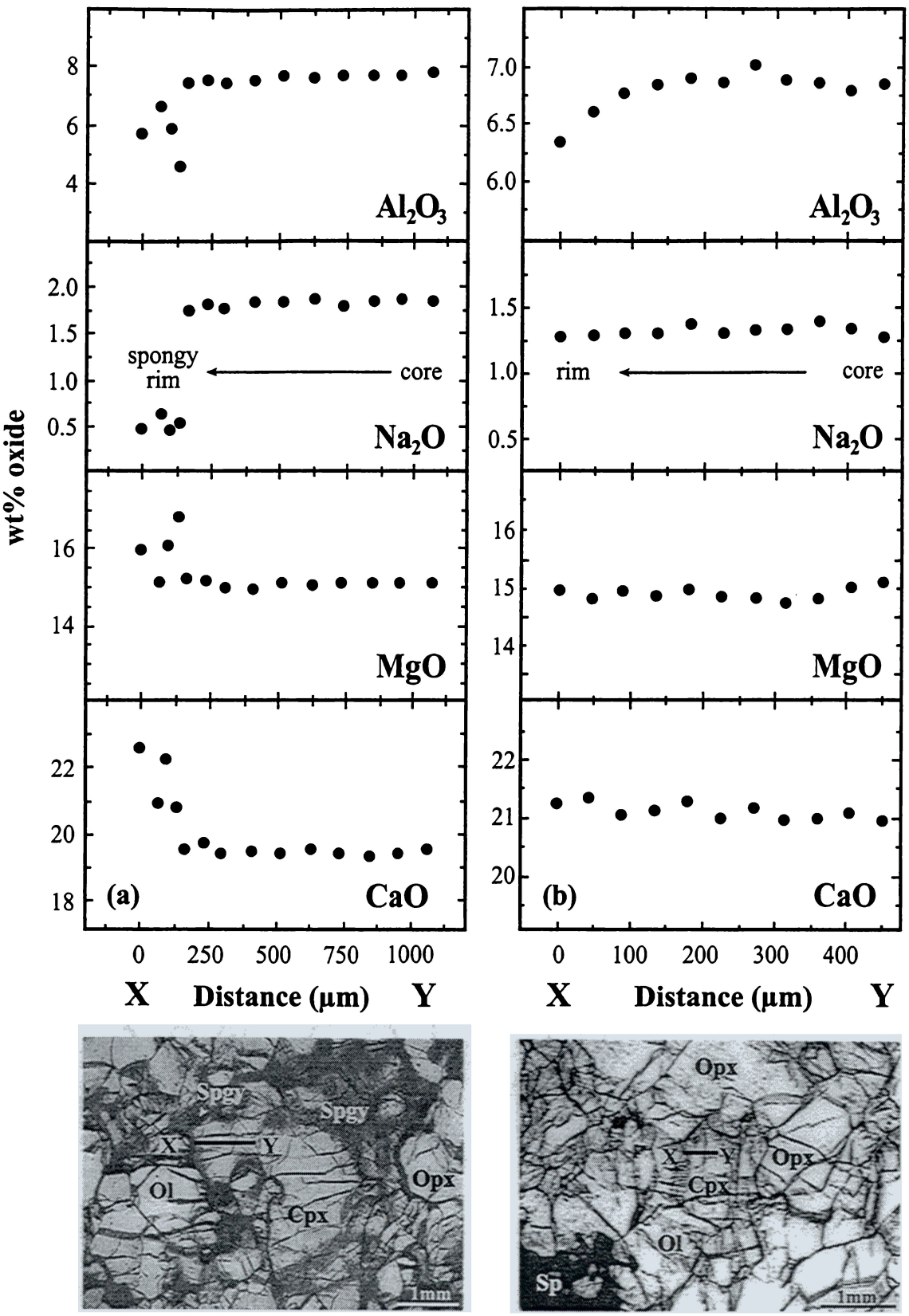

wt% oxide
Al2O3
Na2O
MgO
CaO
spongy rim
core
rim
core
(a)
(b)
X
Distance (μm)
Y
0 250 500 750 1000
0 100 200 300 400
Spgy
Spgy
X
Y
Ol
Opx
Cpx
1mm
Opx
X
Y
Opx
Cpx
Ol
Sp
1mm

Table 7. Selected analyses of spongy rim on clinopyroxene.

Sample:	DC3a	MT7	BP15	BP6	BP31a†
SiO_2	54.7	52.8	48.6	53.2	58.3
TiO_2	0.39	0.71	0.85	0.27	0.40
Al_2O_3	1.86	4.60	15.2	6.23	22.2
Cr_2O_3	1.09	0.63	0.32	0.44	0.09
MgO	25.1	16.1	9.97	19.4	1.34
CaO	11.9	20.0	15.3	8.04	2.28
MnO	0.11	0.12	0.07	0.12	<0.03
FeO	4.42	2.75	2.35	4.98	1.47
Na_2O	0.55	1.14	6.30	1.76	5.36
K_2O	0.20	0.48	1.21	2.67	6.20
Total	100.21	99.4	100.21	97.15	97.72

†This sample is highly metasomatized by host basalts, and its mineral analyses are not included in the present paper.

in the two most refractory Thai mantle xenoliths, i.e., harzburgite (DC3a) and dunite (DC14b) in this study. The relatively high Al^{vi} of the Type II xenoliths is possibly due to the increasing $Al^{vi}Al^{iv} \Leftrightarrow Mg_{-1}Si_{-1}$ (tschermaks) substitution and the increasing Ca^{2+} substitution in the M2 site, thus requiring less Na^{+} to balance the charge.

Although spongy Cpxs are common in the Thai mantle xenoliths, many Cpx grains are fresh and show no textural signs of interaction with fluids or melts. Compositionally, these Cpxs are homogeneous in terms of CaO, MgO, and Na_2O, but develop a gradient of decreasing Al_2O_3 at the grain margins (Fig. 12b). These zoning patterns have been interpreted as caused by differences in diffusion rates among cations during subsolidus cooling (Press et al., 1986; Witt-Eickschen and Seck, 1990), i.e., Al is ~4 times slower than Ca (Brady and McCallister, 1983; Opper and Seck, 1989). Therefore, it can be envisaged that Al has experienced only partial equilibration, resulting in the gradient observed.

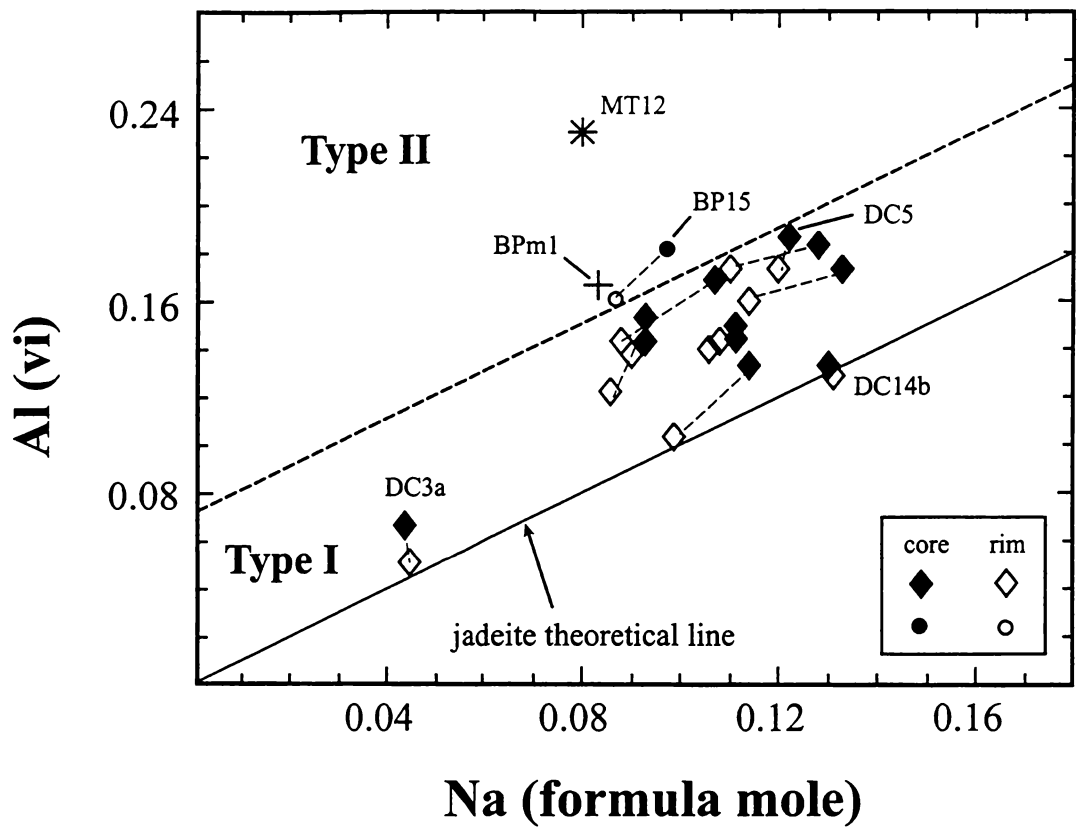


Figure 13. Al (vi) versus Na plot of average clinopyroxene compositions. The solid line with slope 1 represents the theoretical jadeite-substitution. The dashed line is the boundary between Type I and Type II xenoliths for this data set. For the purpose of clarity, only speific samples are labeled.

Thermobarometry

Attainment of equilibrium conditions of Thai ultramafic xenoliths is indicated by homogeneous mineral compositions and strong positive correlations among mg#s of coexisting mineral phases (Fig. 11). Equilibration temperatures were estimated from six thermometers that were calibrated from single minerals, mineral pairs, or mineral assemblages (Wood and Banno, 1973; Herzburg and Chapman, 1976; Bertrand and Mercier, 1986; Brey and Kohler, 1990; Ballhaus et al., 1991; Witt-Eickschen and Seck, 1991), and are reported in Table 8. At the present time, there is no reliable geobarometer for spinel lherzolite. Therefore, the temperatures were calculated at 15 kb, presumably the middle-point for the spinel-lherzolite stability (10-20 kb) under mantle conditions (Green and Ringwood, 1970). The thermometers used are relatively robust; a change in pressure of $\pm$ 5 kb shift the estimated temperatures for the maximum of only $\pm$ 25° C when using Brey and Kohler (1990) thermometer.

The average temperature of Thai ultramafic xenoliths estimated from six geothermometers is in a range of ~1000 to 1130° C (Table 8). Temperature differences obtained from various thermometers are large, giving an average temperature difference of ~260° C. The Herzberg and Chapman (1976) thermometer gives highest temperature estimates in all samples, whereas that of Witt-Eickschen and Seck (1991) produces lowest temperature estimates (Fig. 14a). In addition, the temperatures calculated from two-pyroxene thermometers are generally higher than those obtained from other thermometers. In most samples, the core temperatures are approximately 50° C higher than those of the rims. The Sp-Ol thermometer of Ballhaus et al. (1991) gives the most nonsystematic core to rim temperatures, compared to other thermometers. This

Table 8. Temperature (°C) estimates of mantle xenoliths beneath Thailand.

Geothermometer	Mineral assemblage	Sample											
		BP35	**BP6**	**BP15**	**DC5**	**DC3a**	**DC14b**	**MT1**	**MT7**	**WB3a**	**WB5**	**WB6**	**TM13**
Wood and Banno (1973)	Opx-Cpx	1045[c]	1154	-	1070	1160	-	1094	1050	1070	1088	1079	1057
		1019[r]	1104	-	1081	1138	-	1085	1025	1056	1082	1087	1053
Herzberg and Chapman (1976)	Opx-Cpx	1150	1302	-	1178	1275	-	1216	1149	1191	1177	1159	1173
		1113	1227	-	1190	1245	-	1203	1115	1163	1173	1173	1166
Bertrand and Mercier (1986)	Opx-Cpx	1076	1336	-	1145	1260	-	1208	1095	1095	1218	1247	1090
		977	1197	-	1171	1045	-	1187	1055	1017	1205	1278	1072
Brey and Kohler (1990)	Ca in Opx	924	1133	-	1031	1050	-	1052	957	1002	1033	997	945
		903	1011	-	1020	1025	-	1041	907	947	1027	992	939
Ballhaus et al. (1991)	Sp-Ol	1050	1037	1099	944	996	1085	947	997	947	1031	948	1088
		940	1069	1001	980	1043	1008	960	1034	929	1036	1025	963
Witt-Eickschen and Seck (1991)	Al-Cr in Opx	947	1016	-	978	952	-	982	920	955	899	899	891
		890	995	-	897	950	-	939	870	907	890	907	882
average T		1003	1132	1050	1057	1095	1047	1076	1015	1023	1073	1066	1027
$\Delta \log f(O_2)$	Sp-Ol	-1.00	-1.05	-0.43	-1.37	-0.56	-0.93	-1.43	-3.15	0.34	0.39	0.13	-0.59

Note: Temperature estimates at the top row of each geothermometer (c) were calculated from the mineral cores; those of the bottom row (r) were from the mineral rims. $\Delta \log f(O_2)$ was calculated using temperatures estimated from Ballhaus et al. (1991) thermometer.

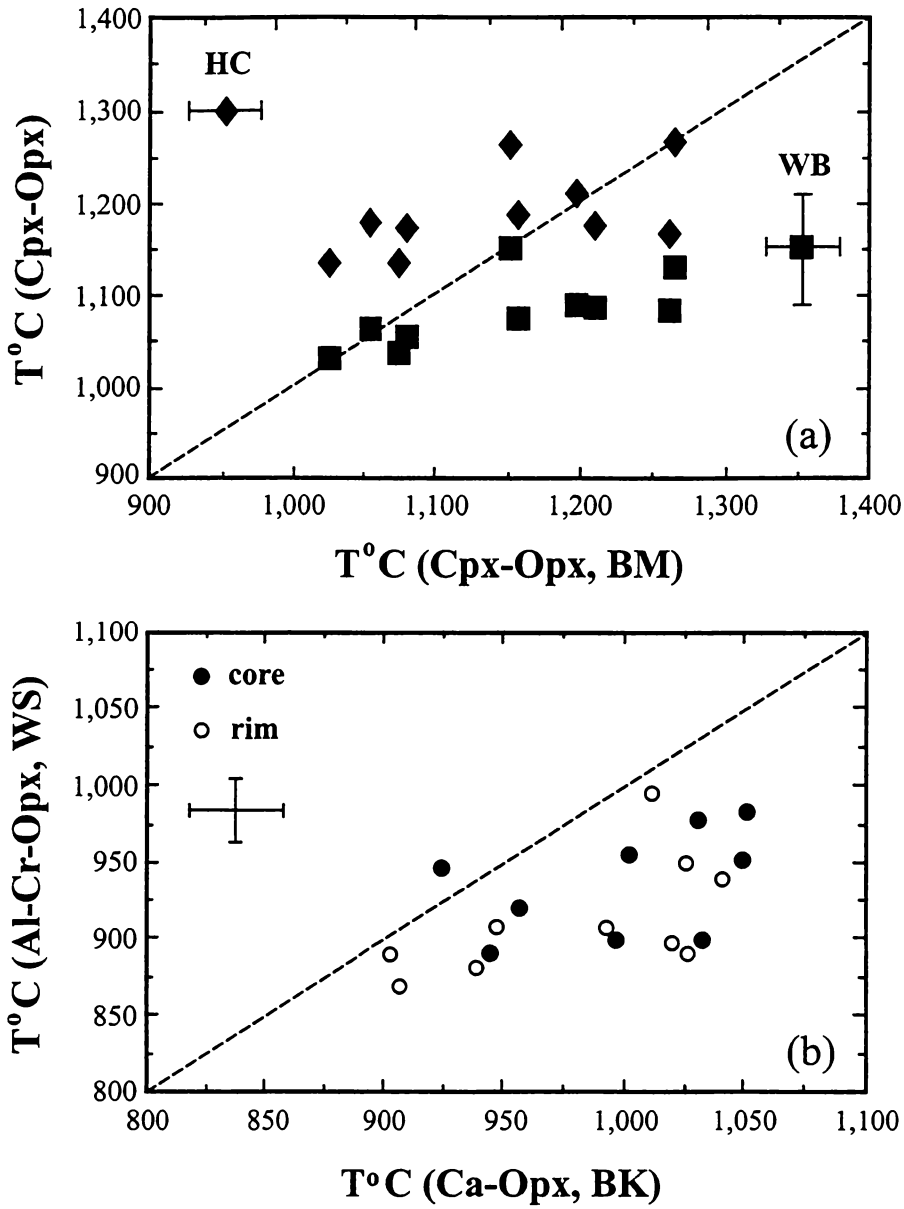


Figure 14. Comparison of estimated temperatures from different thermometers: WB = Wood and Banno (1973); HC = Herzburg and Chapman (1976); BM = Bertrand and Mercier (1986); WS = Witt-Eickschen and Seck (1991); BK = Brey and Kohler (1990). Accuracy of the thermometers, if stated, are indicated by error bars. (a) Relative to BM geothermometer, temperatures obtained from HC are generally higher, whereas those from WB are lower. (b) Ca-Opx thermometer of BK gives higher temperatures than that of WS, probably as a result of heating event.

discrepancy could be the result of differences in closure temperatures of the mineral pairs used, and in experimental calibrations applied for various thermometers. In addition, errors incurred from estimation of Fe^{3+} from electron microprobe data may contribute to this discrepancy (Sobolev et al., 1999).

A useful thermal history of the xenoliths can be deduced by comparing different thermometers. In the event of subsolidus cooling, a temperature calculated using Ca in Opx (Brey and Kohler, 1990) will be lower than that calculated from Cr-Al in Opx (Witt-Eickschen and Seck, 1991). This is due to the higher diffusivity of Ca in Opx, which is more sensitive to temperature changes compared to Cr and Al (Opper and Seck, 1989), thereby attaining complete equilibration at a lower temperature. The temperatures calculated using these two thermometers for the Thai ultramafic xenoliths, however, indicate higher temperatures obtained from the Ca-Opx thermometer than those from the Cr-Al in Opx thermometer (Fig. 14b). Therefore, it is possible that the Thai mantle was reheated, causing the Ca in Opx to record the higher, heating temperature (Promprated et al., 1998). This heating event may have been related to lithospheric thinning and asthenospheric upwelling, a commonly presumed mantle process in this region (Flower et al, 1998; Smith, 1998).

Pressure is difficult to determine for spinel-peridotite xenoliths; an indirect method for pressure estimation is required. The absence of garnet and plagioclase in spinel peridotite limits the equilibrium pressure between 10 and 20 kbar. This pressure range can be translated to depths of 30-60 km.

Redox state of the Thai mantle: A clue for mantle metasomatism under the Indochina microcontinent

Oxygen fugacities, $f(O_2)$, were calculated relative to the fayalite-magnetite-quartz (FMQ) buffer (Table 8), using a semi-empirical oxygen barometer (Ballhaus et al., 1991). The Fe^{3+} contents of spinel used in the calculation were determined from electron microprobe analyses (EMPA) based on perfect stoichiometry. Although a recent work by Sobolev et al. (1999) suggested little correlation between EMPA-calculated and Mossbaur-measured $Fe^{3+}/\Sigma Fe$, the $f(O_2)$ and the $Fe^{3+}/\Sigma Fe$ of spinels obtained from Thai peridotite xenoliths are well correlated. This strong, systematic correlation, combined with small uncertainties of most analyses, affirms the ability to determine meaningful petrologic interpretations based upon the calculated oxygen fugacity. The mantle xenoliths in this study exhibit a range of $f(O_2)$ between FMQ -3 to FMQ +1 (Fig. 15), which is commonly observed in spinel-peridotite xenoliths of shallow Phanerozoic subcontinental lithosphere worldwide (Ballhaus, 1993). It can also be seen that the oxidation states of the Thai xenoliths show a slight positive correlation with cr#, and that spinel-peridotites from the Indochina microcontinent (samples WB3a, WB5, and WB6) are more oxidized (above the FMQ buffer) than those from the Shan-Thai microcontinent. These two important features warrant further discussion.

First, as suggested by Ballhaus (1993), the relative $f(O_2)$ of spinel-peridotites from shallow Proterozoic and Phanerozoic lithosphere is predominantly controlled by Fe^{3+}-Fe^{2+} equilibria in mantle mineralogy. The buffering capacity of mantle material then depends on the ΣFe content and the oxidation state of iron present. Thus, spinel-

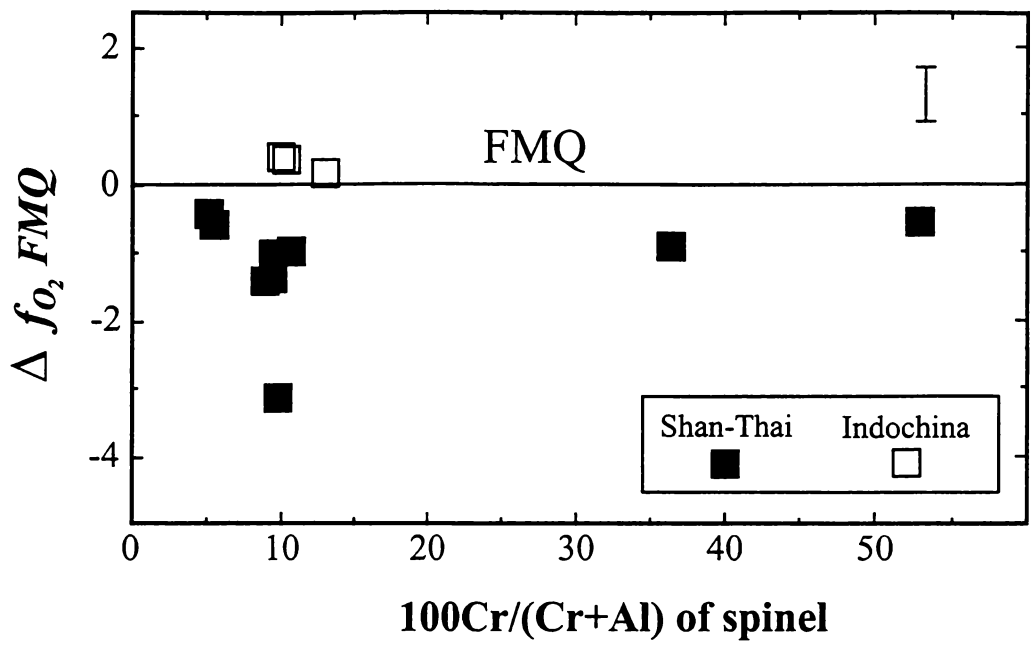


Figure 15. Plot of cr# versus f (O_2) of ultramafic xenoliths from Thailand. Xenoliths of Indochina microcontinent are from the Wichianburi (WB) area; the rest are from Shan-Thai. The Indochina mantle is clearly more oxidized (above FMQ) than Shan-Thai mantle, possibly due to the infiltration of oxidized hydrous fluids beneath the Indochina lithosphere. Error bar represents ± 0.4 log unit of f (O_2).

peridotites with the most refractory lithology (lowest in ΣFe) will have the lowest buffering capacity during oxidation. In other words, the $f(O_2)$ of spinel-peridotite xenoliths in continental basalts will increase, with increasing degree of depletion in basaltic component. This confirms the compositional variation among the Thai mantle xenoliths as an artifact produced by varying degrees of partial melting.

Secondly, the increase in oxidation state of mantle could have been caused by metasomatic reaction from an influx of oxidized fluids or melts (Ballhaus, 1993). These fluids/melts would increase the Fe^{3+} content of the infiltrated mantle, thus raising its oxidation state and contemporaneously lowering its Mg/(Mg+Fe) ratio. The separated and lowered trends of mg# in pyroxenes plotted against Fo in olivine (Fig. 11) for Indochina xenoliths, when compared to those of Shan-Thai, further support this interpretation. Although the compositions and source(s) of these melts/fluids cannot be constrained at the present time, the vicinity of the Nan-River suture to the occurrences of Wichianburi xenoliths may imply the contribution of the fluids from the subducting slab. In fact, Intasopa et al. (1995) observed the incompatible-element enriched signature of the Wichianburi basalts and called for a refertilized depleted mantle (i.e., enriched with subduction components) as a source for the Wichianburi basaltic magmas. This metasomatic event may have contributed to the more extensive basalt volcanism that occurred in close association with the more silicic volcanic rocks in this locality. In addition, the $f(O_2)$ of a partially melted asthenospheric upper mantle increases with falling pressure, thereby suggesting the decompressional melting model as the cause of Cenozoic basaltic volcanism in this region.

Spinel-lherzolite-facies lithosphere beneath Thailand

The occurrences of spinel lherzolite xenoliths, with a lack of garnet lherzolites, in Cenozoic basalts from Thailand suggest that the present-day lithosphere is relatively thin. This is consistent with the interpretation given by Menzies et al. (1993) who studied mantle xenoliths from eastern China. Smith (1998) suggested that the geotherms obtained from mantle xenoliths in Tariat region and eastern China are compatible with the ascent of normal asthenosphere to depths of 75 to 100 km. This corresponds to the presence of low velocity anomalies in seismic-tomographic images of east and Southeast Asia (Zhang and Tanimoto, 1991). These lines of evidence suggest that the thinning of lithosphere beneath Thailand may have been caused by thermal erosion, as a result of heating from the uprising hot asthenosphere. Such mantle process is generally agreed to have caused extensive Cenozoic basalt volcanism in this SE-Asia region.

Conclusions

1. The majority of ultramafic xenoliths in alkali basalts from Thailand are spinel lherzolites of the Type I group. Other Type I xenoliths include harzburgite, dunite, and Ol-websterite. Type II xenoliths in this study include wehrlite, clinopyroxenite, and a clinopyroxene megacryst.

2. Compositional variations of the mantle Type-I xenoliths cover a range of fertile (enriched) to depleted compositions when compared to those of the primitive mantle. Evidence of partial melting is the high cr# of spinels in dunite and harzburgite. In contrast, high modal Opx websterite could have resulted from metasomatic enrichment

of mantle rocks with basaltic melts, perhaps similar to that produced basaltic cumulate xenolith (Type II) observed in this study.

3. Intragrain zonations are observed in clinopyroxene, and to a lesser extent in orthopyroxene. These zonations are caused by two distinct processes: (1) interaction with basaltic melts, and (2) subsolidus cooling. The metasomatic reaction with the host basalts resulted in a decrease of Al_2O_3 and Na_2O with increasing CaO and MgO, and occasionally the production of K-Na rich, feldspathic glass within the spongy rims on clinopyroxenes. Gradients produced by subsolidus reequilibration are recognized by a decrease of Al_2O_3 at the margins of clino- and orthopyroxene, due to the slower diffusivity of Al compared to that of other cations.

4. The positive correlation of mg# in pyroxenes and Fo content in olivines suggest attainment of equilibrium. The equilibration temperatures of these xenoliths are ~1000 to 1130° C, with the core temperatures being ~50° C higher than those of the rims. Calculated temperatures based on diffusion of Ca in Opx are consistently higher than those obtained from Cr-Al in Opx geothermometer. This may indicate a recent heating event that caused re-equilibration of Ca in Opx, but not Cr and Al, with this increase in ambient temperature. Pressures of equilibration are assumed to be within 10-20 kb, based upon the absence of plagioclase and garnet, that can be translated to depths of 30-60 km.

5. Contrasting oxidation states and the mg#s between coexisting pyroxene and olivine from the Shan-Thai microcontinent, compared to those obtained from the Indochina, may indicate the effect of oxidized fluids or melts on the Indochina mantle.

6. The absence of garnet-lherzolite xenoliths in the alkali basalts from Thailand may indicate that garnet-lherzolite mantle was largely removed by thermal erosion, due to the uprising of hot asthenosphere.

References

Ballhaus, C., 1993, Redox states of lithospheric and asthenospheric upper mantle: Contrib. Mineral. Petrol., v. 114, p. 331-348.

Ballhaus, C., Berry, R.F., and Green, D.H., 1991, High-pressure experimental calibration of the olivine-orthopyroxene-spinel oxygen geobarometer: Implications for the oxidation state of the upper mantle: Contrib. Mineral. Petrol., v. 107, p. 27-40.

Barr, S.M., and Dostal, J., 1986, Petrochemistry and origin of megacrysts in Upper Cenozoic basalts, Thailand: J. of SE. Asian Earth Science, v. 1, p. 107-116.

Barr, S.M., and MacDonald, A.S., 1978, Geochemistry and petrogenesis of Late Cenozoic alkaline basalts of Thailand: Geol. Soc. Malaysia Bull. v. 10, p. 25-52.

Barr, S.M., and MacDonald, A.S., 1979, Palaeomagnetism, age, and geochemistry of the Denchai basalt, northern Thailand: Earth Planet. Sci. Lett., v. 46, p. 113-124.

Barr, S.M., and MacDonald, A.S., 1981, Geochemistry and geochronology of Late Cenozoic basalts of Southeast Asia: Geol. Soc. Am. Bull., v. 92, p. 1069-1142.

Barr, S.M., and MacDonald, A.S., 1991, Toward a late Paleozoic - early Mesozoic tectonic model for Thailand: J. of Thai Geosci., v. 1, p. 11-22.

Barr, S.M., and James, D.E. (1990), Trace-element characteristics of Upper Cenozoic basaltic rocks of Thailand, Kampuchea, and Vietnam, J. of Southeast Asian Earth Sciences, v. 4, no. 3, p. 233-242.

Bertrand, P., and Mercier, J.C.C., 1985, The mutual solubility of coexisting ortho- and clinopyroxene: Toward an absolute geothermometer for the natural system: Earth Planet. Sci. Lett., v. 76, p. 109-122.

Brady, J.B., and McCallister, R.B., 1983, Diffusion data for clinopyroxenes from homogenization and self-diffusion experiments: American Mineralogist, v. 68, no. 1-2, p. 95-105.

Brey, G.P., and Kohler, T., 1990, Geothermobarometry in four-phases lherzolites II: New thermobarometers, and practical assessment of existing thermobarometers: J. of Petrology, v. 31, no. 6, p. 1353-1378.

Bunopas, S., 1981, Paleogeographic history of western Thailand and adjacent parts of southeast Asia: A plate tectonic interpretation: Ph.D. Thesis, Victoria University of Wellington, New Zealand, 810 p, reprinted 1982 as Geological Survey paper no.5, Department of Mineral Resources, Thailand.

Bunopas, S., and Vella, P., 1992, Geotectonic and geologic evolution of Thailand: Proceedings of a National Conference on Geologic Resources of Thailand: Potential for Future Development, Department of Mineral Resources, Thailand, p. 209-228.

Department of Mineral Resources, Thailand, 1987, Geological Map of Thailand, scale 1 : 2,5000,000.

Dick, H.J.B., and Sinton, J.M., 1979, Compositional layering in alpine peridotites: Evidence for pressure solution creep in the mantle, J. Geol., v. 87, p. 403-416.

Donaldson, C.H., 1978, Petrology of the upper most mantle deduced from spinel lherzolite and harzburgite nodules at Calton Hill, Derbyshire: Contrib. Mineral. Petrol., v. 65, p. 363-377.

Flower, M.F.J., Tamaki K., and Hoang, N., 1998, Mantle extrusion: A model for dispersed volcanism and DUPAL-like asthenosphere in East Asia and the Western Pacific, *in* Flower M.F.J., Chung S.-L., Lo C.-H., Lee T.-Y., eds., Mantle Dynamics and Plate Interactions in East Asia, Amer. Geophys. Union, Geodynamics Series, v. 27, p. 67-87.

Frey, F.A., and Green, H.D., 1974, The mineralogy, geochemistry, and origin of lherzolite inclusions in Victorian basanites: Geochim. et Cosmochim. Acta, v. 38, p. 1023-1059.

Frey, F.A., and Prinz, M., 1978, Ultramafic inclusions from San Carlos, Arizona: Petrologic and geochemical data bearing on their petrogenesis: Earth and Planet. Sci. Lett., v. 38, p. 129-176.

Frey, F.A., Suen, C.F., and Stockman, H.W., 1985, The Ronda high temperature peridotite: Geochemistry and petrogenesis: Geochim. et Cosmochim. Acta, v. 49, p. 2469-2491.

Green, D.H., and Ringwood, A.E., 1970, Mineralogy of peridotite compositions under upper mantle conditions: Phys. Earth Planet. Int., v. 3, p. 359-371.

Hart, S.R., and Zindler, A., 1986, In search of a bulk-earth composition, Chemical Geology, v. 57, p. 247-267.

Herzberg, C.T., and Chapman, N.A., 1976, Clinopyroxene geothermometry of spinel-lherzolites: Amer. Mineral., v. 61, p. 626-637.

Hofmann, A.W., 1988, Chemical differentiation of the Earth: The relationship between mantle, continental crust, and oceanic crust, *in* Isotope geochemistry; the Crafoord symposium, Earth Planet. Sci. Lett., v. 90, no. 3, p. 297-314.

Hutchison, C.S., 1989, Geological evolution of Southeast Asia: Clarendon Press, Oxford, U.K., 368 pp.

Intasopa, S., Dunn, T., and Lambert, R. StJ., 1995, Geochemistry of Cenozoic basaltic and silicic magmas in the central portion of the Loei-Phetchabun volcanic belt, Lop Buri, Thailand: Can. J. Earth Sci., v. 32, p. 393-409.

Jezek, D.A., Sinton, J.M., Jarosewich, E., and Obermeyer, C.R., 1978, Fusion of rock mineral powder for electron microprobe analysis: Smithsonian Contributions to Earth Sciences, v. 22, p. 46-52.

Kelemen, P.B., 1990, Reaction between ultramafic rock and fractioning basaltic magma I: Phase relations, the origin of calc-alkaline magma series, and the formation of discordant dunite: Jour. of Petro., v. 31, no. 1, 51-98.

Kelemen, P.B., Joyce, D.B., Webster, J.D., and Holloaway, J.R., 1990, Reaction between ultramafic rock and fractioning basaltic magma II: Experimental Investigation of reaction between olivine tholeiite and harzburgite at 1050-1150 °C and 5 kb: J. of Petro., v. 31, no. 1, p. 99-134.

Kelemen, P.B., Dick, J.B.H., and Quick, J.E., 1992, Formation of harzburgite by pervasive melt/rock reaction in the upper mantle: Nature, v. 358, p. 635-641.

McDonough, W.F., 1990, Constraints on the composition of the continental lithospheric mantle: Earth Planet Sci. Lett, v. 101, p. 1-18.

Menzies, M.A., Fan, W., and Zhang, M., 1993, Paleozoic and Cenozoic lithoprobes and the loss of >120 km of Archean lithosphere, Sino-Korean craton, China, *in* Prichard, H.M., Alabaster, T., Harris, N.B.W., and Neary, C.R. eds., Magmatic processes and plate tectonics: London, London Geol. Soc. Spec. Publ. No. 76, p. 71-81.

Mitchell, A.H.G., 1981, Phanerozoic plate boundaries in mainland southeast Asia, the Himalayas, and Tibet, J. Geophys. Soc. London, v. 135, p. 109-122.

Mukasa, S.M., Fischer, G.M., and Barr, M.S., 1996, The character of the subcontinental mantle in southeast Asia: Evidence from isotopic and elemental compositions of extension-related Cenozoic: Geophysical Monograph 95, p. 233-252.

Negro, D.A., Carbonin, S., Domeneghetti, C., Molin, G.M., Cundari, A., and Piccirillo, E.M., 1984, Crystal chemistry and evolution of the clinoyroxene in a suite of

high pressure ultramafic nodules from the Newer Volcanics of Victoria, Australia: Contrib. Min. Petrol, v. 86, no. 3, p. 221-229.

Nickel, K.G., and Green, D.H., 1984, The nature of the upper-most mantle beneath Victoria, Australia as deduced from ultramafic xenoliths: Kimberlites II: The Mantle and Crust-Mantle Relationships, Kornprobst, J. ed., p. 161-178.

Opper, D., and Seck, H.A., 1989, Diffusionsverhalten von elementen in pyroxen aus aufgeheizten mantelperidotiten, abgeleitet aus dem Konzentrationsgradienten: Eur J. Mineral., Bh. 1:141.

Palm, H., and Nickel, K.G., 1985, Ca/Al ratio and composition of the Earth's upper mantle: Geochim. et Cosmochim. Acta, v. 49, p. 2123-2132.

Press S., Witt, G., Seck, H.A., Eonov, D., and Kovalenko, V.I., 1986, Spinel peridotite xenoliths from the Tariat Depression, Mongolia I: Major element chemistry and mineralogy of a primitive mantle xenolith suite: Geochimica et Cosmochimica Acta, v. 50, p. 2587-2599.

Promprated, P., Taylor, L.A., and Snyder, G.A., 1998, Compositional and thermal history of the mantle beneath Thailand: Evidence from spinel-lherzolite xenoliths, *abstract,* EOS, Transactions, v. 79, no. 45, p. F946.

Qi, Q., Taylor, L.A., and Zhou, X., 1995, Petrology and geochemistry of mantle peridotite xenoliths from SE China: J. of Petrology, v. 36, no. 1, p. 55-79.

Sasada, M., Ratanasatien, B., and Soponpongpipat, R., 1987, New K/Ar ages from the Lampang Basalt, Northern Thailand: Geol. Surv., Japan Bull., v. 38, no. 1, p. 13-20.

Smith, A.D., 1998, The geodynamic significance of the DUPAL anomaly in Asia, *in* Flower M.F.J., Chung S.-L., Lo C.-H., Lee T.-Y., eds., Mantle Dynamics and Plate Interactions in East Asia, Amer. Geophys. Union, Geodynamics Series, v. 27, p. 89-105.

Snyder, G.A., Taylor, L.A., Jin, Y., and Taylor, D.-H., 1997, Mantle-lherzolites xenoliths from eastern China: Petrogenesis and development of secondary textures: Inter. Geol. Rev., v. 39, p. 671-687.

Sobolev, N.V., McCammon, C.A., Taylor, L.A., Snyder, G.A., and Sobolev, N.V., 1999, Precise Mossbauer milliprobe determination of ferric iron in rock-forming minerals and limitations of electron microprobe analysis: American Mineralogist, v. 84, p. 78-85.

Stauffer, P.H., 1983, Unraveling the mosaic of Paleozoic crustal blocks in southest Asia: Geol. Rundsch., v. 72, p. 1061-1080.

Sun, S.S., 1982, Chemical composition and origin of the earth's primitive mantle: Geochim. et Cosmochim. Acta, v. 46, p. 179-192.

Suthirat, C., Charusiri, P., Farrar, E., and Clark, A.H., 1994. New $^{40}Ar/^{39}Ar$ geochronology and characteristics of some Cenozoic basalts in Thailand: Proceedings of the International Symposium on Stratigraphic Correlation of Southeast Asia. Bangkok, Thailand, p. 306-321.

Tapponnier, P., Peltzer, G., and Armijo, R., 1986, On the mechanics of the collision between India and Asia, in Colision Tectonics, Coward, M.P. and Reis, A.C., eds.: Geol. Soc. London Spec. Pub., v. 19, p. 115-157.

Vichit, P., Vudhichativanich, S, and Hansawek, R., 1979, The distribution and some characteristics of corundum-bearing basalts in Thailand: Department of Mineral Resources, Thailand, Special Report M4, p. 1-38.

Wass, S.Y., 1980, Geochemistry and origin of xenolith-bearing and related alkali basaltic rocks from the Southern Highlands, New South Wales, Australia: Amer. J. Sci., v. 280-A, p. 639-665.

Wood, B.J., and Banno, S., 1973, Garnet-orthopyroxene and orthopyroxene-clinopyroxene relationships in simple and complex systems: Contrib. Min. Petrol, v. 42, p. 109-124.

Wilshire, H.G., and Shervais, J.W., 1975, Al-augite and Cr-diopside ultramafic xenoliths in basaltic rocks from Western United States, *in* Ahrens, L.H., Press F., Runcorn, S.K., Urey, H.C., eds., Phys. Chem. Earth 9, Pergamon Press, New York, p. 257-272.

Witt-Eickschen, G., and Seck, H.A., 1991, Solubility of Ca and Al in orthopyroxene from spinel peridotite: An improved version of an empirical geothermometer: Contrib. Mineral. Petrol., v. 106, p. 431-439.

Zhang, Y-S, and Tanimoto, T., 1991, Global Love wave phase velocity variation in its significance to plate tectonics, Phys. Earth. Planet. Int., v. 66, p. 160-202.

Zhou, P., and Mukasa, S.B., 1997, Nd-Sr-Pb isotopic, and major- and trace-element geochemistry of Cenozoic lavas from the Khorat Plateau, Thailand: Sources and petrogenesis: Chemical Geology, v. 137, p. 175-193.

PART 3

TRACE-ELEMENT CHARACTERISTICS OF THE SPINEL-PERIDOTITE XENOLITHS FROM THAILAND: MELTING AND METASOMATISM OF MANTLE BENEATH A SUTURE ZONE

Abstract

Trace-element characteristics of clinopyroxenes in spinel-peridotite xenoliths from Thailand were used to evaluate the partial melting and metasomatism that occurred in the mantle beneath a suture zone. Clinopyroxene trace-element modelings demonstrate that most xenoliths experienced small degrees (<6%) of partial melting, with up to 16% in one clinopyroxene-poor sample (5% modal Cpx). This partial melting may have been decompressional in nature, as indicated by the pronounced LREE-depleted clinopyroxenes (La/Lu = 0.01), believed to be the product of garnet breakdown.

Clinopyroxenes in a number of xenoliths display LREE-enriched patterns, with pronounced depletions of high-field strength elements (Ti, Zr, Hf). Such patterns may indicate metasomatic enrichment by carbonate-rich fluids. Bulk-mixing calculations indicate that this metasomatism contributed as much as 30% trace-element concentrations in clinopyroxenes, resulting in a "concave downward" LREE-elevated pattern (65 times chondrite for Ce). It is possible that these metasomatic fluids were originated from subduction slab (s), or were a consequence of asthenospheric upwelling in the Cenozoic.

This study also demonstrates that pronounced negative Eu anomalies in whole rocks could be an artifact of weathering during which Eu-depleted components were deposited along grain boundaries.

Introduction

In Mesozoic, accretion of subduction complexes was the dominant tectonic activity of the Eurasian margin, which stretches from north of the Russian Far East (Sikhote-Alin) through Korea, eastern China, and into SE Asia (Faure and Natal'in,

1992). This was followed by the opening of rift basins and intense basaltic volcanism in the Cenozoic (e.g., Deng et al., 1998). Among basalts erupted in this region, the alkalic types are particularly interesting, since they contain significant amounts of mantle-derived xenoliths (e.g., Barr and Dostal, 1986; Ionov et al., 1995; Xu et al., 2000). In Thailand, however, only minor amounts of mantle xenoliths have been found in small, localized alkali-basalt eruptions. Despite their rarity, these xenoliths are of particular importance as they represent the only known mantle materials in this region of SE Asia.

The mantle xenoliths are from two separate lithospheric blocks, known as the Shan-Thai and the Indochina microcontinents (Fig. 1), which were united by Mesozoic subduction. The remnant of this continent-continent collision is recognized as the Nan-River suture zone. Potentially, some of these xenoliths may also represent "mantle-wedge" samples, which could be affected by the Mesozoic subduction. A preliminary study of the Thai xenoliths (Promprated et al., 1999) indicated a substantial range of major-element compositions (e.g., 32.7-43.2 wt% MgO in bulk rocks). Previous geochemical data of the xenoliths, however, have only permitted limited interpretations as to the extent and nature of mantle processes. In the present study, we have expanded the preliminary results with additional major-element and new trace-element analyses. These data are used to evaluate quantitatively the extent of partial melting and metasomatism experienced by these xenoliths, as well as defining the characteristics of the metasomatic fluids. This information, in conjunction with geothermometry, provides us with an increased understanding of the evolution of the mantle beneath SE Asia.

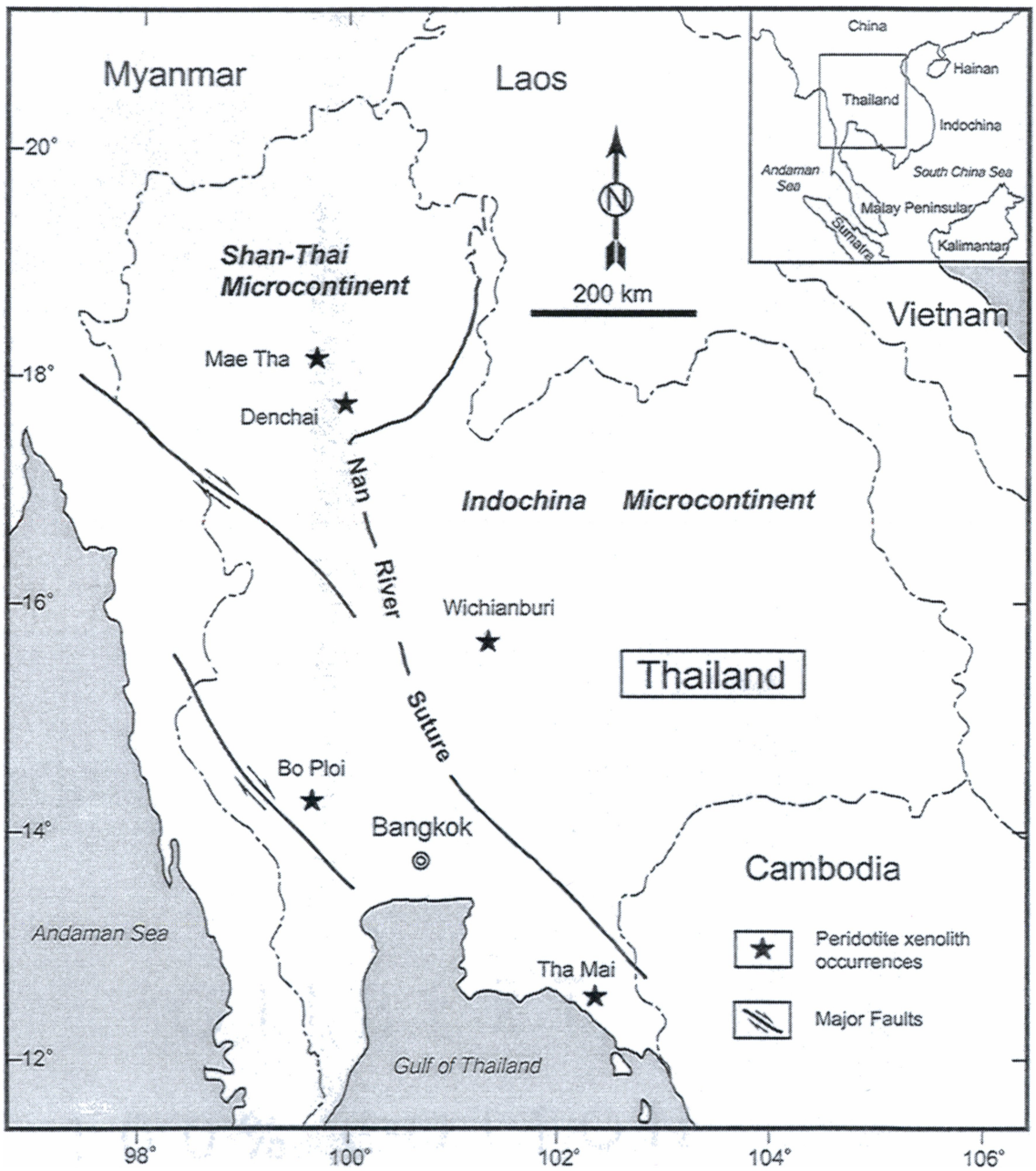


Figure 1. Major occurrences of peridotite xenoliths in Thailand.

Sample Preparation and Analytical Technique

Most mantle-derived xenoliths found in Thailand are spinel-peridotites, with small numbers of harzburgites, and rare wehrlite, websterite, and dunite. They mostly occur in basaltic flows or plug remnants of the Shan-Thai or western microcontinent (WMC). Only one xenolith locality (at Wichianburi) is situated on the Indochina or eastern microcontinent (EMC; Fig. 1). Detailed petrography of most samples have been previously described (Promprated et al., 1999), and that of additional xenoliths is given in the appendix A-1.

Major elements of minerals and whole-rock samples were determined with a fully automated CAMECA SX-50 electron microprobe (EMP) at the University of Tennessee. Whole-rock compositions were obtained from EMP analyses on glass beads, which were prepared by fusing the whole-rock powders on a molybdenum-strip heater in a nitrogen atmosphere. This technique, prescribed by Jezek et al. (1978), has been shown to be a reliable method for obtaining major- and minor-element concentrations for small samples (Schuraytz and Ryder, 1990). The EMP analytical conditions employed an accelerating potential of 15 kV, with 20 nA and 10 μm electron beam for fused glass beads, or with 30 nA and 5 μm beam for minerals. The counting time was 20 s for all elements, and all data were corrected with a ZAF procedure. Loss on ignition (LOI) of whole-rock samples was determined by heating a known amount of sample at 1000° C for 1 hour. A correction was then applied to this weight loss due to the oxidation of FeO.

In-situ trace-element compositions of polished samples were determined by laser ablation-inductively coupled plasma-mass spectrometry (LA-ICP-MS) at the Institute of Geoscience, the University of Tsukuba, Japan. The laser microprobe system

consisted of a Quantel Brilliant-ω, Q-switched Nd:YAG laser, with a frequency quadrupled-output generating a UV (266 nm) wavelength at a pulse repetition rate of 10 Hz and a pulse energy of 0.2 to 3 mJ. The laser sampling was carried out by using a defocusing beam to prevent catastrophic ablation and sample fracturing, producing spot sizes of 50-70 microns, with a dwelling time of 5-30 msec. The ICP-MS system was a Perkin-Elmer Sciex ELAN6000 ICP-MS operated at an RF power of 1050 W, and nebuliser Ar gas flow of 0.73 liter/min with platinum sampling and skimmer cones. The gas flow was adjusted to produce ThO^+/Th^+ less than 0.5% in NIST SRM 612 glass. These conditions yielded maximum sensitivity on the mass range of interest and minimum oxide interference for REE measurements.

Data acquisition was performed by a peak hopping (one point per isotope) in pulse counting mode. Prior to beginning laser ablation, the backgrounds were collected for 60 seconds, and then the data were acquired for an additional 60 seconds. Data reduction was performed using the software LAMTRACE (Jackson et al., 1992; Longerich et al., 1996). Ca (mass 42) was used as internal standard for clinopyroxene analyses, and ^{57}Fe was used for analyses of olivine, orthopyroxene and spinel. This permitted correction for inter-element fractionation and differences in the absolute amount of material that was ablated and transported during an individual analysis. The elemental concentrations of the internal standards were predetermined by electron microprobe. The external standard NIST SRM 612 was used for the analyses of clinopyroxene, and NIST SRM 610 for analyses of olivine, orthopyroxene and spinel. Detection limits were typically in the 0.2-2.0 parts per billion (ppb) range for most heavy elements (atomic mass >80), and 1-10 ppb for lighter elements, except for Si, Ca, and Ti

which were in the range of 1, 6, and 100 parts per million (ppm), respectively. Typical analytical error was less than 5% for most elements and 5-10% for Zn and Pb using the above analytical conditions.

Additional Cpx trace-element analyses were performed at the University of Notre Dame, where the laser microprobe system is a Nd:YAG Spectron SL-282, with the laser quadrupled to 266 nm generating a UV pulse energy of 0.1 to 2.0 mJ. The laser sampling was carried out by slowly increasing the laser energy until a controlled ablation for the material was achieved. This technique produced a spot size of 30-50 microns. The ICP-MS system was a FISONS-VG Elemental PlasmaQuad model PQII, operated at an RF power of 1350 W. The nebuliser Ar gas flow was 1.10 liter/min and was adjusted to produce maximum sensitivity on La and CeO^+/Ce^+. Nickel sampling and skimmer cones were used, and data acquisition and reduction were similar to the procedure employed at the University of Tsukuba.

Trace-element concentrations of the peridotite whole-rocks were determined by ICP-MS, also at the University of Notre Dame. Each xenolith was dissected to obtain a mass of ~5 g, then powdered using a tungsten-carbide mill. Approximately 50-mg split of the sample powder was dissolved using standard HF/HNO_3 techniques on a hot plate set at 120°C. The solution was then dried and subsequently treated with 40 drops of HNO_3. The residue was dissolved on a hot plate for 24 hours, dried again and further treated with 40 drops of HNO_3. The sample was then allowed to dissolve at room temperature for 24 hours. After completing a third drying stage, the final residue was treated with two 1-2 ml washes of concentrated HNO_3, then diluted to 100 g using a 5% v/v HNO_3 matrix. All acids used were doubly distilled, resulting in a full procedural

blank generally at the sub-ppt (part per trillion) level. Standard addition and external calibration procedures were used to quantify elements in the unknowns (modified from Jenner et al., 1990). Internal standards used were As (as the matrix contained no Cl- and, hence no ArCl interference on mass 75), Te, and In. BHVO-1 basalt standard was run as unknowns in order to check calibrations. Blanks were periodically run to ensure there were no memory effects.

Major-element Chemistry and Temperature Estimates

Major-element compositions of whole rocks and minerals analyzed in the present study (Table 1 and appendices A-2 to A-5) were evaluated with the analyses previously obtained (Promprated, 1999). Whole-rock compositions of the Thai spinel-peridotite xenoliths have a considerable range of MgO contents (~32-50 wt%) that form well-defined negative correlations with other major-oxides (Fig. 2). The correlations are accentuated with plots of clinopyroxene compositions (Fig. 3). The mg#s of Cpx in Denchai xenoliths are the highest, and those of Wichainburi xenoliths are among the lowest. Comparison with the spinel-peridotite xenoliths from other western Asia-Pacific localities shows good agreement (e.g., SE China; Xu et al., 2000; and SE Russia; Ionov et al., 1995). Such relationships have been interpreted as characteristics of residues after basaltic-melt extraction (e.g., Frey et al., 1985).

Temperature estimates in the present study, combined with those previously determined (Promprated et al., 1999), are reported in Table 2. Among the thermometers used, the 2-pyroxene thermometers (Wood and Banno; 1973; Herzberg and Chapman; 1976; Bertrand and Mercier, 1986) yielded a higher range of temperatures (~980 to1370°

Table 1. Modal abundances and whole-rock compositions of peridotite xenoliths and host basalts from Thailand.

Sample:	BP6*	BP15	BP35	BP38	DC1	DC3a	DC5	DC8*	DC14b	MT1*
Modal abundances (vol%)										
Ol	55.4	58.2	62.0	66.8	75.3	67.8	51.8	73.8	95.2	50.5
Opx	26.6	-	23.9	14.3	20.7	26.4	28.8	21.9	-	31.2
Cpx	15.3	41.0	11.9	15.9	3.5	5.1	16.2	3.3	3.7	16.2
Sp	2.7	0.8	2.2	3.0	0.5	0.7	3.2	1.0	1.1	2.1
Whole-rock compositions (wt%)										
SiO_2	44.4	41.5	42.5	42.4	41.6	43.3	44.4	43.4	44.6	45.6
TiO_2	0.13	0.30	0.10	0.15	<0.03	0.12	0.12	0.05	0.08	0.15
Al_2O_3	4.31	3.40	2.94	4.28	1.02	3.04	4.50	1.65	2.26	4.12
Cr_2O_3	0.50	0.14	0.32	0.43	0.54	0.39	0.38	0.30	0.39	0.45
MgO	38.6	38.3	41.2	38.4	49.0	40.9	37.6	44.5	40.5	37.5
CaO	3.28	4.93	2.35	3.70	0.52	2.49	3.01	0.86	2.12	3.47
MnO	0.13	0.14	0.13	0.13	0.10	0.13	0.11	0.14	0.15	0.14
FeO	8.50	9.19	7.77	8.04	6.19	7.45	7.69	8.91	8.45	7.92
NiO	0.22	0.04	0.05	0.09	0.05	0.07	0.06	0.30	0.03	0.19
Na_2O	0.27	0.09	0.05	0.16	<0.03	0.10	0.15	0.08	0.06	0.34
K_2O	<0.03	<0.03	<0.03	0.04	<0.03	<0.03	<0.03	<0.03	0.03	<0.03
P_2O_5	n.a.	0.03	0.03	<0.03	<0.03	0.03	<0.03		0.03	n.a.
LOI	n.a.	1.84	2.10	2.36	2.24	2.07	2.14	n.a.	1.72	n.a.
Total	100.32	99.91	99.53	100.26	101.28	100.16	100.14	100.22	100.45	99.88
mg#	89.0	88.1	90.4	89.5	93.4	90.7	89.7	89.9	89.5	89.4

(continues)

Table 1. (continued)

Sample:	MT7*	TM7	TM13*	TM16*	WB2	WB3a	WB5	WB6	DCbs3 (basalt)	WBbs8 (basalt)
Modal abundances (vol%)										
Ol	45.7	67.5	23.3	70.6	53.8	46.7	41.1	42.2	-	-
Opx	29.2	18.2	54.1	15.0	31.8	32.4	39.6	38.0	-	-
Cpx	22.4	12.7	19.7	10.6	10.2	17.4	15.7	17.6	-	-
Sp	2.7	1.6	2.9	3.8	4.2	3.5	3.6	2.2	-	-
Whole-rock compositions (wt%)										
SiO_2	45.7	43.3	48.5	42.5	44.6	44.9	45.0	44.1	46.3	48.1
TiO_2	0.16	0.08	0.13	0.07	0.13	0.13	0.16	0.11	2.30	2.10
Al_2O_3	4.55	3.07	5.80	3.50	3.60	4.85	4.94	3.90	16.1	17.2
Cr_2O_3	0.53	0.40	0.38	0.62	0.40	0.39	0.42	0.40	<0.03	<0.03
MgO	35.7	42.0	32.7	42.1	38.5	36.9	34.1	37.0	7.91	6.96
CaO	4.74	2.29	4.53	2.26	3.41	3.71	3.62	3.60	7.83	7.34
MnO	0.13	0.14	0.13	0.13	0.13	0.11	0.17	0.13	0.15	0.16
FeO	7.43	7.69	7.25	8.75	7.87	7.89	9.69	8.30	8.55	8.76
NiO	0.17	0.06	0.11	0.29	0.06	0.07	0.08	0.06	<0.03	<0.03
Na_2O	0.44	0.10	0.29	0.20	0.16	0.18	0.21	0.16	4.30	3.20
K_2O	<0.03	<0.03	<0.03	<0.03	<0.03	<0.03	0.04	<0.03	1.81	1.84
P_2O_5	n.a.	<0.03	n.a.	n.a.	<0.03	0.04	0.06	0.04	0.75	0.10
LOI	n.a.	1.24	n.a.	n.a.	1.58	1.44	1.59	2.58	3.36	2.91
Total	99.59	100.46	99.80	100.41	100.44	100.58	100.11	100.42	100.15	98.82
mg#	87.9	90.7	88.9	89.6	89.7	89.3	86.3	88.8	62.2	58.6

Note: Chemical analyses were performed on whole-rock fused beads using EMP. For small samples (indicated with *), reconstructed whole-rock compositions were calculated from mineral analyses and modal abundances. Modal abundances were determined by point counting, up to 5000 points per thin section. Abbreviations: Ol, Opx, Cpx, Sp = Olivine, Clinopyroxene, Orthopyroxene, Spinel, respectively; n.a. = not analysed; LOI = Loss on ignition. mg# = molar (Mg/Mg+Fe).

Figure 2. Plot of selected major-element concentrations versus MgO of whole-rock lherzolite xenoliths (data from this study and Promprated et al., 1999). Data of the xenoliths from SE China (Xu et al., 2000) and from SE Russian (Ionov et al.,1995) are included for comparison. Negative correlations of SiO_2, Al_2O_3, CaO, Na_2O, and TiO_2 with the MgO contents suggest a major control by partial melting process. Abbreviations: DC = Denchai, TM = Tha Mai, BP = Bo Ploi, MT = Mae Tha, WB = Wichianburi. PM is the primitive mantle composition of McDonough and Sun (1995).

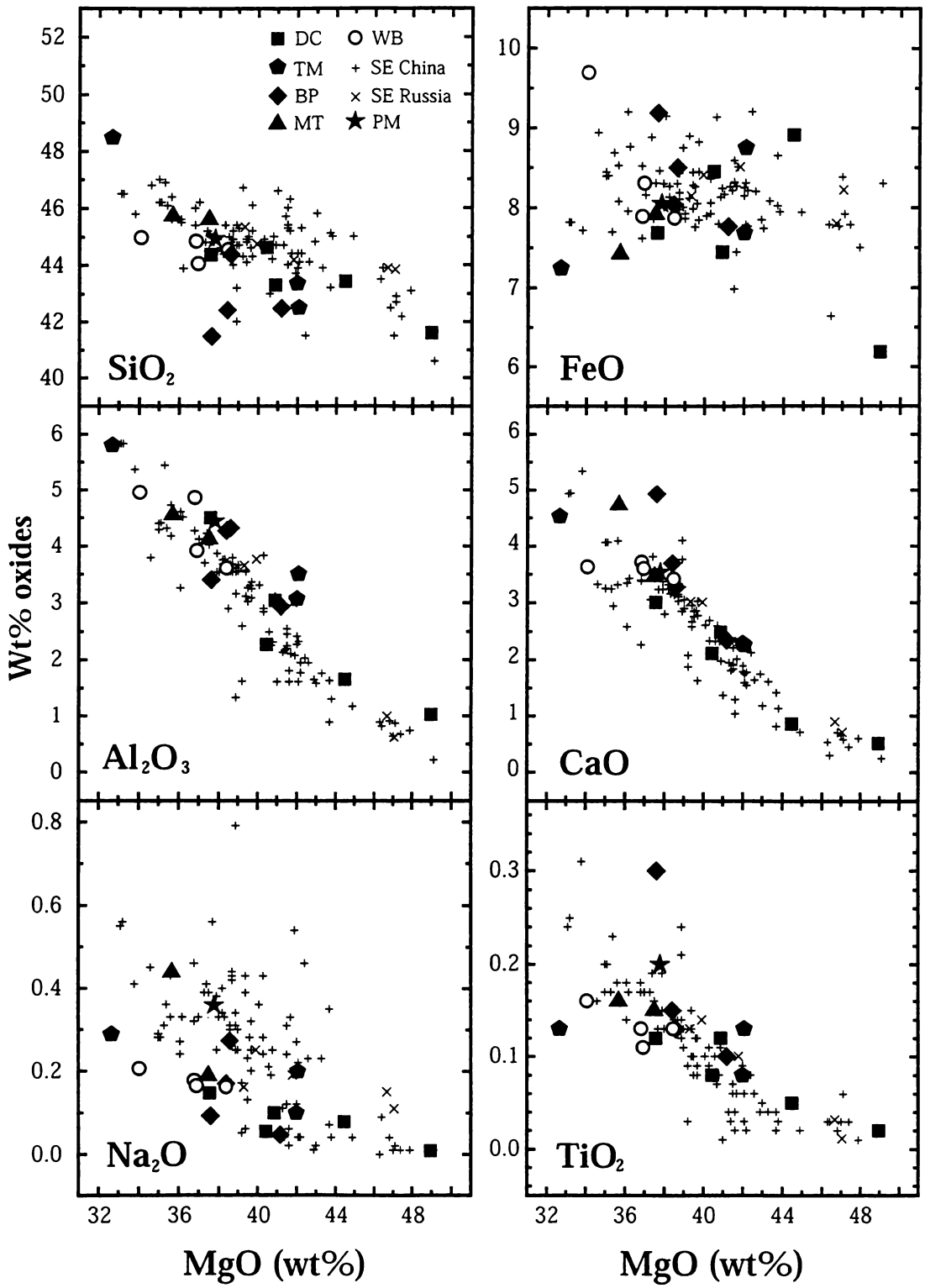

DC
WB
TM
SE China
BP
SE Russia
MT
PM
SiO2
FeO
Al2O3
CaO
Na2O
TiO2
Wt% oxides
MgO (wt%)
MgO (wt%)

Figure 3. Clinopyroxene major-element compositions of lherzolite xenoliths from Thailand compared with those from other world localities. The most fertile samples of the Thai xenoliths are from Wichianburi (WB), whereas Denchai (DC) clinopyroxenes indicate the most depleted compositions. See Figure 2 for abbreviations and references for Chinese and Russian data. Mt. Shadwell data are from Norman (1998).

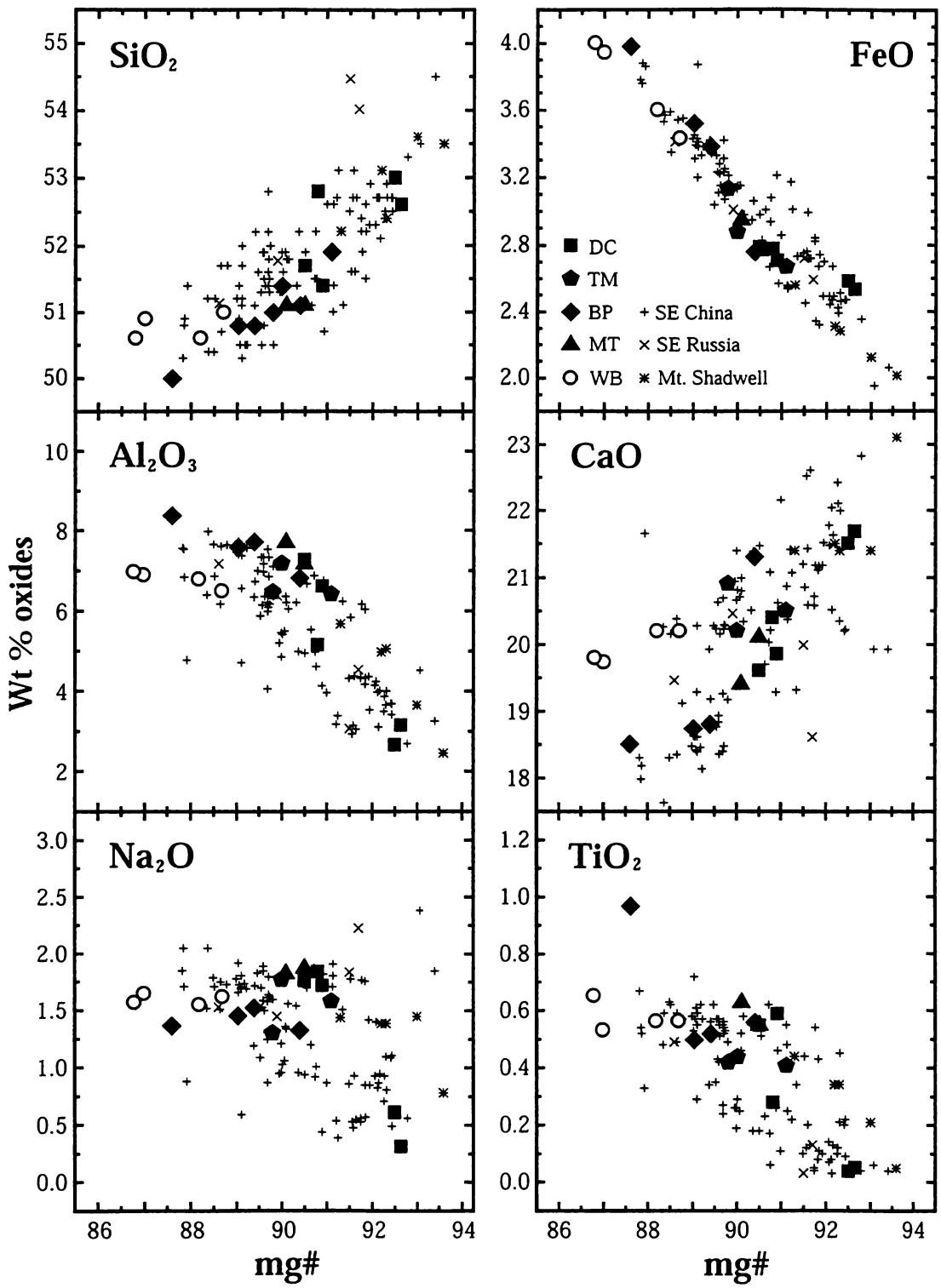

SiO2
FeO
Al2O3
CaO
Na2O
TiO2
Wt % oxides
mg#
mg#
DC
TM
BP
MT
WB
SE China
SE Russia
Mt. Shadwell

Table 2. Estimated temperatures (°C) of peridotite xenoliths from Thailand[†].

	Thermometer[‡]						
Sample	**WB73**	**HC76**	**BM86**	**BK90**	**B91**	**WS91**	**Avg**
BP6*	1154	1302	1336	1133	1037	1016	1163
BP15*	-	-	-	-	1099	-	1099
BP35*	1045	1150	1076	924	1050	947	1032
BP38	1175	1321	1373	1163	1010	995	1173
DC1	1152	1256	1283	1056	1010	1019	1129
DC3a*	1160	1275	1260	1050	996	952	1116
DC5*	1070	1178	1145	1031	944	978	1058
DC8	1078	1173	1173	1019	1000	986	1072
DC14b*	-	-	-	-	1085	-	1085
MT1*	1094	1216	1208	1052	947	982	1083
MT7*	1050	1149	1095	957	997	920	1028
TM7	1063	1147	1096	975	968	1055	1051
TM13*	1057	1173	1090	945	1088	891	1041
TM16	1024	1095	984	924	888	976	982
WB2	1072	1203	1101	1022	-	945	1069
WB3a*	1070	1191	1095	1002	947	955	1043
WB5*	1088	1177	1218	1033	1031	899	1074
WB6*	1079	1159	1247	997	948	899	1055

[†]Temperatures were calculated from core compositions, using 15 kb pressure.

[‡]Abbreviations: WB73 = Wood and Banno (1973); HC76 = Herzburg and Chapman (1976); BM96 = Bertrand and Mercier (1986); BK90 = Brey and Köhler (1990); B91 = Ballhaus et al. (1991); WS91 = Witt-Eickschen and Seck, (1991).

*From Promprated et al. (1999).

C), compared to those obtained from the Opx- and Ol-Sp thermometers (~890 to1160° C; Brey and Kohler, 1990; Witt-Eickschen and Seck, 1991; Ballhaus et al., 1991). The higher temperatures obtained from the 2-pyroxene thermometers are largely due to the slower Mg-Fe diffusion in pyroxenes, compared to that in olivine and spinel, resulting in higher closure temperatures (Witt-Eickschen and Kramm, 1997).

Whole-rock Trace-element Chemistry

Representative samples from each locality were selected for trace-element analyses (Table 3), based mainly on their relative freshness. Two host basalts from Denchai and Wichianburi were also analyzed in order to address the possibility of metasomatism of the xenoliths by basaltic magmas.

Selected trace elements of whole-rock samples are plotted against MgO, which is a good indicator of the degree of depletion in mantle peridotites (Fig. 4). For the compatible trace elements, Ni is positively correlated with MgO, with an exception of sample DC1, whereas Co shows no such correlation, possibly due to its strong dependence on FeO contents (Glassley and Piper, 1978). The moderately incompatible elements (Sc, Sr, Y, and Zr) show well-defined negative correlations, with Sr being more dispersed, possibly due to its higher mobility. Similar trends are observed in spinel-peridotite xenoliths from NE China (Xu et al., 1998), but with noticeably lower Sr and Zr contents (Fig. 4).

Rare earth element (REE) patterns of most whole-rock samples are approximately 2X chondrite (Anders and Grevesse, 1989) for HREE, coupled with either LREE enrichment or depletion (Fig. 5). Interestingly, most samples exhibit prominent negative

Table 3. Trace-element compositions of whole-rock peridotites and host basalts (in ppm) analyzed by ICP-MS[†].

Sample:	DC1	DC3a		DC5		BP15		BP38	
Set:	a	a	b	a	b	a	b	a	b
Sc	8.9	13.6	10.9	17.0	14.6	16.9	16.0	15.0	14.5
V	31.4	55.9	55.6	70.1	74.7	89.9	97.7	70.4	82.4
Cr	3133	2503	2437	2680	2519	770	790	3050	2927
Co	110	326	228	272	258	125	109	170	154
Ni	2303	2347	2311	2188	2020	2131	2068	1982	2003
Cu	5.3	18.6	21.5	21.6	26.5	29.9	37.7	27.5	34.7
Zn	36.8	56.0	59.8	47.5	63.6	46.5	65.4	44.8	73.1
Ga	2.18	5.14	5.68	4.71	6.62	3.29	3.63	3.81	5.00
Rb	0.28	1.33	0.73	0.69	0.58	2.40	1.81	1.29	0.81
Sr	9.03	13.70	17.42	15.15	22.19	40.20	40.17	17.71	24.29
Y	0.15	2.41	2.52	3.29	3.84	4.72	5.41	3.52	4.11
Zr	4.16	10.07	7.56	9.25	8.06	11.57	9.46	7.24	6.31
Nb	0.36	5.55	3.70	6.91	5.56	1.40	1.17	2.95	2.28
Ba	8.41	9.73	7.90	0.59	0.63	14.30	13.17	15.39	14.34
La	0.08	0.50	0.49	0.19	0.20	0.97	0.98	0.47	0.47
Ce	0.17	1.28	1.26	0.68	0.68	2.73	2.76	1.06	1.11
Pr	0.03	0.16	0.17	0.12	0.13	0.39	0.43	0.14	0.15
Nd	0.08	0.82	0.82	0.73	0.71	2.15	2.23	0.82	0.94
Sm	0.03	0.28	0.19	0.28	0.30	0.77	0.66	0.30	0.27
Eu	b.d.*	0.02	0.08	0.04	b.d.	0.25	0.09	0.06	b.d.
Gd	0.03	0.36	0.36	0.52	0.53	1.05	1.04	0.52	0.56
Tb	b.d.	0.07	0.05	0.07	0.10	0.14	0.14	0.10	0.09
Dy	0.04	0.42	0.40	0.58	0.65	0.94	1.04	0.60	0.66
Ho	0.01	0.09	0.09	0.12	0.12	0.19	0.19	0.14	0.14
Er	0.01	0.29	0.23	0.36	0.40	0.50	0.59	0.39	0.41
Tm	0.01	0.04	0.04	0.06	0.07	0.07	0.07	0.06	0.07
Yb	0.04	0.32	0.27	0.44	0.44	0.49	0.51	0.39	0.38
Lu	0.01	0.04	0.04	0.06	0.08	0.06	0.07	0.06	0.06
Hf	0.07	0.18	0.17	0.20	0.26	0.36	0.33	0.22	0.26
Pb	0.15	0.45	0.26	0.36	0.29	0.60	0.57	0.83	1.13
Th	0.02	0.09	0.08	0.03	0.03	0.09	0.09	0.15	0.15
U	0.01	0.05	0.04	0.03	0.03	0.12	0.11	0.03	0.04

(continues)

Table 3. (continued)

Sample:	TM7		WB3		WB5		DCbs3‡	WBbs8‡
Set:	a	b	a	b	a	b	b	b
Sc	13.5	11.6	18.3	14.9	14.4	12.4	18.9	15.7
V	72.5	55.7	82.4	84.3	63.5	66.1	253.3	159.6
Cr	3477	2388	3223	2857	2816	2867	264.2	89.2
Co	198	144	164	194	284	197	59.0	53.7
Ni	2644	2314	1757	2201	1896	2164	179.3	98.6
Cu	24.9	11.9	8.4	10.8	7.9	9.5	68.5	73.8
Zn	66.2	63.5	51.0	64.1	65.4	73.6	129.7	154.4
Ga	17.47	11.74	4.48	5.39	4.95	6.29	b.d.	21.21
Rb	0.47	0.39	0.57	0.15	0.87	0.56	38.88	32.15
Sr	25.60	16.93	40.95	38.77	47.14	53.58	751.1	1861
Y	2.80	2.33	3.77	3.86	3.52	3.61	23.54	27.28
Zr	8.16	3.70	15.97	13.58	13.10	10.06	246.2	323.4
Nb	3.17	2.00	4.69	3.16	3.94	2.31	69.83	119.4
Ba	17.79	11.99	7.76	6.64	8.31	6.91	470.5	666.5
La	0.19	0.20	1.74	1.65	1.57	1.54	27.90	64.84
Ce	0.69	0.51	4.80	4.47	5.40	5.29	61.98	150.0
Pr	0.10	0.08	0.53	0.52	0.80	0.80	6.86	15.80
Nd	0.51	0.37	2.03	1.83	3.53	3.49	28.28	59.09
Sm	0.23	0.14	0.43	0.39	0.66	0.71	5.78	9.41
Eu	0.08	0.06	0.13	0.01	0.15	0.26	1.74	2.71
Gd	0.43	0.30	0.62	0.56	0.73	0.83	6.78	8.50
Tb	0.07	0.06	0.08	0.09	0.10	0.11	0.83	0.97
Dy	0.38	0.34	0.60	0.69	0.66	0.64	4.64	5.18
Ho	0.10	0.07	0.13	0.14	0.11	0.14	0.84	0.97
Er	0.32	0.23	0.40	0.42	0.34	0.42	2.33	2.47
Tm	0.04	0.04	0.06	0.07	0.05	0.07	0.31	0.35
Yb	0.34	0.27	0.42	0.35	0.37	0.42	1.88	2.14
Lu	0.05	0.04	0.06	0.07	0.06	0.06	0.28	0.33
Hf	0.17	0.09	0.28	0.32	0.25	0.36	4.79	5.68
Pb	0.78	0.50	0.33	0.20	0.51	0.49	3.23	6.42
Th	0.04	0.02	0.12	0.12	0.07	0.07	4.29	7.81
U	0.04	0.02	0.05	0.04	0.06	0.06	1.40	2.01

†Replicate analyses (a,b) were performed on most samples using the same sample powders.
‡DCbs3 and WBbs8 are host basalts from Denchai and Wichianburi xenoliths, respectively.
*b.d., below detection limit.

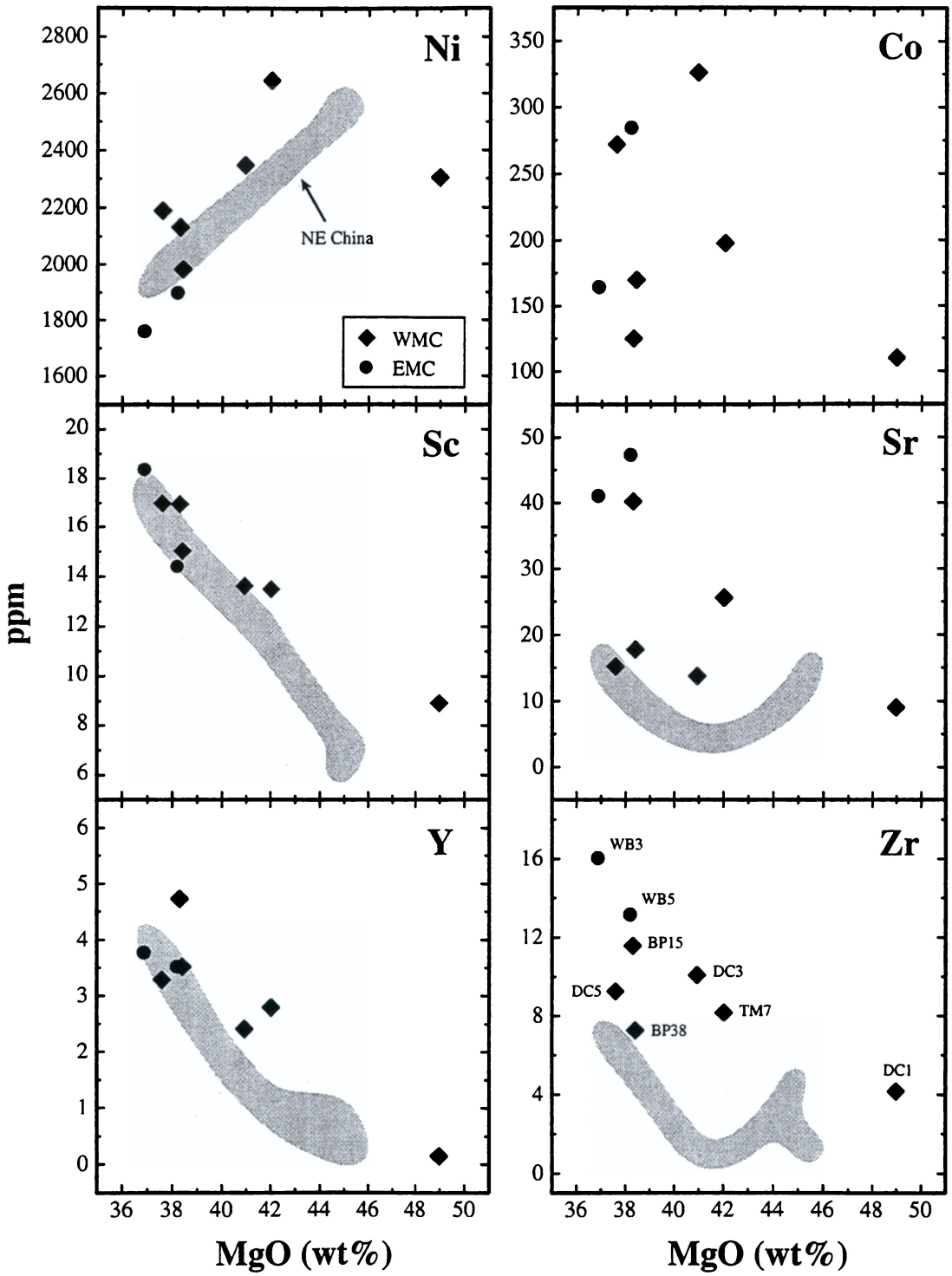
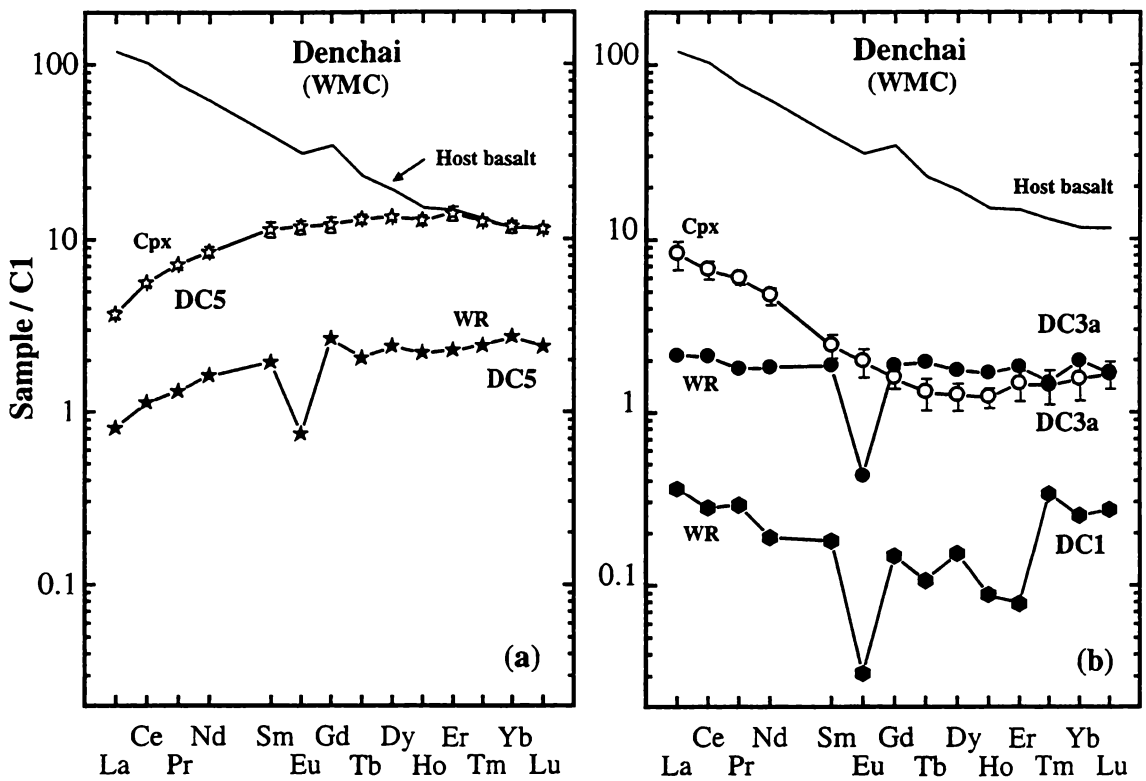


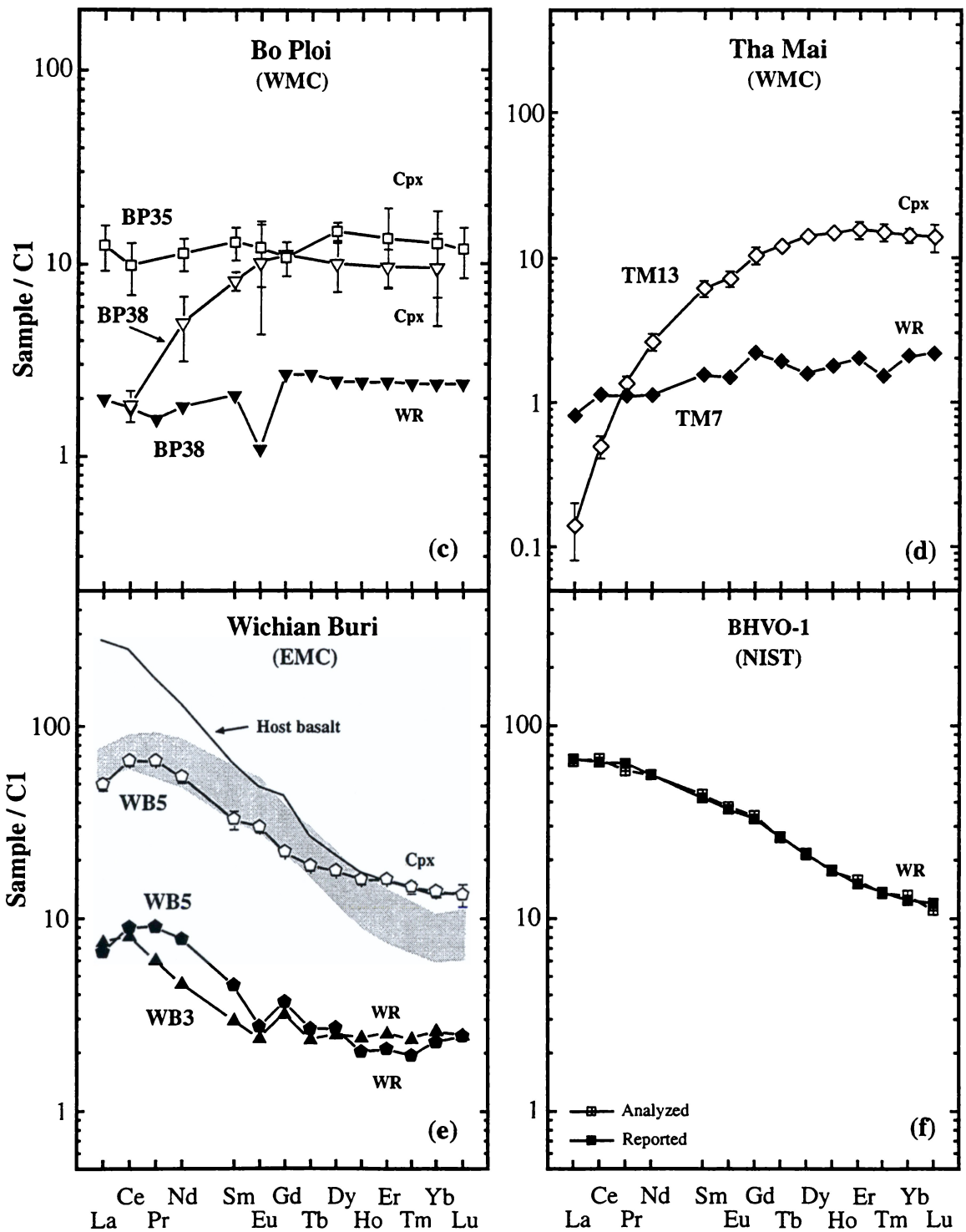
Figure 4. Variation diagrams of MgO contents versus selected trace elements in whole rocks. Each data point is labeled in the Zr plot for reference. NE China xenoliths (shaded trends) are from Xu et al. (1998).



(continues)

Figure 5. REE concentrations (C1 normalized) of whole-rock lherzolite xenoliths (WR), compared with their clinopyroxenes (Cpx; shown with 2 σ error bars). Notice prominent negative Eu anomalies in whole-rock analyses from Denchai, Bo Ploi, and Wichianburi that are absent in Cpx from the same samples (a-e). Differences in REE patterns between whole-rocks and Cpx suggest REE contribution from contaminants residing along grain boundaries. Shaded pattern in (e) represents amphibole-bearing sp-lherzolite from SE China (Xu et al., 2000) and SE Russia (Ionov et al., 1995). (f) Absence of negative Eu anomalies in the NIST reference material (BHVO-1) rules out the possibility of analytical artifacts.

(continued)


Bo Ploi
(WMC)
Cpx
BP35
BP38
Cpx
WR
BP38
(c)
Tha Mai
(WMC)
Cpx
TM13
WR
TM7
(d)
Wichian Buri
(EMC)
Host basalt
WB5
Cpx
WB5
WB3
WR
WR
(e)
BHVO-1
(NIST)
WR
Analyzed
Reported
(f)
Sample / C1
100
10
1
0.1
Ce Nd Sm Gd Dy Er Yb
La Pr Eu Tb Ho Tm Lu

Eu anomalies, which are absent in corresponding clinopyroxene analyses. Sample DC1 is the most depleted sample in this study, based on its overall REE abundances (<0.4X chondrite). By contrast, Wichianburi xenoliths (WB3 and WB5) exhibit the most elevated LREE abundances (up to ~10X chondrite), with concave downward patterns and, perhaps, slight positive Gd anomalies.

Trace-element Chemistry of Minerals

Trace-element analyses of mineral phases were performed using the LA-ICP-MS technique. One of the benefits of this technique is that the *in-situ* analyses can be achieved such that effects of contaminants residing along grain boundaries or cracks can be avoided (Norman, 1998). For each mineral phase in a sample, 5 to 8 analyses were performed on cores and rims (~50 μm from grain boundaries) of a single grain, and usually 3 grains in a sample were analyzed. The results, particularly for the REE, show insignificant core-to-rim variations; thus, average analyses are presented (Tables 4 to 7).

In anhydrous spinel peridotites, clinopyroxenes usually host most of the incompatible trace elements, which are sensitive to both partial melting and metasomatism. As shown in Figure 6, the selected incompatible trace elements (Y, Yb, Zr, and Hf) correlate positively with Ti, in agreement with that observed in the larger data set of Chinese xenoliths (Xu et al., 2000). Additional features are revealed in trace-element profiles (Fig. 7) that show significant variations in the trace-element concentrations, particularly the depletion of high-field-strength element such as Ti, Zr, and Hf. Such variations suggest the interplay between partial melting and metasomatism occurred to the xenoliths. It is interesting to note that the clinopyroxene REE profiles of

Table 4. Trace-element compositions (in ppm) of clinopyroxene in spinel-lherzolite xenoliths from Thailand, analyzed by LA-ICP-MS.

Sample:	DC3a	DC5	TM13	BP35	BP38	WB5
n†:	6	6	6	5	8	6
Sc	74.6 (33)‡	77.6 (35)	77.9 (123)	54.5 (57)	56.2 (76)	76.4 (15)
Ti	295 (10)	3979 (51)	2869 (379)	2952 (379)	1119 (107)	4386 (64)
V	194 (14)	261 (6)	342 (78)	181 (16)	250 (8)	252 (4)
Cr	7530 (1635)	4531 (603)	2645 (568)	5630 (627)	7160 (388)	4704 (713)
Co	26.5 (18)	22.8 (34)	38.0 (359)	15.5 (30)	31.7 (12)	27.7 (3.6)
Ni	430 (31)	342 (31)	543 (452)	n.a.*	n.a.	423 (53)
Ga	2.01 (36)	4.63 (101)	5.40 (121)	n.a.	n.a.	6.41 (182)
Rb	0.09 (5)	0.31 (33)	0.07 (1)	6.15 (125)	<4.51	0.13 (8)
Sr	45.2 (16)	65.7 (54)	6.40 (35)	201 (13)	21.9 (15)	307 (22)
Y	1.61 (9)	17.7 (4)	19.7 (5)	17.6 (22)	15.5 (12)	21.9 (2)
Zr	2.81 (9)	29.1 (11)	6.83 (37)	95.3 (86)	15.3 (14)	42.4 (27)
Nb	0.58 (3)	0.17 (5)	0.37 (29)	1.34 (16)	<0.90	0.44 (12)
Ba	0.37 (20)	0.20 (8)	<0.13	110 (10)	<9.22	0.31 (16)
La	1.92 (18)	0.86 (2)	0.03 (1)	2.95 (28)	<0.81	11.7 (44)
Ce	4.03 (24)	3.38 (6)	0.30 (3)	5.95 (71)	1.12 (10)	39.8 (12)
Pr	0.53 (2)	0.63 (1)	0.12 (1)	n.a.	n.a.	5.85 (15)
Nd	2.13 (12)	3.81 (13)	1.19 (8)	5.15 (40)	2.23 (41)	24.6 (87)
Sm	0.36 (3)	1.67 (9)	0.91 (6)	1.91 (60)	1.20 (7)	4.78 (26)
Eu	0.11 (1)	0.66 (3)	0.40 (2)	0.68 (19)	0.57 (16)	1.66 (5)
Gd	0.31 (2)	2.38 (12)	2.04 (14)	2.12 (45)	2.19 (0)	4.35 (9)
Tb	0.05 (1)	0.47 (1)	0.43 (1)	n.a.	n.a.	0.68 (2)
Dy	0.30 (3)	3.23 (6)	3.39 (6)	3.56 (59)	2.41 (34)	4.30 (12)
Ho	0.07 (1)	0.71 (2)	0.82 (2)	n.a.	n.a.	0.89 (3)
Er	0.23 (2)	2.21 (10)	2.46 (17)	2.14 (43)	1.53 (17)	2.53 (5)
Tm	0.03 (1)	0.30 (1)	0.36 (2)	n.a.	n.a.	0.35 (1)
Yb	0.25 (3)	1.90 (8)	2.31 (13)	2.06 (42)	1.55 (39)	2.23 (7)
Lu	0.04 (1)	0.28 (1)	0.34 (4)	0.29 (3)	<0.40	0.32 (2)
Hf	0.10 (3)	1.07 (1)	0.58 (5)	1.93 (35)	0.72 (14)	1.46 (16)
Ta	0.10 (1)	0.02 (1)	0.10 (11)	0.46 (5)	<0.30	0.08 (1)
Pb	0.15 (5)	0.16 (6)	0.08 (3)	n.a.	n.a.	0.43 (15)
Th	0.11 (1)	0.02 (0)	<0.01	0.69 (1)	<0.38	0.26 (10)
U	0.03 (1)	0.03 (2)	<0.01	<0.20	<0.21	0.08 (8)

†number of analyses used in the average.

‡units in parentheses represent 1 standard deviation of replicate analyses in terms of last unit cited.

*not analyzed.

Table 5. Trace-element compositions (in ppm) of orthopyroxene in spinel-lherzolite xenoliths from Thailand, analyzed by LA-ICP-MS.

Sample:	**DC3a**	**DC5**	**TM13**	**WB5**
n:	5	5	6	6
Sc	17.9 (8)*	13.9 (9)	16.6 (17)	15.0 (87)
Ti	119 (36)	622 (62)	532 (68)	729 (71)
V	83.8 (55)	92.0 (30)	131 (13)	87.3 (27)
Co	61.3 (11)	62.2 (15)	66.4 (27)	65.8 (22)
Ni	808 (29)	727 (18)	797 (17)	793 (32)
Zn	58.2 (36)	53.7 (126)	53.4 (84)	85.2 (327)
Ga	2.42 (51)	3.86 (22)	6.47 (360)	5.26 (125)
Rb	0.36 (8)	<0.05	0.21 (9)	0.12 (7)
Sr	0.39 (32)	0.15 (4)	0.17 (16)	0.72 (22)
Y	0.17 (2)	0.95 (10)	1.47 (54)	1.30 (5)
Zr	0.69 (53)	1.68 (50)	0.58 (25)	2.43 (58)
Ce	0.10 (10)	0.01 (0)	<0.02	0.14 (4)
Ho	<0.01	0.04 (0)	0.06 (2)	0.05 (1)
Er	<0.04	0.16 (2)	0.23 (7)	0.20 (2)
Yb	0.07 (2)	0.25 (3)	0.36 (6)	0.31 (4)
Lu	0.01 (0)	0.04 (1)	0.07 (1)	0.06 (1)
Ni/Co	13.2	11.7	12.0	12.0
$\mathbf{Ti_{opx}/Ti_{cpx}}$	0.40	0.16	0.19	0.17
$\mathbf{Zr_{opx}/Zr_{cpx}}$	0.25	0.06	0.09	0.06
$\mathbf{Yb_{opx}/Yb_{cpx}}$	0.28	0.13	0.16	0.14
mg#	91.5	90.1	89.3	88.5

n: number of analyses used in the average

*units in parentheses represent 1 standard deviation of replicate analyses in terms of last unit cited.

Table 6. Trace-element compositions (in ppm) of olivine in spinel-lherzolite xenoliths from Thailand, analyzed by LA-ICP-MS.

Sample:	DC3a	DC5	TM13	WB5
n†:	6	6	5	6
Al	85.4 (156)‡	106 (35)	97.1 (24)	106 (18)
Ca	510 (15)	<739	385 (46)	<500
Sc	3.47 (76)	2.68 (68)	2.29 (19)	2.54 (32)
Ti	<0.01	14.8 (22)	14.2 (56)	13.8 (14)
V	4.17 (108)	2.91 (36)	2.41 (14)	2.93 (76)
Cr	178 (43)	51.9 (20)	23.8 (26)	44.3 (48)
Mn	1074 (169)	1239 (200)	1213 (43)	1418 (22)
Co	136 (21)	168 (6)	165 (5)	168 (5)
Ni	2853 (452)	3299 (122)	3263 (100)	3203 (115)
Fo	90.4	89.4	88.7	88.4
Ni/Co	20.9	20.1	19.8	19.1

†number of analyses used in the average.
‡units in parentheses represent 1 standard deviation of replicate analyses in terms of last unit cited.

Table 7. Trace-element compositions (in ppm) of spinel in spinel-lherzolite xenoliths from Thailand, analyzed by LA-ICP-MS.

Sample:	DC3a	DC5	TM13	WB5
n†:	5	6	4	5
Sc	4.21 (131)‡	<4.34	<0.66	0.86 (12)
Ti	293 (37)	424 (37)	395 (7)	475 (45)
V	927 (78)	362 (78)	475 (22)	352 (34)
Mn	1173 (145)	707 (145)	755 (9)	957 (99)
Co	263 (32)	236 (32)	252 (6)	243 (15)
Ni	1629 (295)	3446 (295)	3477 (184)	3440 (234)
Zn	1143 (119)	1092 (120)	1151 (103)	1302 (106)
Ga	46.3 (63)	85.6 (63)	82.9 (2.8)	79.8 (59)
Zr	0.38 (6)	<0.46	0.13 (10)	0.69 (78)
Nb	0.44 (5)	<0.22	0.05 (1)	0.18 (14)
Cr#	52.9	9.4	5.6	10.0

†number of analyses used in the average.
‡units in parentheses represent 1 standard deviation of replicate analyses in terms of last unit cited.

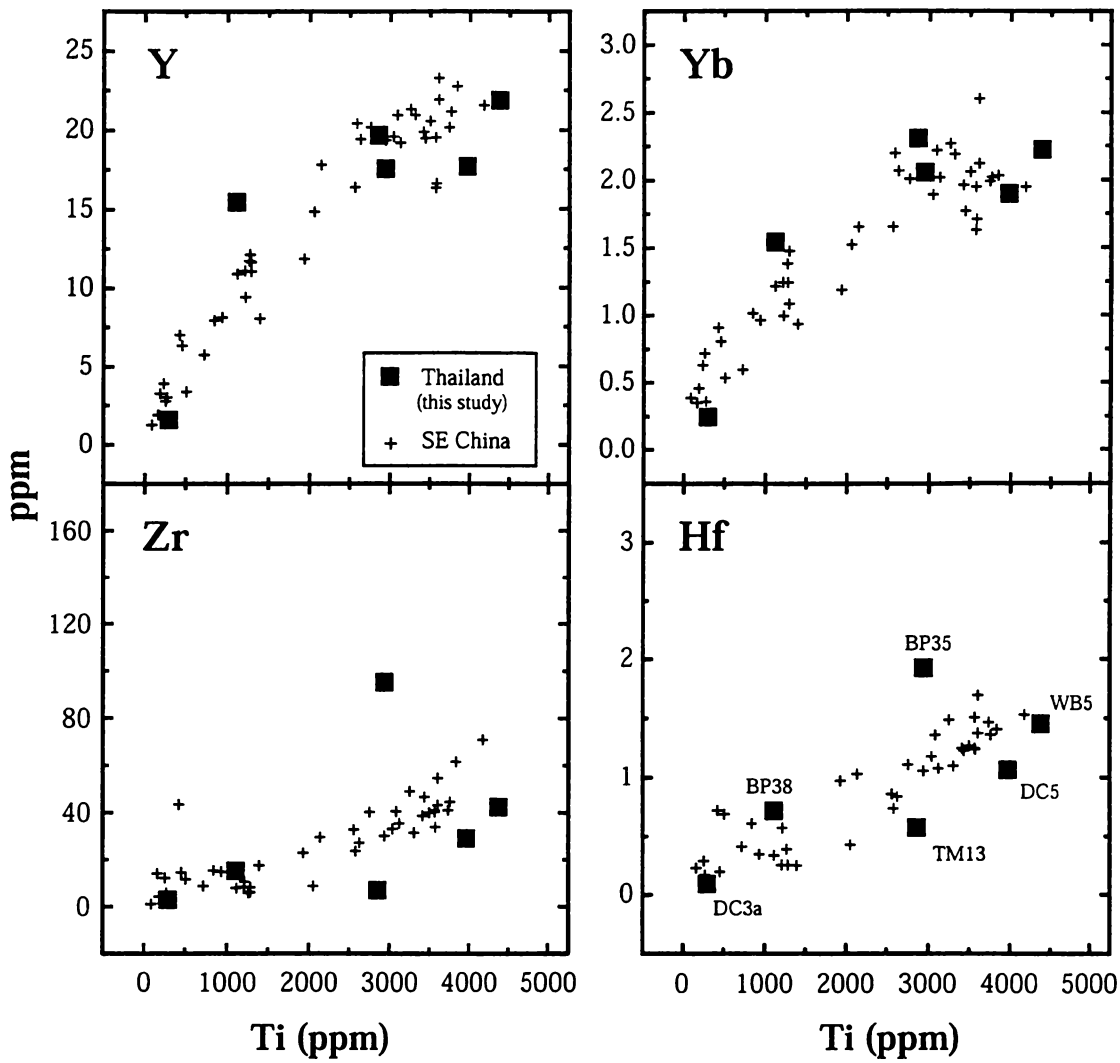


Figure 6. Incompatible trace elements in clinopyroxene showing strong positive correlation with Ti contents. These correlations are strengthen when clinopyroxene compositions of SE China spinel-peridotite xenoliths (Xu et al., 2000) are plotted for comparison.

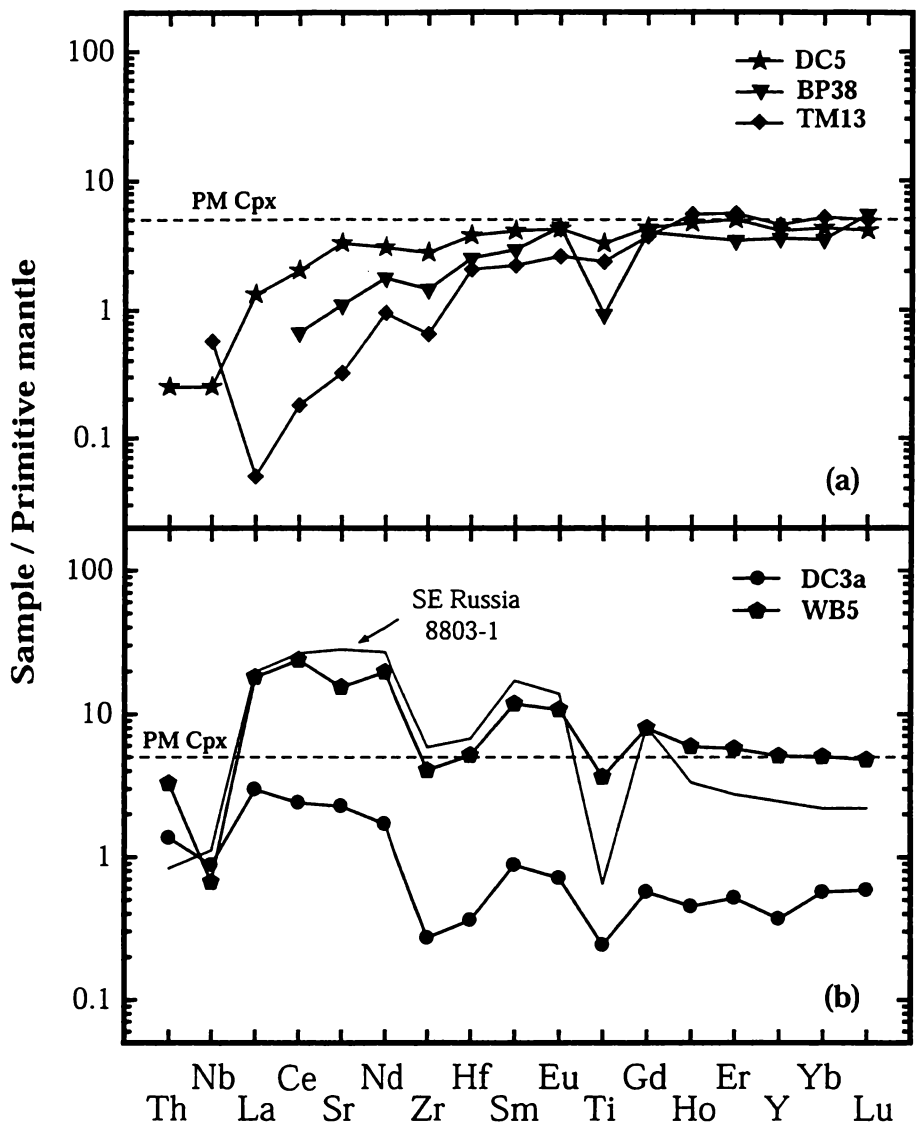


Figure 7. Trace-element patterns of clinopyroxenes (primitive mantle normalized) showing variable degrees of depletion (a) and enrichment (b) in these elements. Notice pronounced HFSE (Zr, Hf, Ti) depletion in (b) that suggest metasomatism by carbonate-rich fluids. SE-Russian sample, which shows evidence of carbonate metasomatism, is from Ionov et al. (1995). Clinopyroxene compositions of the Primitive mantle (PM Cpx) are taken as 5 times those of hypothetical bulk PM (McDonald and Sun, 1995).

samples DC5 and WB5 mimic those of whole-rocks (with the exception of Eu). This similarity, however, is not observed in other samples (Fig. 5).

Analyses of orthopyroxene (Table 5) show that the high-field-strength elements (HFSE), particularly Ti, are negatively correlated with mg#. In addition, there is a general increase in partitioning of HFSE (Ti, Zr, Hf) between Opx and Cpx from fertile to depleted xenoliths. This is consistent with previous conclusions that the HFSE depletion in Cpx is partially compensated for by the enrichment in the coexisting Opx (Rampone et al., 1991; McDonough et al., 1992; Norman, 1998; Xu, 2000). Ni/Co ratios of Opx are relatively constant (~12-13), in agreement with the range observed in Mt. Shadwell low-Ca pyroxenes (Norman, 1998).

Limited amounts of trace elements were measurable in olivines and spinels (Tables 6 and 7). It is noticeable that the Ni/Co increases systematically with increasing Fo contents (Table 6), in agreement with a partial melting trend (Norman, 1998). In spinels, the concentrations of Zn and Co vary within narrow ranges (~1090-1300 and 230-260 ppm, respectively). High Nb contents were observed in TM13, consistent with the elevated Nb contents seen in Cpx of this sample.

Discussion

Negative Eu anomalies in peridotites

The presence of negative Eu anomalies in all analyzed whole-rock peridotites is surprising, especially when the anomalies are absent in clinopyroxenes from the same samples. The results of a second set of determinations (Table 3) reconfirm the presence of negative Eu anomalies, ruling out the possibility of analytical artifacts. This is also

strengthened by the absence of such anomalies in the analyzed reference material BHVO-1 in both sets of analyses. The likelihood of the anomalies caused by other primary phases such as orthopyroxene, olivine, and spinel is at best remote, since these phases contain insignificant amounts of the REE.

It is conceivable that the negative Eu anomalies in the whole-rock analyses have been contributed by unknown phases residing along grain boundaries. Such REE-rich phases as apatite might lend their large negative Eu anomalies to the overall whole-rock patterns. However, no apatite was seen in the petrographic examination or detected in whole-rock analyses (i.e., P_2O_5 <0.03; Table 1), although minute amounts of apatite could have been omitted from these particular thin-sections studied. In similar studies (e.g., Ionov et al., 1995; Rudnick et al., 1993; Hauri et al., 1993), even the presence of apatite is confirmed, the whole-rock REE patterns posses no negative Eu anomalies. Therefore, apatite may not be the cause of the negative Eu anomalies observed in these whole-rock analyses. The negative Eu anomalies caused by host-basalt contamination is possible. However, this process would probably result in an enrichment of all LREE without preferentially excluding the Eu, rendering the host basalts unlikely sources of the anomalies.

Condie (1993) demonstrated that negative Eu anomalies are characteristics of upper continental crust (UCC) of all ages. Furthermore, Bau et al. (1998) concluded that the negative Eu anomalies are "fingerprints" of boundary films coating primary mineral grains in mildly weathered igneous rocks (Fig. 8). These studies establish that upon weathering, surface or ground water would precipitate the Eu-depleted components as thin films along grain boundaries of rocks exposing to surficial conditions. The xenoliths

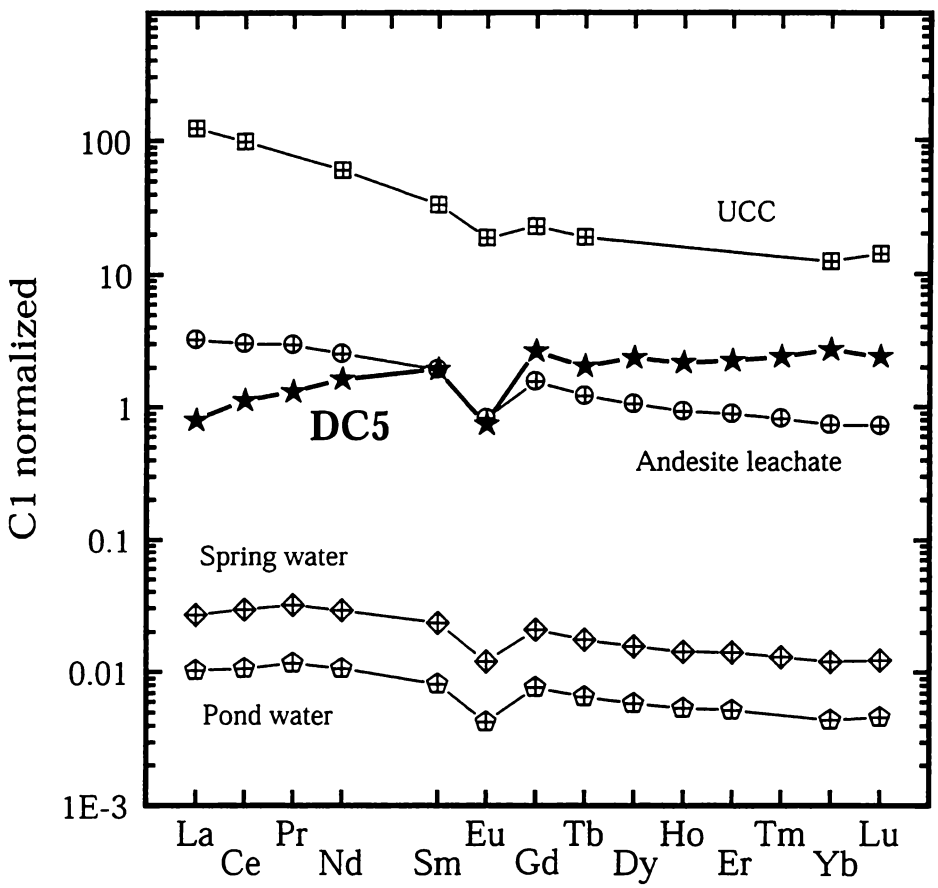


Figure 8. REE abundances (chondrite normalized) of whole-rock DC5 showing prominent negative Eu anomaly similar to other surface materials. UCC is the average upper continental crust from Condie (1993). Andesite leachate, spring and pond water are from Bau et al. (1998).

in this study have shown variable degrees of weathering on the surfaces. Therefore, we prefer to attribute the negative Eu anomalies to the secondary effects of weathering.

Clinopyroxene trace-element modeling

Partial melting

Clinopyroxene trace-element modeling has been widely used to evaluate the degrees of partial melting experienced by the sp-peridotite xenoliths (e.g., Johnson et al., 1990; Norman, 1998; Xu et al., 2000). In quantifying the extents of partial melting in this study, specific assumptions were made to the nature of melting process: (1) a single stage of melting occurred, and (2) mineral-melt distribution coefficients were constant throughout the melting period. A non-modal fractional melting equation will be used here to obtain more realistic results (Norman, 1998). The equation and parameters involved are shown below:

$$C_{cpx} = C_o/(1-F)*[(1-PF)/D_o]^{(1/P)}$$

where,

C_{cpx} is the concentration of an element in the residual clinopyroxene.

C_o is the starting Cpx composition of the source rock, which is taken as the primitive mantle (PM) of McDonough and Sun (1995). The modal abundance of this "primitive" Cpx in the source rock is assumed to be 20%. Therefore, concentration of the REE in Cpx is considered to be 5 times that of PM.

F is the degree of partial melting.

P is the Cpx/melt distribution coefficient for an element at the Cpx melt-mode of 0.67 (Kinzler, 1997). The Cpx/melt distribution coefficients are as follows: Th = 0.035, Nb = 0.004, La = 0.049, Ce = 0.07, Sr = 0.095, Nd = 0.178, Zr = 0.119, Hf = 0.20, Sm = 0.293, Eu = 0.37, Ti = 0.31, Gd = 0.40, Er = 0.41, Y = 0.412, Yb = 0.40, Lu = 0.449 (Johnson, 1998; Hauri et al., 1994; Green, 1994; Norman, 1998).

D_o is the Cpx/melt distribution coefficient in the source rock.

The results, obtained from a series of trace elements (Fig. 9a), suggest that xenoliths DC5, BP38, and TM13 underwent small degrees (up to ~6%) of partial melting. The extent of melting of LREE-enriched DC3a was constrained at ~16% in the plot of Y_n versus Yb_n (Fig. 9b).

Metasomatism

Clinopyroxenes in samples DC3a and WB5 show LREE-enriched patterns that require metasomatic addition of the incompatible elements. Quantifying the extent of this process requires knowledge of the type of metasomatic agents, hence their compositions. The absence of mineralogical evidence hinders a direct identification of metasomatic fluids. Nevertheless, studies of the spinel-peridotite xenoliths elsewhere in Asia (Ionov et al., 1995; Xu et al., 2000) have shown evidence of metasomatism by both silicate (basaltic) and carbonatitic melt. Therefore, these two types of metasomatic agent will be evaluated here.

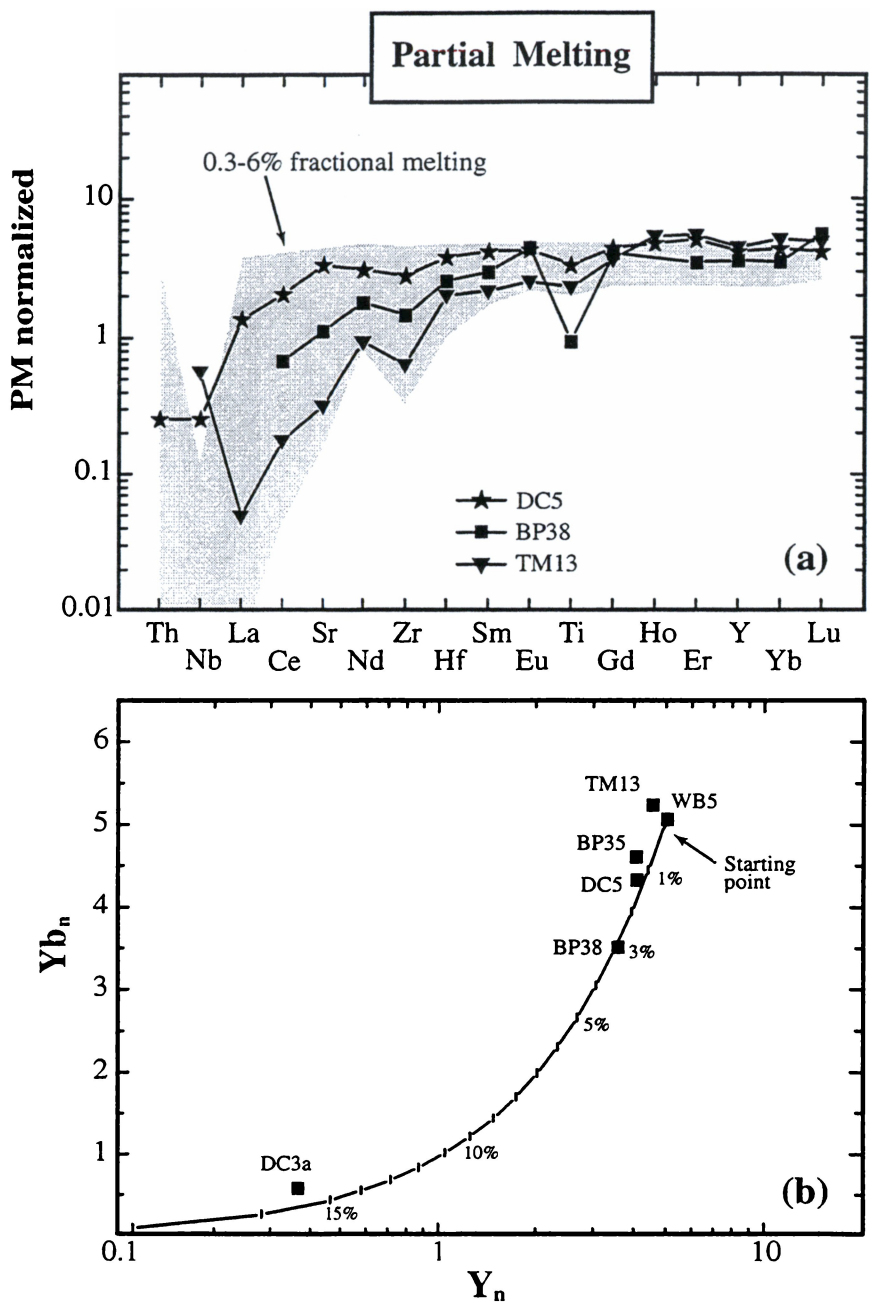


Figure 9. Clinopyroxene trace-element modeling showing variable degrees of partial melting experienced by spinel-peridotite xenoliths. (a) Up to 6% melting could explain patterns observed in DC5, BP38, and TM13. (b) Yb_n-Y_n modeling (n = PM normalized) constrains the partial melting of DC3a at ~16 %.

For basaltic metasomatism, compositions of the xenolith host-basalts (Table 3) were used in a simple "bulk" mixing calculation with primitive mantle Cpx composition, and with residual Cpx that previously experienced 16% partial melting (Fig. 10a). It is apparent that the calculated Cpx compositions show no depletion of HFSE (Nb, Zr, Hf, Ti) as observed in the analyzed data. In contrast, when a carbonatitic-melt composition (Nelson et al., 1988) was used, the resulting Cpx trace-element patterns show close similarity with the observed data (Fig. 10b). Indeed, carbonatite melts are known to posses this characteristic HFSE depletion (Rudnick et al., 1993). The mixing calculations show that Cpx in sample DC3a requires up to 6% trace-element contribution from carbonatitic melts, whereas Cpx in WB5 needs as much as 30%.

Figure 11 illustrates the calculated compositions of carbonate-rich fluids that may have been in equilibrium with xenoliths DC3a and WB5, using the relationship $K_D = C_{cpx}/C_{liq}$ and the partition coefficients from Blundy and Dalton (2000) and Klemme et al. (1995). The calculated melts have overall shapes similar to erupted carbonatites (Nelson et al., 1988). Discrepancies observed could have caused by near-surface fractionation and/or crustal contamination of the erupted carbonatites (Ionov et al., 1993). Alternatively, these carbonate-rich fluids may contain some proportions of basaltic melt $\pm$ H_2O, as suggested by Xu et al. (2000).

The lithospheric mantle beneath Thailand

The spinel-lherzolite xenoliths in this study show no conclusive evidence of the effects of Mesozoic subduction that created the Nan-River suture. Ionov et al. (1995) postulated a scenario in which the subduction-derived fluids were exhausted in their

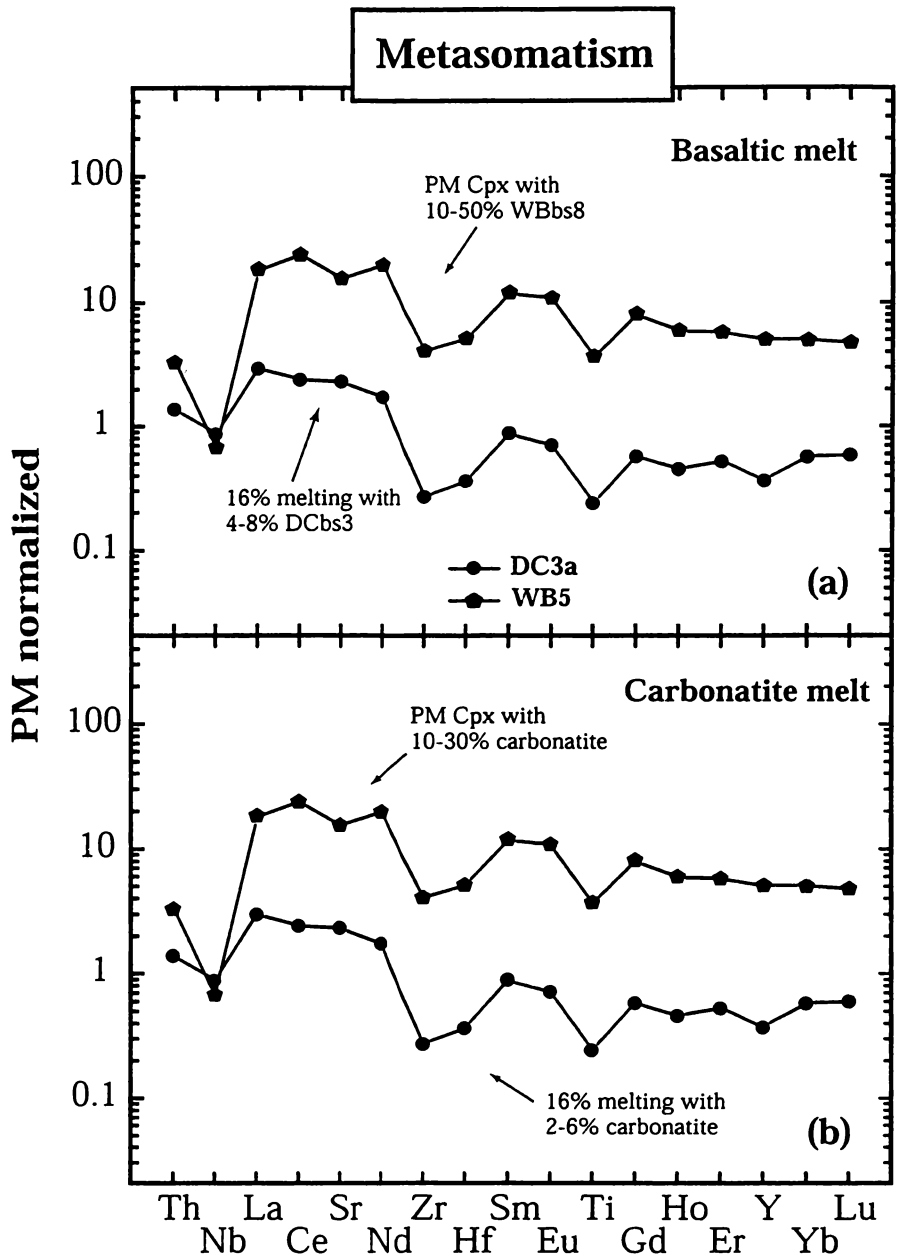


Figure 10. Estimation of the degrees of metasomatic enrichment using two possible metasomatic agents and pre-matasomatized clinopyroxenes of samples DC3a and WB5. (a) Host basalts as metasomatic agents produce generally good fits for the REE, but significant discrepancies for Nb, Zr, Hf, and Ti. (b) A calcite-rich carbonatite (Nelson et al., 1988) creates better fits with the analyzed data.

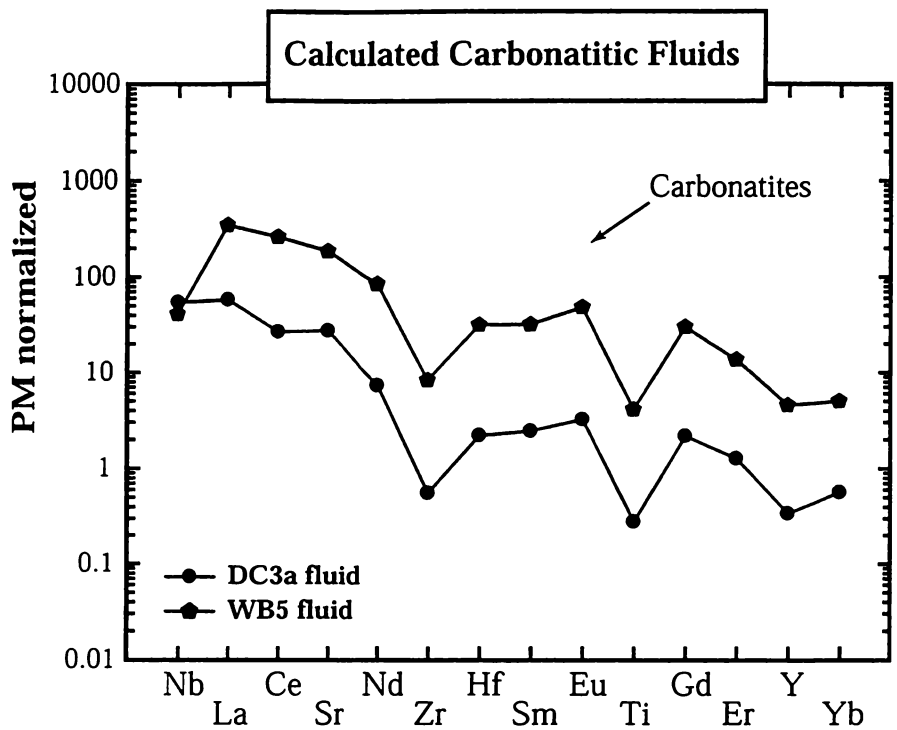


Figure 11. Calculated carbonate-rich fluids in equilibrium with clinopyroxenes of samples DC3a and WB5, using partition coefficients of Blundy and Dalton (2000) and Klemme et al. (1995). Selected carbonatite compositions are from Nelson et al. (1988).

hydrous component by reacting with the deep mantle section above the slab. Consequently, the residual fluids reaching the upper-most mantle may predominantly consist of CO_2, which became carbonate-rich fluids/melts. This scenario may also be applicable to portions of the lithospheric mantle beneath Thailand. Alternatively, the carbonatitic metasomatism that interacted with the Thai mantle xenoliths may have occurred in an intraplate setting, such as in continental rifts associated with basin developments (Norman, 1998), or in an ocean-island environment (Hauri et al., 1993; Gregoire et al., 2000).

Clinopyroxenes in sample TM13 are strongly LREE depleted ($[La/Lu]_N = 0.01$; Fig. 5d), similar to observations in other studies (e.g., Johnson et al., 1990; Witt-Eickschen and Kramm, 1997). This LREE depletion/HREE enrichment perhaps indicates the former existence of garnet from which clinopyroxene inherits its REE signature. Johnson et al. (1990) concluded, based on studies of abyssal peridotites, that the extreme LREE-depleted patterns in Cpx were the result of *decompressional* melting associated with garnet (Gt) breakdown. This is shown as: Ol + Gt = 2.5 Opx + 0.75 Cpx + Sp. If this is true for sample TM13, the approximate lithospheric thickness in this region is ~60 km, near the garnet-spinel transitional zone (i.e., ~20 kb).

Conclusions

Trace-element data obtained from the spinel-peridotite xenoliths from Thailand have permitted a quantitative evaluation of partial melting and metasomatism occurred to the mantle in this SE-Asia region. As demonstrated by clinopyroxene trace-element modeling, the majority of the xenoliths in this study experienced small degrees (up to

~6%) of partial melting, whereas the most depleted sample analyzed (DC3a) was subjected to ~16% melting. Sample WB5 appears to have remained fertile, or its previous melting history was effectively erased by a subsequent metasomatic enrichment. The metasomatic agents affecting some xenoliths were probably carbonate-rich, as indicated by the pronounced depletion of HFSE (Ti, Zr, Hf). Mixing calculations indicated that up to 6% carbonatite melt was necessary to produce the trace-element pattern observed in DC3a, while as much as 30% carbonatite was required for sample WB5. Furthermore, the present study also reveals a weathering artifact, apparent as negative Eu anomalies in the whole-rock analyses.

Mineralogical and geochemical evidence of the spinel-peridotite xenoliths suggests a thin, approximately 60 km, lithosphere beneath Thailand, possibly as a result of asthenospheric upwelling. This is supported by the presence of "garnet-like" REE profile in clinopyroxenes of a Tha Mai sample (TM13) that resulted from the breakdown of garnets entering spinel-peridotite facies. This mantle process is commonly believed to have caused lithosphere thinning as a result of thermal erosion, and the eventual Cenozoic basalt-volcanism of the Western Pacific regions.

References

Anders, E., and Grevesse, N, 1989, Abundances of the elements: meteoritic and solar: Geochim. Cosmochim. Acta, v. 53, p. 197-214.

Ballhaus, C., Berry, R.F., and Green, D.H., 1991, High-pressure experimental calibration of the olivine-orthopyroxene-spinel oxygen geobarometer: Implications for the oxidation state of the upper mantle: Contrib. Mineral. Petrol., v. 107, p. 27-40

Barr, S.M. and Dostal, J., 1986, Petrochemistry and origin of megacrysts in Upper Cenozoic basalts, Thailand: J. of SE Asian Earth Science, v. 1, p. 107-116.

Bau, M., Usui, A., Pracejus, B., Mita, N., Kanai, Y., Irber, W., and Dulski, P., 1998, Geochemistry of low-temperature water-rock interaction: Evidence from natural waters, andesite, and iron-oxyhydride precipitates at Nishiki-numa iron-spring, Hokkaido, Japan: Chem. Geol., v. 151, p. 293-307.

Bertrand, P., and Mercier, J.C.C., 1985, The mutual solubility of coexisting ortho- and clinopyroxene: Toward an absolute geothermometer for the natural system: Earth Planet. Sci. Lett., v. 76, p. 109-122.

Blundy, J., and Dalton, J., 2000, Experimental comparison of trace element partitioning between clinopyroxene and melt in carbonate and silicate systems, and implications for mantle metasomatism, Contrib Mineral Petrol, v. 139, p. 356-371.

Blundy, J.D., Robinson, J.A.C., Wood, B.J., 1998, Heavy REE are compatible in clinopyroxene on the spinel lherzolite solidus: Earth Planet. Sci. Lett., v. 160, p. 493-504.

Bodinier, J.L., Dupuy, C., Dostal, J., 1988, Geochemistry and petrogenesis of eastern Pyrenean peridotites, Geochim et Cosmochim Acta, 52, 2893-2907.

Brey, G.P. and Kohler, T., 1990, Geothermobarometry in four-phases lherzolites II: New thermobarometers, and practical assessment of existing thermobarometers: J. of Petrology, v. 31, no. 6, p. 1353-1378.

Condie, K.C., 1993, Chemical composition and evolution of the upper continental crust: contrasting results from surface samples and shales, Chem Geol, 104, 1-37.

Deng, J., Zhao, H., Luo, Z., Guo, Z., and Mo, X., 1998, Mantle plumes and lithosphere motion in East Asia, *in* Flower, M.F., Chung, S.L., Lo, C.H., and Lee, T.Y. (eds), Mantle Dynamics and Plate Interactions in East Asia, American Geophysical Union, Geodynamics Series, v. 27, p. 59-65.

Faure, M., and Natal'in, B., 1992, The geodynamic evolution of the eastern Eurasian margin in Mesozoic times, Tectonophysics, v. 208, p. 397-411.

Frey, F.A., Suen, C.J., and Stockman, H.W., 1985, The Rhonda high temperature peridotite: Geochemistry and petrogenesis, Geochim Cosmochim Acta, 49, p. 2469-2491.

Glassley, W.E., and Piper, D.Z., 1978, Cobalt and scandium partitioning versus iron contents for crystalline phases in ultramafic nodules, Earth Planet Sci Lett, 39, 173-178.

Green, T.H., 1994, Experimental studies of trace-element partitioning applicable to igneous petrogenesis: Sedona 16 years later, Chem Geol, 117, 1-36.

Gregoire, M., Moine, B.N., O'Reilly, S.Y., Cottin, J.Y., and Giret, A., 2000, Trace element residence and partitioning in mantle xenoliths metasomatized by highly alkaline, silicate- and carbonate-rich melts (Kerguelen islands, Indian Ocean), J Petrol, v. 41, p. 477-509.

Hauri, E., Shimizu, N., Dieu, J., and Hart, R., 1993, Evidence for hot spot-related carbonatite metasomatism in the oceanic upper mantle, Nature, 365, 221-227.

Hauri, E.H., Thomas, P.W., Timothy, L.G., 1994, Experimental and natural partitioning of Th, U, Pb, and other trace elements between garnet, clinopyroxene, and basaltic melts, Chem Geol, 117, 149-166.

Herzberg, C.T., and Chapman, N.A., 1976, Clinopyroxene geothermometry of spinel-lherzolites: Amer. Mineral., v. 61, p. 626-637.

Ionov, D.A., Prikhod'ko, V.S., O'Reilly, S.Y., 1995, Peridotite xenoliths in alkali basalts from the Sikhote-Alin, southeastern Siberia, Russia: trace-element signatures of mantle beneath a convergent continental margin, Chem Geol, 120, 275-294.

Ionov, D.V., Dupuy, C., O'Reilly, S.Y., Kopylova, M.G., and Genshaft, Y.S., 1993, Carnonated peridotite xenoliths from Spitsbergen: Implications for trace element signature of mantle carbonate metasomatism: Earth Planet. Sci. Lett, v. 119, p. 283-297.

Jackson, S. E., Longerich, H. P., Dunning, G. R. and Fryer, B. J., 1992, The Application of laser-ablation microprobe-inductively coupled plasma-mass spectrometry (LAM-ICP-MS) to in situ trace element determinations in minerals: Can. Mineral., v. 30, p. 1049-1064.

Jenner, G.A., Longerich, H.P., Jackson, S.E., and Fryer, B.J., 1990, ICP-MS --- A powerful tool for high precision trace-element analysis in Earth sciences: Evidence from analysis of selected U.S.G.S. reference samples: Chemical Geology, v. 83, p.

133-148.

Jezek, D.A., Sinton, J.M., Jarosewich, E., and Obermeyer, C.R., 1978, Fusion of rock mineral powders for electron microprobe analysis: Smithsonian Contributions to Earth Sciences, v. 22, p. 46-52.

Johnson, K.T.M., Dick, H.J., Shimizu, N., 1990, Melting in the oceanic upper mantle: An ion microprobe study of diopsides in abyssal peridotites: J. Geophys. Res., v. 95, p. 2662-2678.

Kinzler, R.J., 1997, Melting of mantle peridotite at pressures approaching the spinel to garnet transition: application to mid-ocean ridge basalt petrogenesis: J. Geophys Res., v. 102, p. 853-874.

Klemme, S., van der Laan, S.R., Foley, S.F., Günther, D., 1995, Experimentally determined trace and minor element partitioning between clinopyroxene and carbonatite melt under upper mantle conditions, Earth Planet Lett, v. 133, p. 439-448.

Longerich, H. P., Jackson, S. E., Gunther, D., 1996, Laser ablation inductively coupled plasma mass spectrometric transient signal data acquisition and analyte concentration calculation: J. Anal. At. Spectrosc., v. 11, p. 899-904.

McDonough, W.F., and Sun, S.S., 1995, The composition of the Earth: Chem.Geol., v. 120, p. 223-253.

McDonough, W.F., Stosch, H.G., Ware, N.G., 1992, Distribution of titanium and the rare earth elements between peridotitic minerals: Contrib. Mineral. Petrol., v. 110, p. 321-328.

Nelson, D.R., Chivas, A.R., Chappel, B.W., and McCulloch, M.T., 1988, Geochemical and isotopic systematics in carbonatites and implications for the evolution of ocean-island sources, Geochim Cosmochim Acta, v. 52, p. 1-17.

Norman, M.D., 1998, Melting and metasomatism in the continental lithosphere: laser ablation ICPMS analysis of minerals in spinel lherzolites from Australia: Contrib. Mineral. Petrol., v. 130, p. 240-255.

Promprated, P, Taylor, L.A., and Snyder, G.A., 1999, Petrochemistry of the mantle beneath Thailand: Evidence from peridotite xenolith: INT. GEOL. REV., v. 41, p. 506-530.

Rampone, E., Bottazzi, P., Ottolini, L., 1991, Complimentary Ti and Zr anomalies in orthopyroxene and clinopyroxene from mantle peridotites, Nature, v. 354, p. 518-521.

Rudnick, L.R., McDonough, W.F., Chappel, B.W., 1993, Carbonatite metasomatism in the northern Tanzanian mantle: petrographic and geochemical characteristics: Earth Planet. Sci. Lett., v. 114, p. 463-475.

Schuraytz, B.C., and Ryder, G., 1990, An evaluation of the reliability and usefulness of microprobe fused bead analyses for petrogenetic interpretations: Abstr, 21st Lunar and Planet. Sci. Conf, p. 1113-1114.

Witt-Eickschen, G., and Kramm, U., 1997, Mantle upwelling and metasomatism beneath central Europe: Geochemical and isotopic constraints from mantle xenoliths from the Rhön (Germany): J. Petrol., v. 38, p. 479-493.

Witt-Eickschen G., and Seck H.A., 1991, Solubility of Ca and Al in orthopyroxene from spinel peridotite: An improved version of an empirical geothermometer: Contrib. Mineral. Petrol., v. 106, p. 431-439.

Wood, B.J. and Banno, S., 1973, Garnet-orthopyroxene and orthopyroxene-clinopyroxene relationships in simple and complex systems: Contrib Min Petrol, v. 42, p. 109-124.

Xu, X., O'Reilly, S.Y., Griffin, W.L., and Zhou, X., 1998, The nature of the Cenozoic lithosphere beneath Nushan, East Central China, *in* Flower, M.F., Chung, S.L., Lo, C.H., and Lee, T.Y. (eds): Mantle Dynamics and Plate Interactions in East Asia, American Geophysical Union, Geodynamics Series, v. 27, p. 167-169.

Xu, X., O'Reilly, Y.S., Griffin, W.L., and Zhou, X., 2000, Genesis of young lithospheric mantle in southeastern China: an LAM-ICPMS trace-element study: J. Petrol., v. 41, p. 111-148.

Appendices

A-1: Petrographic descriptions of additional peridotite xenoliths from Thailand.

BP38 Spinel lherzolite with protogranular texture. Grain sizes are coarsest for olivine and orthopyroxene (3-6 mm), relatively finer for clinopyroxene (1-5 mm), and finest for spinel (0.5-2 mm). Some large olivine grains exhibit stress feature known as "kink bands", while clinopyroxenes typically show grungy reaction texture with the host basalt ("spongy rinds").

DC1 & DC8 Spinel harzburgite with protogranular texture. Grain sizes progressively decrease from olivine (2-5 mm), orthopyroxene (1-3 mm), clinopyroxene (mostly 1 mm), to spinel (mostly <0.5 mm). No spongy rinds were observed on clinopyroxenes, but kink bands are abundant on olivines.

TM7 & TM16 Spinel lherzolite with porphyroclastic texture. Relict orthopyroxene, and less commonly olivine, porphyroclasts (4-6 mm) are set in the finer groundmass (mostly 1 mm) of recrystallized olivine, ortho- and clinopyroxene, with interstitial spinel (<0.5 mm). Rare, poorly developed, exsolution lamellae were seen on orthopyroxenes. Olivine kink bands are common.

WB2 Spinel lherzolite with prophyroclastic texture. Orthopyroxene porphyroclasts (up to 8 mm) occur within a recrystallized groundmass of olivine, ortho- and clinopyroxene (0.5-2 mm), and spinel (<0.5). Olivine grains form recognizable parallel orientation.

Table A-2. Major-element compositions of clinopyroxene in spinel-peridotite xenoliths from Thailand.

Sample:	BP38	DC1	DC8	TM7	TM16	WB2
$n^{\dagger}$:	10	10	16	7	11	8
SiO_2	50.8 (1)[‡]	52.6 (3)	51.4 (4)	51.9 (2)	51.4 (1)	50.9 (1)
TiO_2	0.50 (3)	0.05 (2)	0.59 (3)	0.41 (3)	0.44 (3)	0.53 (2)
Al_2O_3	7.58 (14)	3.15 (6)	6.61 (10)	6.42 (35)	7.17 (15)	6.88 (10)
Cr_2O_3	0.80 (4)	1.11 (7)	1.20 (8)	0.91 (10)	1.06 (8)	0.77 (5)
MgO	16.0 (1)	17.9 (0)	15.1 (1)	15.3 (1)	14.6 (4)	14.8 (1)
CaO	18.7 (3)	21.7 (1)	19.8 (2)	20.5 (3)	20.2 (4)	19.7 (2)
MnO	0.10 (3)	0.09 (2)	0.08 (2)	0.09 (2)	0.08 (3)	0.10 (2)
FeO	3.52 (10)	2.53 (3)	2.71 (6)	2.67 (6)	2.88 (11)	3.94 (8)
Na_2O	1.46 (1)	0.32 (2)	1.73 (4)	1.59 (9)	1.78 (6)	1.65 (2)
Total	99.56	99.37	99.26	99.74	99.66	99.30
Cations on the basis of 6 oxygens						
Si	1.846	1.917	1.872	1.882	1.870	1.863
Ti	0.014	0.002	0.016	0.011	0.012	0.015
Al^{iv}	0.154	0.083	0.128	0.118	0.130	0.137
Al^{vi}	0.171	0.053	0.157	0.157	0.177	0.160
Cr	0.023	0.032	0.035	0.026	0.031	0.022
Mg	0.869	0.972	0.823	0.826	0.790	0.810
Ca	0.729	0.847	0.775	0.796	0.787	0.774
Mn	0.003	0.003	0.003	0.003	0.003	0.003
Fe	0.107	0.077	0.082	0.081	0.088	0.121
Na	0.103	0.023	0.122	0.112	0.125	0.117
Σ	4.018	4.009	4.013	4.012	4.012	4.021
mg#	89.0	92.6	90.9	91.1	90.0	87.0
En	51.0	51.3	49.0	48.5	47.4	47.5
Fs	6.3	4.1	4.9	4.8	5.3	7.1
Wo	42.7	44.6	46.1	46.7	47.3	45.4

[†]number of analyses (core) used in the average.
[‡]units in parentheses represent 1 standard deviation of replicate analyses in terms of last unit cited.

Table A-3. Major-element compositions of orthopyroxene in spinel-peridotite xenoliths from Thailand.

Sample:	BP38	DC1	DC8	TM7	TM16	WB2
$n^{\dagger}$:	11	6	13	9	12	10
SiO_2	53.8 (2)[‡]	55.8 (2)	54.8 (4)	54.7 (5)	55.1 (3)	54.1 (3)
TiO_2	0.15 (1)	0.02 (1)	0.14 (2)	0.12 (3)	0.13 (1)	0.12 (1)
Al_2O_3	5.83 (8)	2.93 (4)	4.11 (8)	4.84 (54)	4.38 (23)	4.83 (38)
Cr_2O_3	0.43 (3)	0.72 (3)	0.52 (4)	0.46 (9)	0.40 (5)	0.38 (10)
MgO	32.0 (2)	33.7 (1)	33.2 (1)	32.7 (9)	33.1 (3)	31.9 (2)
CaO	1.17 (4)	1.14 (4)	0.73 (5)	1.15 (82)	0.67 (9)	0.81 (3)
MnO	0.16 (2)	0.12 (2)	0.13 (1)	0.14 (3)	0.15 (2)	0.17 (3)
FeO	6.56 (11)	5.48 (11)	6.34 (10)	6.04 (16)	6.49 (13)	7.50 (9)
Na_2O	0.14 (1)	0.03 (1)	0.10 (1)	0.11 (6)	0.07 (1)	0.11 (1)
Total	100.24	99.98	100.10	100.24	100.50	99.93
Cations on the basis of 6 oxygens						
Si	1.863	1.926	1.895	1.888	1.896	1.884
Ti	0.004	0.001	0.004	0.003	0.003	0.003
Al^{iv}	0.137	0.074	0.105	0.112	0.104	0.116
Al^{vi}	0.101	0.045	0.063	0.084	0.074	0.082
Cr	0.012	0.020	0.014	0.013	0.011	0.011
Mg	1.649	1.734	1.712	1.680	1.700	1.656
Ca	0.044	0.042	0.027	0.042	0.025	0.030
Mn	0.005	0.004	0.004	0.004	0.004	0.005
Fe	0.190	0.158	0.183	0.174	0.187	0.218
Na	0.010	0.002	0.007	0.008	0.005	0.007
Σ	4.013	4.005	4.014	4.008	4.009	4.013
mg#	89.7	91.6	90.3	90.6	90.1	88.4
En	87.6	89.6	89.1	88.6	88.9	87.0
Fs	10.1	8.2	9.5	9.2	9.8	11.4
Wo	2.3	2.2	1.4	2.2	1.3	1.6

[†]number of analyses (core) used in the average.
[‡]units in parentheses represent 1 standard deviation of replicate analyses in terms of last unit cited.

Table A-4. Major-element compositions of olivine in spinel-peridotite xenoliths from Thailand.

Sample:	BP38	DC1	DC8	TM7	TM16	WB2
$n^{\dagger}$:	21	18	23	17	11	9
SiO_2	40.6 (2)[‡]	40.9 (3)	40.3 (4)	40.9 (1)	40.8 (3)	40.4 (1)
MgO	49.2 (2)	50.0 (4)	49.5 (3)	49.7 (1)	49.3 (4)	48.1 (2)
CaO	0.11 (2)	0.10 (1)	0.06 (1)	0.05 (1)	0.03 (1)	0.07 (1)
MnO	0.14 (2)	0.12 (2)	0.14 (3)	0.14 (3)	0.13 (3)	0.15 (3)
FeO	10.4 (2)	8.75 (9)	9.92 (10)	9.60 (9)	9.93 (23)	11.2 (2)
NiO	0.34 (3)	0.38 (4)	0.40 (4)	0.40 (2)	0.39 (5)	0.36 (3)
Total	100.66	100.33	100.30	100.75	100.61	100.33
Cations on the basis of 4 oxygens						
Si	0.992	0.996	0.988	0.995	0.996	0.995
Mg	1.792	1.816	1.808	1.803	1.794	1.765
Ca	0.003	0.003	0.002	0.001	0.001	0.002
Mn	0.003	0.003	0.003	0.003	0.003	0.003
Fe	0.212	0.178	0.203	0.196	0.203	0.231
Ni	0.007	0.008	0.008	0.008	0.008	0.007
Σ	3.008	3.004	3.013	3.005	3.004	3.005
Fo	89.4	91.1	89.9	90.2	89.8	88.4

[†]number of analyses used in the average.
[‡]units in parentheses represent 1 standard deviation of replicate analyses in terms of last unit cited.

Table A-5. Major-element compositions of spinel in spinel-peridotite xenoliths from Thailand.

Sample:	BP38	DC1	DC8	TM7	TM16	WB2
$n^{\dagger}$:	13	9	19	12	12	6
SiO_2	0.10 (4)[‡]	0.06 (1)	0.03 (1)	0.03 (1)	<0.03	0.05 (1)
TiO_2	0.18 (2)	0.09 (2)	0.14 (2)	0.11 (2)	0.10 (1)	0.11 (2)
Al_2O_3	57.4 (4)	32.5 (2)	53.1 (3)	55.3 (2)	54.9 (2)	53.7 (8)
V_2O_3	0.08 (1)	0.17 (2)	0.07 (1)	0.07 (2)	0.07 (1)	0.07 (1)
Cr_2O_3	9.32 (14)	35.6 (4)	14.3 (2)	11.9 (2)	11.8 (2)	10.3 (1)
MgO	20.8 (2)	17.1 (1)	20.0 (2)	20.2 (2)	19.6 (1)	19.3 (2)
MnO	0.10 (1)	0.12 (2)	0.08 (2)	0.09 (1)	0.11 (2)	0.11 (2)
FeO	10.8 (3)	13.1 (2)	10.8 (1)	10.8 (1)	12.1 (1)	15.2 (8)
NiO	0.37 (4)	0.20 (4)	0.35 (4)	0.39 (4)	0.36 (4)	0.39 (4)
ZnO	0.06 (4)	0.08 (4)	0.12 (6)	0.11 (6)	0.17 (4)	0.10 (6)
Total	99.27	98.88	99.06	99.09	99.32	99.26
Cations on the basis of 4 oxygens						
Si	0.003	0.002	0.001	0.001	0.001	0.001
Ti	0.003	0.002	0.003	0.002	0.002	0.002
Al	1.761	1.119	1.663	1.717	1.711	1.694
V	0.002	0.004	0.002	0.002	0.002	0.002
Cr	0.192	0.823	0.300	0.248	0.248	0.218
Mg	0.809	0.745	0.794	0.794	0.774	0.771
Mn	0.002	0.003	0.002	0.002	0.002	0.003
Fe	0.236	0.320	0.240	0.238	0.268	0.340
Ni	0.008	0.005	0.007	0.008	0.008	0.009
Zn	0.001	0.002	0.002	0.002	0.003	0.002
Σ	3.017	3.023	3.014	3.014	3.018	3.041
mg#	77.4	70.0	76.8	76.9	74.3	69.4
cr#	9.8	42.4	15.8	12.6	12.6	11.4

[†]number of analyses (core) used in the average.
[‡]units in parentheses represent 1 standard deviation of replicate analyses in terms of last unit cited.

PART 4

NATURE OF THE LOWER CRUST BENEATH THAILAND: A RECORD FROM GRANULITE XENOLITHS

Abstract

Granulite-suite xenoliths in alkali basalts of the Chantaburi-Trat area of Thailand represent the only known occurrence of lower crustal material in this region. These mafic xenoliths (43-49% SiO_2) can be classified into 3 groups: (1) olivine-garnet clinopyroxenite, (2) garnet-rich granulite, and (3) clinopyroxene-rich granulite. All possess similar geochemical features in the whole rocks, including high normative olivine, plagioclase, and diopside; low and generally flat REE abundances (~0.5-6.0 xC1 for HREE); and positive Eu anomalies. These characteristics indicate cumulate origins, possibly from underplating basaltic magmas. Subsolidus reequilibration resulted in the transformation of original cumulate mineralogy to granulite-facies mineralogy, mainly by the formation of garnet and clinopyroxene at the expense of plagioclase and olivine. P-T estimates indicate that this reequilibration occurred at ~1100 to 1200° C and 15 to18 kbar. The upper limit of this P-T range appears to mark the appearance of corundum inclusions in the garnet-rich granulites. Extensive kelyphitization of garnets is probably due to decompression, while the xenoliths were en route to the surface. The occurrence of granulite xenoliths in the Thai region may indicate prolonged periods of basaltic magmatism that eventually resulted in alkali basalt volcanism in the Cenozoic.

Introduction

Granulite-facies rocks are generally considered a direct representation of lower continental crust. These lower crustal samples are emplaced at the Earth's surface as: (1) regional granulite-facies terrains, and (2) granulite xenoliths in rapidly erupted basalts or kimberlites. Typically, the former tends to be dominated by intermediate to felsic

compositions, whereas the latter is predominantly mafic, commonly believed to have originated from underplating basaltic magmas (Rudnick, 1992).

In Thailand, samples of lower crustal origin have never before been documented. The lower crustal samples found in this study are granulite xenoliths, whose only known occurrence, thus far, is in alkali basalts from the Chantaburi-Trat provinces (Fig. 1). These samples, therefore, provide an excellent opportunity to constrain compositions of the lower crust in this region, and to understand the processes responsible for its formation and modification. Moreover, some samples are of special significance since they contain corundum inclusions that could provide crucial information about the petrogenesis of gem corundum in this region.

The Chantaburi-Trat area is located within an accretional complex of the Mesozoic subduction that created the Nan-River suture (Bunopas and Vella, 1992). This tectonic infrastructure is believed to be the locus of asthenospheric upwelling that, in the Cenozoic, led to eruption of alkali basalts (e.g., Bunopas and Vella, 1992; Mukasa et al., 1996). Most basalts found here range from nephelinite to basanite, dated around 1-3 Ma (Barr and MacDonald, 1981; Barr and James, 1990; Sutthirat et al., 1994). Besides the granulite xenoliths, the alkali basalts in this and other regions of Thailand also entrained mantle peridotites, which were the subject of a separate study (Promprated et al., 2001, in prep.).

Samples and Petrography

The basaltic flows in which the suite of granulite xenoliths occurs, lie approximately 10 m beneath the surface, and were recently exposed by gem-corundum

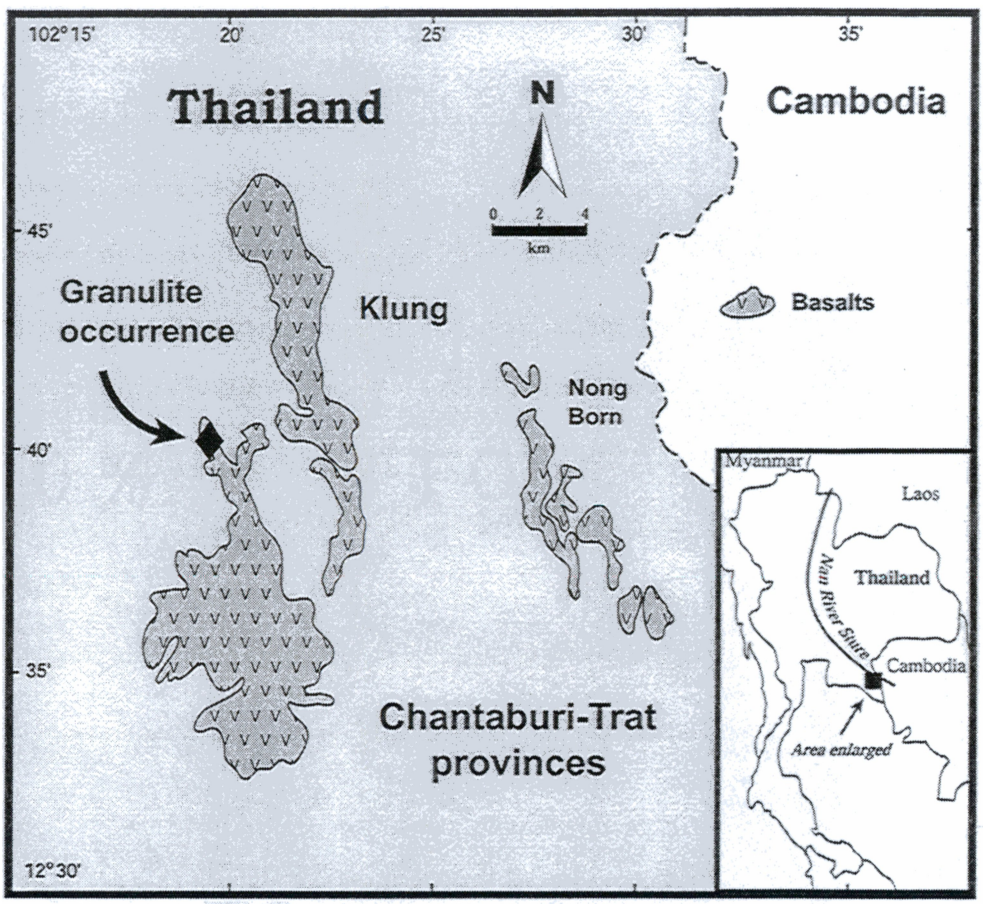


Figure 1. Occurrence of granulite-xenolith locale in Thailand.

mining (Vichit 1992). Ten xenoliths selected for this study consist of nine garnet granulites and a rare olivine-garnet clinopyroxenite. Most are 5 to 8 cm across, except one being roughly 12 cm. As a suite, these xenoliths will be referred to as garnet granulites.

Usually, the samples display granoblastic equigranular, mostly polygonal texture, with common 120° C triple-junction grain boundaries. Some samples also exhibit millimeter-scale banding, but without stress features, i.e., kink bands. Clinopyroxene (Cpx) is almost always the largest mineral present (up to 5 mm), but commonly has similar grain sizes (0.5 to 2.0 mm) as plagioclase (Pl) and garnet (Gt). Minor minerals include olivine (Ol; 0.5 to1.0 mm), spinel (Sp; ~0.2 mm), and corundum (Cor). Based on mineralogy and chemistry, the samples can be broadly classified into three groups: (1) olivine-bearing garnet clinopyroxenite, (2) garnet-rich granulite, the most common type, and (3) pyroxene-rich garnet granulite (Table 1). Further descriptions of each group follow.

Group 1: Olivine-garnet clinopyroxenite

The only olivine-garnet clinopyroxenite in this collection is xenolith KL9. It exhibits well-defined banding mainly as discontinuous trains of garnets similar to the "fish-net fabric" described by Pearson et al. (1992). It appears that the initial nucleation of garnets in this and samples of other groups is along Pl-Pl or Pl-Cpx grain boundaries that commonly progresses into plagioclases. In KL9, garnets are moderately altered to

Table 1. Reconstructed primary modal abundances of granulite xenoliths from Thailand†.

Sample	Cpx	Pl	Gt	Ol	Sp
Ol-Gt clinopyroxenite					
KL9	38.4	-	43.5	14.6	3.5
Gt-rich granulite					
KL12	39.4	29.6	31.0	-	-
KL4a	21.3	27.9	50.8	-	-
KL11	19.5	21.4	59.1	-	-
KL5	17.2	27.7	55.1	-	-
KL13*	23.6	23.9	52.5	-	-
KL10*	22.2	39.4	36.0	-	2.4
KL14	27.7	45.8	26.5	-	-
Cpx-rich granulite					
KL8	43.7	28.7	27.6	-	-
KL7	44.3	27.3	28.4	-	-

†Determined by point counting usually 3000-5000 points per thin section. Kelyphites were counted as primary garnets. Abbreviations: Cpx = Clinopyroxene; Pl = Plagioclase; Gt = Garnet; Ol = Olivine; Sp = Spinel.

*Contain trace amounts of corundum inclusions.

kelyphite[1], observed as brown, radially arranged fibrous-like rinds (kelyphitic rims; Fig. 2). This kelyphite is extremely fine-grained ($\ll 1\mu m$) such that individual minerals cannot be resolved petrographically or by electron microprobe (EMP). In addition, garnets usually contain microcracks, often circular, which have been interpreted as the evidence of decompression (Rudnick, 1992).

[1]Kelyphite is defined as rims or reaction coronas surrounding garnet (Schrauf, 1882). It is commonly formed by metasomatic reaction with kimberlites or basalts (e.g., Garvie and Robinson, 1984). Secondary minerals that commonly occur in the kelyphite include, for instance, pyroxenes, spinel, phlogopite, amphibole, chlorite, and plagioclase.

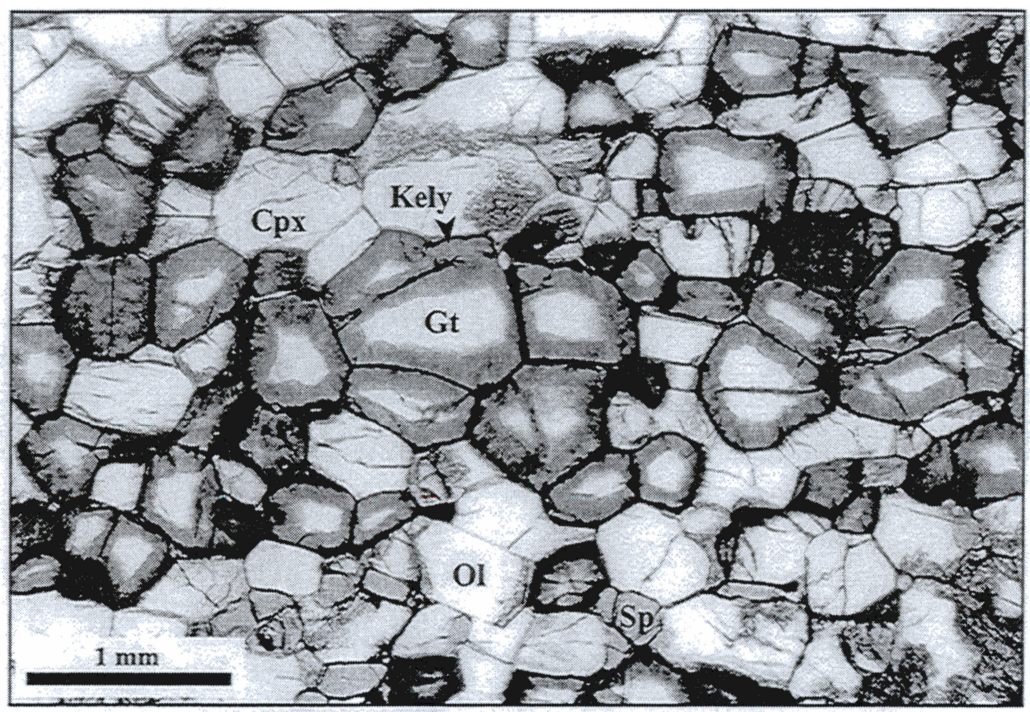


Figure 2. Olivine-garnet clinopyroxenite showing "trains" of garnets (plane-polarized light). Notice extensive kelyphitic rims (Kely) on the garnet cores. Gt = garnet; Cpx = clinopyroxene; Ol = olivine; Sp = spinel.

Clinopyroxenes are generally fresh, and have no exsolution lamellae. It is common, however, to find "spongy rim" developed along margins or cracks of Cpx. This reaction feature of Cpx consists of secondary green spinel and clinopyroxene (Cpx_2). According to Taylor and Neal (1989), spongy rims occur when Na and Al from primary clinopyroxene are "leached" into metasomatic fluids. The consequence of this is the volume decrease, resulting in the cracking of the affected clinopyroxene, but without disrupting the optical continuity of the margins with the core. Snyder et al. (1997) explained this texture observed in lherzolite xenoliths from China by the reaction: Cpx_1 + K-rich fluids = Cpx_2 + alkali feldspar $\pm$ sulfide $\pm$ titanomagnetite.

Olivines are typically subhedral tabular, with minor alteration to serpentine. In addition, a small amount of spinels also occurs interstitially, and appears to be the last phase to crystallize.

Group 2: Garnet-rich granulite

Granulite xenoliths in the garnet-rich group contain abundances of garnets or plagioclases significantly higher than clinopyroxenes (Table 1). The Cpx-rich KL12, however, is included in this group because its mineral chemistry (see below) is similar to that of Gt-rich samples. Generally, clinopyroxenes and plagioclases are fresh, except in KL10 in which clinopyroxenes are extensively metasomatized to secondary Cpx and Sp. Garnets often contain circular cracks, and are extensively or completely overprinted by kelyphite, becoming dark brown and turbid. Fine banding, due to contrasting proportions of minerals, is observed in most samples, except in KL5, KL11, and KL12. In KL14,

Cpx grains form aggregates or "islands" that enhance the overall layering appearance. Some of these Cpx islands contain interstitial K-rich feldspathic glasses.

Samples KL13 and KL10 are especially important, since they contain corundum inclusions that occur mostly in plagioclases (Fig. 3a), with a few cases in kelyphitized garnets. These inclusions are generally subhedral prismatic (up to 300 μm), some with bladed or trigonal shapes. The occurrence of corundum inclusions in the relatively fresh KL13 suggests that their origin is not involved with external melts/fluids. In highly metasomatized KL10, many corundum inclusions were transformed to spinels, some of which were further reacted to plagioclases (Fig. 3b).

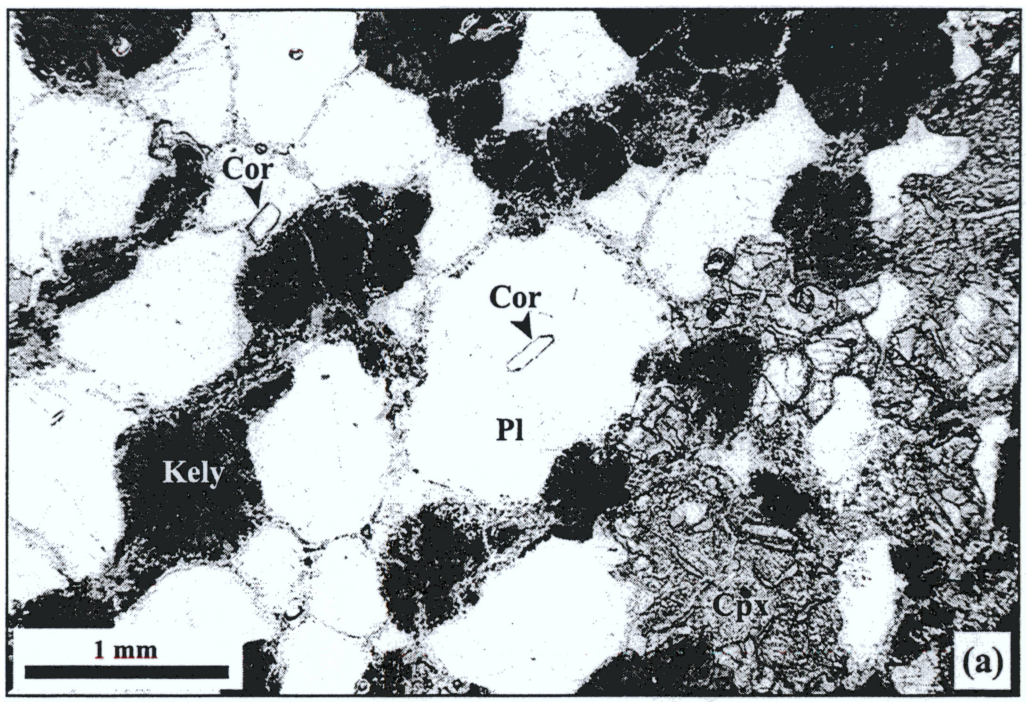
Group 3: Clinopyroxene-rich granulite

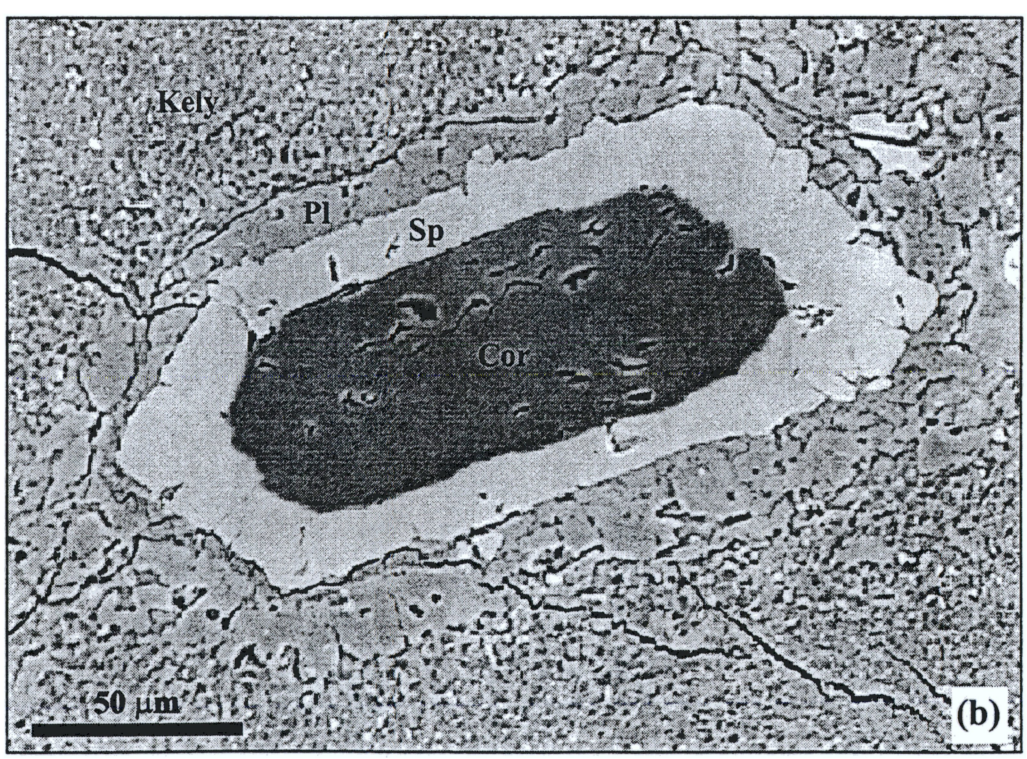
The two clinopyroxene-rich granulite xenoliths (KL7 and KL8) contain Cpx roughly 44% (Table 1), with no banding observed. Garnets in both samples are completely kelyphitized. Although relatively fresh in KL7, plagioclases and clinopyroxenes in KL8 show rinds of metasomatic partial melting. This is observed on the clinopyroxene as spongy rims, constituting of secondary Cpx and Pl, and in some cases with interstitial K-rich feldspathic glasses. On plagioclase, the partial melting rims are corroded, with increasing anorthite contents of the "residual" plagioclase on the rims when compared to the primary core (see below).

Analytical Technique

Major elements of minerals and whole-rock samples were determined with a fully automated CAMECA SX-50, four-spectrometer electron microprobe (EMP), at the

Figure 3. Corundum-bearing garnet granulite (KL10) showing complete kelyphitization of garnets. (a) Fresh corundum inclusions (Cor) in plagioclase (plane-polarized light). (b) Back scattered electron (BSE) image of a metasomatized corundum inclusion in kelyphite. The corundum is mantled by spinel (Sp), which is further reacted to plagioclase (Pl) at the outer rims. Cpx = clinopyroxene.


Cor
Cor
Pl
Kely
Cpx
1 mm
(a)


Kely
Pl
Sp
Cor
50 µm
(b)

University of Tennessee. Data were collected using wavelength-dispersive techniques and corrected with a ZAF procedure. EMP analyses of whole-rock samples were performed on fused glass beads, which were prepared by fusing sample powders on molybdenum-strip heaters under a nitrogen atmosphere (Jezek et al.,1978). Instrumental conditions for glass-bead analyses employed an accelerating potential of 15 kV, an electron beam of 20 nA with a 20-30 μm beam size, and 20 s counting times for all elements. For mineral analyses, similar analytical conditions were used, but with a 30-nA beam current and a 5-μm beam size.

Trace-element concentrations of the granulite whole-rocks were obtained with a FISONS-VG Elemental PlasmaQuad II inductively coupled plasma-mass spectrometry (ICP-MS) at the University of Notre Dame. Details of the ICP-MS analytical conditions and procedures can be found in Jenner et al (1990).

Whole-rock Chemistry

Representative samples of all three xenoliths groups and a host basalt were analyzed for major and trace elements (Tables 2 and 3). Based on the major-element chemistry, all granulite xenoliths analyzed are mafic (~43-49 wt% SiO_2), similar to tholeiitic or subalkali basaltic magmas, with normative nepheline-olivine or hypersthene-olivine.

In major-element plots (Fig. 4), MgO is negatively correlated with SiO_2 and alkalis (Na_2O+K_2O). Notice in Al_2O_3 plot that the two Cpx-rich samples (KL8 and KL12) do not follow the trends formed by the majority of samples. Similar deviation is shown, although to a lesser degree, in CaO plot. These two samples appear to follow the

Table 2. Whole-rock compositions and CIPW normative mineralogy of granulite xenoliths and host basalt.

Sample:	KL9	KL5	KL13	KL4	KL12	KL10	KL8	KLbs11 (basalt)
Whole-rock compositions (wt%)[1]								
SiO_2	43.1	44.8	45.0	45.7	48.1	45.9	48.6	42.2
TiO_2	0.09	0.08	0.13	0.09	0.23	0.19	0.45	3.00
Al_2O_3	16.9	21.4	21.4	20.9	18.2	22.1	17.2	13.1
Cr_2O_3	0.06	<0.03	0.07	0.07	0.18	0.03	0.07	<0.03
MgO	18.8	13.1	12.3	11.7	10.5	10.1	9.18	9.96
CaO	9.49	11.1	12.0	12.0	14.0	11.5	12.0	9.71
MnO	0.12	0.08	0.10	0.09	0.08	0.08	0.13	0.16
FeO	7.49	4.99	4.96	5.37	4.28	5.08	6.73	11.0
NiO	0.04	n.a.[4]	n.a.	n.a.	n.a.	n.a.	n.a.	0.04
Na_2O	1.07	1.33	1.43	1.54	2.12	2.24	2.76	3.65
K_2O	0.09	0.47	0.30	0.13	0.16	0.45	0.72	2.18
P_2O_5	<0.03	<0.03	<0.03	<0.03	0.03	0.06	0.03	0.72
LOI[2]	2.49	2.28	2.10	2.34	1.83	1.98	1.23	2.34
Total	99.81	99.72	99.90	99.90	99.64	99.73	99.11	98.00
mg#[3]	81.8	82.4	81.6	79.5	81.4	78.0	70.8	61.9
CIPW normative mineralogy (%)[5]								
Qtz	0	0	0	0	0	0	0	0
Cor	0	0	0	0	0	0	0	0
Or	0.53	2.77	1.77	0.77	0.94	2.66	4.25	12.87
Ab	9.04	11.24	11.98	13.02	16.26	15.27	19.16	2.64
An	41.02	51.01	51.06	49.71	39.65	48.90	32.40	12.92
Ne	0	0	0.06	0	0.90	1.99	2.26	15.29
Di	4.69	3.09	6.64	7.70	23.58	6.21	21.72	24.78
Hy	1.24	1.84	0	3.89	0	0	0	0
Ol	39.07	26.29	24.94	21.29	15.10	21.25	15.86	17.81
Mt	1.42	0.95	0.94	0.97	0.81	0.96	1.28	2.08
Ilm	0.17	0.15	0.25	0.17	0.44	0.36	0.86	5.71
Ap	0	0	0	0.05	0.06	0.12	0.06	1.56

[1]Obtained from EMP analyses (average of 20-25 analyses) on fused glass beads.
[2]Loss on ignition: weight loss after heating a known amount of sample at 1000°C for 1 hr, and corrected for the oxidization from Fe^{2+} to Fe^{3+}.
[3]mg# = (100Mg/Mg + ∑Fe).
[4]n.a. = not analysed.
[5]Calculated using software Magma2 (Ken Wohletz, 1996), assuming $Fe_2O_3/FeO = 0.15$. Mineral abbreviations: Cpx = clinopyroxene; Pl = plagioclase; Gt = garnet; Ol = olivine; Sp = spinel; Qtz = quartz; Cor = corundum; Ab = Albite; An = anorthite; Ne = nepheline; Di = diopside; Hy = hysperthene; Mt = magnetite; Ilm = ilmenite; Ap = apatite.

Table 3. Trace-element analyses (in ppm) of whole-rock granulite xenoliths, analyzed by ICP-MS.

Sample:	KL9	KL5	KL13	KL4	KL12	KL10	KL8
Sc	6.2	5.5	11.5	11.7	27.3	7.3	34.3
V	18.5	15.6	37.3	42.2	90.5	27.4	201.9
Cr	343.6	121.5	358.1	394.4	960.5	64.6	422.3
Co	313.5	163.4	165.1	186.8	136.1	109.1	129.8
Ni	592.6	280.6	280.7	207.2	235.5	311.0	108.7
Cu	72.2	69.9	51.1	115.9	77.2	110.3	66.8
Zn	63.5	35.6	39.8	40.2	34.5	42.1	58.8
Ga	13.03	11.19	13.06	11.03	12.27	12.76	14.05
Rb	1.41	7.45	4.81	0.14	1.74	6.57	8.87
Sr	148.6	272.4	284.1	176.6	236.7	235.1	200.4
Y	1.02	1.36	2.86	1.95	4.09	2.22	9.20
Zr	2.91	2.69	5.00	2.94	9.58	10.46	13.57
Nb	8.35	3.88	3.32	3.44	4.74	4.93	4.42
Ba	3.31	37.17	20.58	17.06	22.97	37.29	54.38
La	0.37	0.33	0.40	0.44	1.39	2.21	1.60
Ce	0.93	0.90	1.15	1.04	2.94	4.62	3.88
Pr	0.12	0.15	0.18	0.13	0.37	0.56	0.56
Nd	0.59	0.79	1.00	0.62	1.74	2.28	2.89
Sm	0.18	0.28	0.31	0.19	0.49	0.46	0.96
Eu	0.10	0.27	0.21	0.29	0.16	0.24	0.48
Gd	0.21	0.39	0.53	0.34	0.76	0.52	1.60
Tb	0.03	0.04	0.07	0.06	0.11	0.07	0.25
Dy	0.22	0.30	0.51	0.34	0.66	0.42	1.62
Ho	0.03	0.06	0.10	0.07	0.14	0.09	0.33
Er	0.09	0.16	0.30	0.17	0.40	0.18	0.96
Tm	0.02	0.03	0.05	0.03	0.06	0.03	0.14
Yb	0.16	0.18	0.26	0.12	0.34	0.19	0.92
Lu	0.02	0.02	0.05	0.02	0.05	0.03	0.13
Hf	0.13	0.13	0.20	0.09	0.27	0.27	0.52
Pb	1.65	0.95	0.46	1.16	0.52	0.95	1.42
Th	0.07	0.02	0.04	0.02	0.19	0.31	0.25
U	0.05	0.02	0.02	0.01	0.09	0.08	0.09

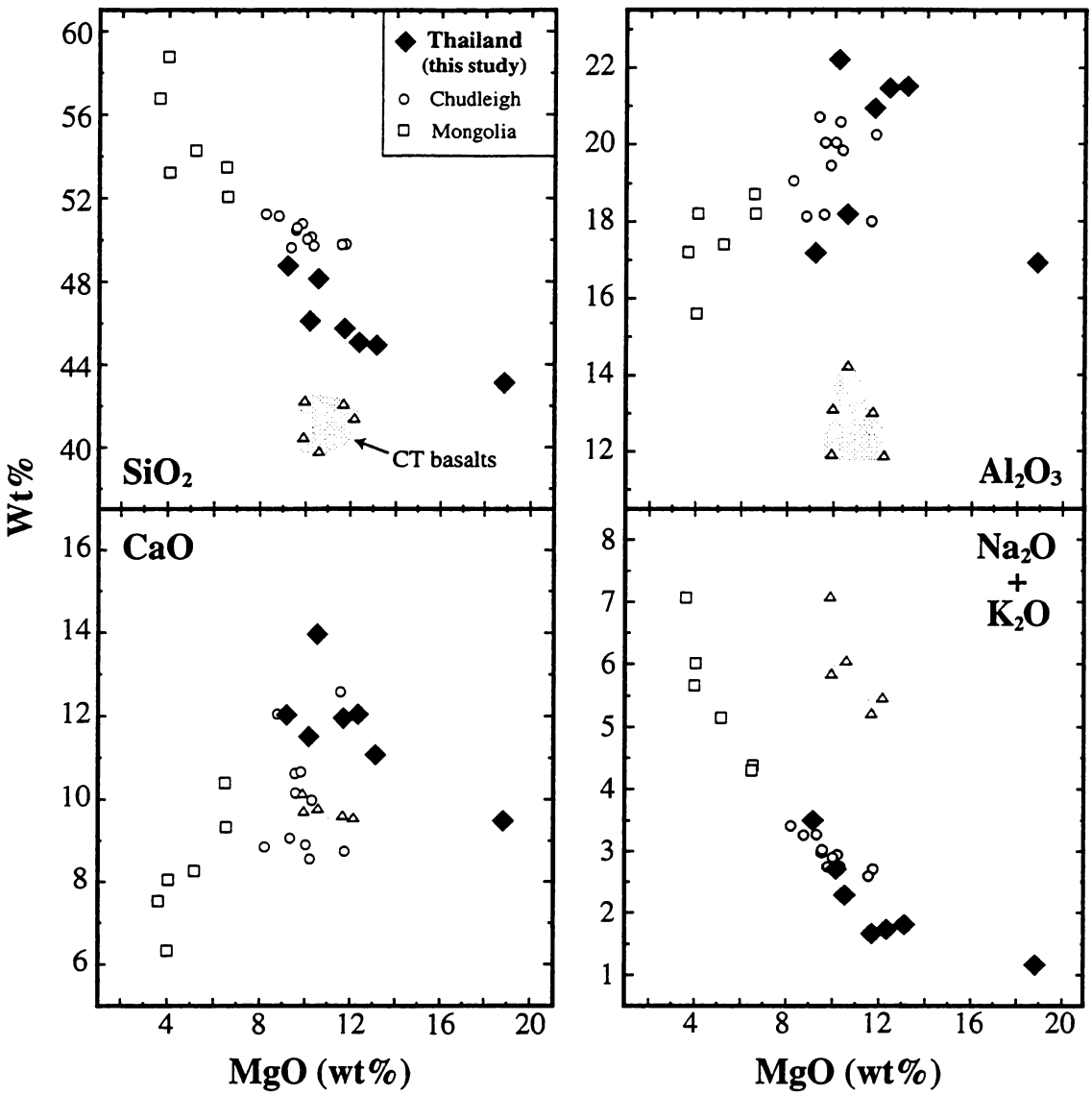


Figure 4. Whole-rock compositions of Thai granulite xenoliths compared to those of Chudleigh (Rudnick et al., 1986) and Mongolia (Stosch et al., 1995). Well-defined negative trends of MgO versus SiO_2 and alkali (Na_2O + K_2O) suggest an igneous fractionation. Deviations from the trends of the two Thai samples in Al_2O_3 and CaO plots could be the result of clinopyroxene fractionation. The host basalts, i.e., Chantaburi-Trat (CT) basalts from this study and Mukasa et al.(1996), appear unrelated with the granulite xenoliths.

arrays formed by the more evolved granulite xenoliths from Chudleigh (Australia) and Mongolian (Rudnick and Taylor, 1991; Stosch, et al., 1995, respectively). The host basalts (CT basalts) are compositionally distinct from their entrained granulite xenoliths, suggesting a lack of genetic relationship between the two rock types (Fig. 4).

Trace-element concentrations also vary systematically with MgO (Fig. 5). For instance, compatible Ni and Co correlate positively with MgO, as expected when olivine is a crystallizing phase. This in turn results in negative correlations with the moderately incompatible Zr, Hf, and La, but with small deviations for the olivine-garnet clinopyroxenite, possibly due to metasomatic addition from the host basalt. For highly incompatible elements, Ba concentrations vary in a limited range. In contrast, U and Th are scattered, and elevated in some samples when compared with the well-defined negative trends of the Chudleigh data. Rudnick et al. (1985) suggested that metamorphic fluid-fluxes could disturb the concentrations of highly mobile U and Th.

Rare earth element (REE) concentrations, normalized to chondrite compositions of Anders and Grevesse (1989), show overall flat patterns, with noticeable light REE (LREE) enrichment in some samples (Fig. 6). All but one sample (KL12) show positive Eu anomalies (Eu/Eu* up to 3.4), suggesting plagioclase accumulation. It is interesting to note that the olivine-garnet clinopyroxenite (KL9), which contains no plagioclase in the modal mineralogy, also displays a positive Eu anomaly. In addition, the lowest REE contents of KL9 and the highest in KL8 are consistent with the former being most primitive, while the latter being the most evolved among the samples in this study.

Figure 5. Selected trace-element plots as a function of MgO contents in whole-rock granulite xenoliths. Basaltic fractionation is suggested by the positive correlation seen in plots of compatible trace elements (Ni and Co), and by the negative correlation observed in the plots of incompatible trace elements (Zr, Hf, La, Ba). U and Th contents are scattered, possibly due to the disturbance by post-crystallization processes.

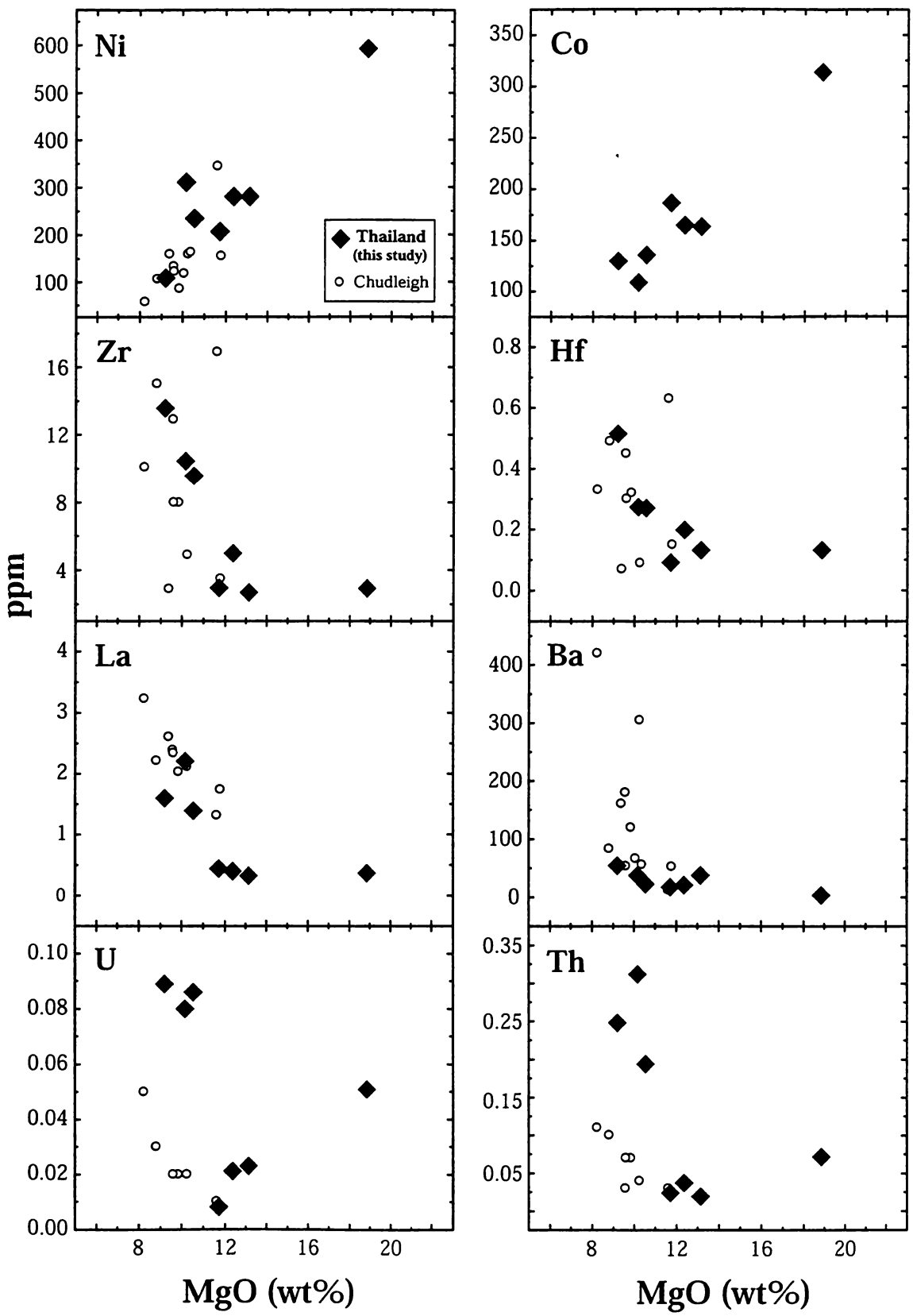
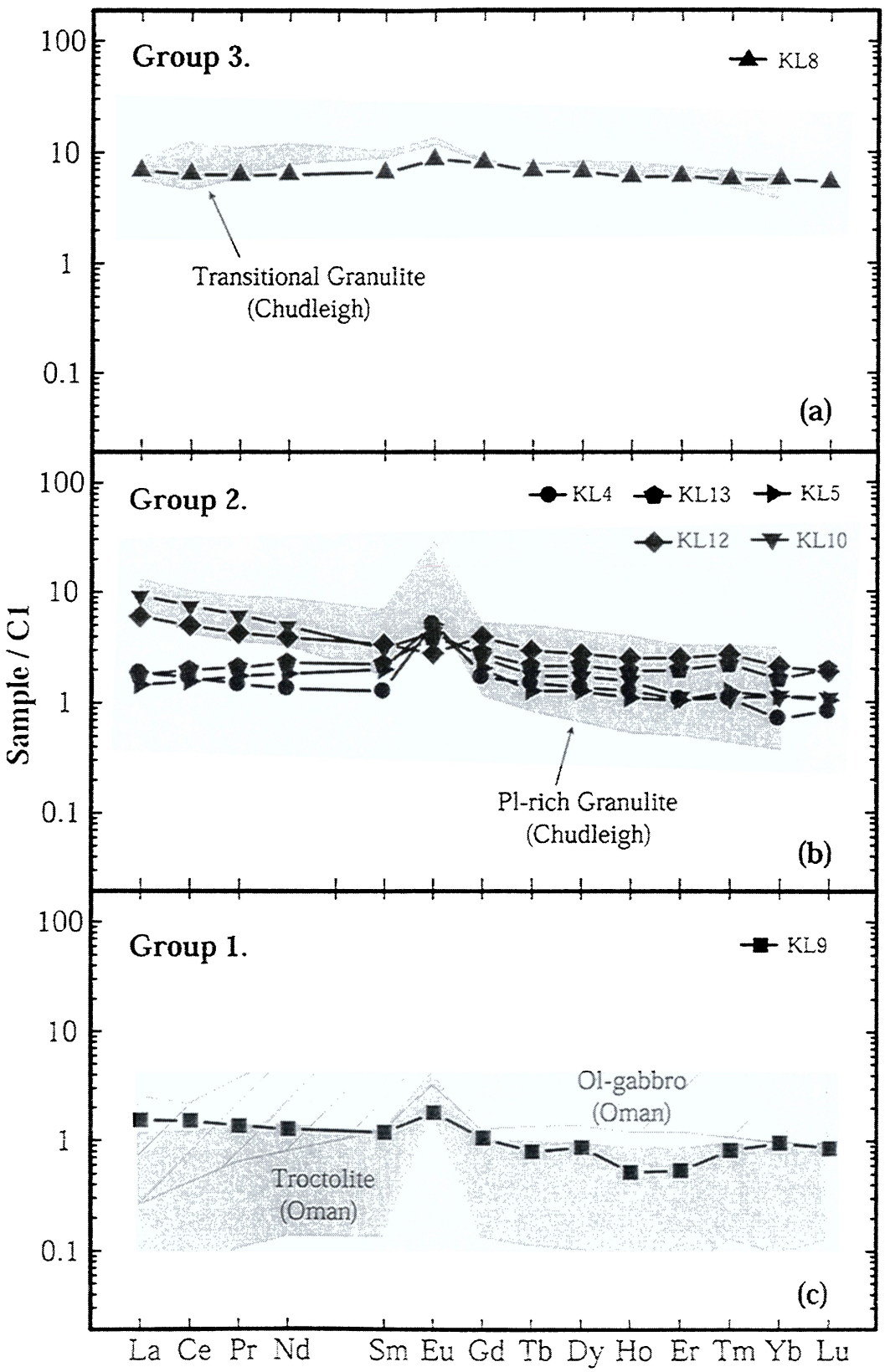

Ni
Co
Zr
Hf
La
Ba
U
Th
Thailand (this study)
Chudleigh
ppm
MgO (wt%)
MgO (wt%)

Figure 6. Whole-rock REE profiles (chondrite normalized) of three granulite xenolith groups showing general similarity with the Chudleigh granulite xenolits (Rudnick et al., 1986) and the Oman ophiolite cumulates (Benoit et al., 1996). Positive Eu anomalies, observed in almost all samples (except KL12), suggest plagioclase accumulation. "Trapped" melts may have caused the absence of a positive Eu anomaly in KL12.


Group 3.
KL8
Transitional Granulite
(Chudleigh)
(a)
Group 2.
KL4
KL13
KL5
KL12
KL10
Pl-rich Granulite
(Chudleigh)
(b)
Group 1.
KL9
Ol-gabbro
(Oman)
Troctolite
(Oman)
(c)
Sample / C1
100
10
1
0.1
La Ce Pr Nd Sm Eu Gd Tb Dy Ho Er Tm Yb Lu

Mineral Chemistry

Clinopyroxene. Compositional variations of clinopyroxene (Table 4) form well-defined trends when selected major elements are plotted against MgO (Fig. 7). The three groups of xenoliths, i.e., (1) Ol-Gt clinopyroxenite, (2) Gt-rich granulite, and (3) Cpx-rich granulite, are well delineated in these plots. Sample KL12 is unique; the composition of whole rock is similar to that of Cpx-rich samples, but that of Cpx is akin to Gt-rich samples. The most striking feature of the Cpx compositions is the high-Al_2O_3 contents (~8 to16 wt%), associated with low Na_2O (mostly <2 wt%). This corresponds to a higher proportion of Ca-Tschermak (CaTs) versus jadeite ($NaAl^{VI}$) molecules in group 2, while the opposite situation is present for groups 1 and 3 (Table 4). Besides, the Al-rich nature is further accentuated when corundum is present in granulite xenoliths KL13 and KL10, and in xenoliths of similarly mafic compositions elsewhere (e.g., Beni Bousera: Kornprobst et al., 1990; Yakutia: Qi et al., 1997).

Two opposite trends of chemical zonation are also noticeable in clinopyroxenes from individual samples: (1) a gradual decrease in Al_2O_3 (up to ~0.5 wt%) with increasing MgO from core to rim, and (2) a reverse trend of up to ~3 wt% increase in Al_2O_3 at rims (Fig. 7 and 8). The first zoning pattern is typical for a "cooling" profile in Cpx (Loock et al., 1990; Pearson et al., 1995), while the latter may be a chemical gradient developed during the course of fractional crystallization.

Chemical heterogeneity is also observed within the spongy texture on Cpx rims. When compared with the primary Cpx at cores, the residual "secondary" Cpx becomes profoundly depleted in Al_2O_3 and Na_2O, concomitant with the increase in MgO, CaO, and FeO contents (Tables 4 and 5). Taylor and Neal (1989) and Snyder et al. (1997)

Table 4. Representative compositions of clinopyroxene in granulite xenoliths from Thailand.

Sample:	KL9		KL12		KL4a		KL11		KL5		KL13	
	c	r	c	r	c	r	c	r	c	r	c	r
SiO_2	52.2	52.7	49.1	49.9	48.1	48.7	48.1	48.2	47.2	47.5	47.3	47.6
TiO_2	0.12	0.13	0.34	0.36	0.25	0.27	0.23	0.25	0.27	0.30	0.34	0.34
Al_2O_3	9.10	8.78	11.4	10.7	12.2	11.5	13.1	12.8	14.4	14.1	14.5	14.1
Cr_2O_3	0.07	0.03	0.35	0.25	0.31	0.10	0.21	0.19	0.27	0.16	<0.03	0.05
MgO	13.6	13.8	12.7	13.2	12.3	12.8	12.0	12.1	11.5	11.9	11.4	11.7
CaO	17.6	17.9	21.1	21.3	21.4	21.3	21.4	21.5	21.2	21.1	21.5	21.3
MnO	0.08	0.06	0.07	0.03	<0.03	<0.03	<0.03	0.03	<0.03	<0.03	0.04	0.04
FeO	3.52	3.68	2.92	2.73	3.08	3.14	2.98	3.05	2.58	2.60	2.52	2.74
Na_2O	2.84	2.74	1.45	1.41	1.32	1.23	1.52	1.49	1.69	1.64	1.53	1.51
Total	99.16	99.85	99.34	99.78	98.95	99.11	99.60	99.54	99.17	99.29	99.10	99.36
Cations based on 6 oxygens												
Si	1.890	1.896	1.790	1.808	1.764	1.782	1.752	1.756	1.723	1.731	1.725	1.734
Ti	0.003	0.004	0.009	0.010	0.007	0.007	0.006	0.007	0.007	0.008	0.009	0.009
Al	0.388	0.373	0.488	0.457	0.527	0.496	0.562	0.549	0.620	0.604	0.623	0.605
Cr	0.002	0.001	0.010	0.007	0.009	0.003	0.006	0.005	0.008	0.005	0.001	0.002
Mg	0.743	0.743	0.688	0.711	0.671	0.699	0.650	0.655	0.628	0.647	0.623	0.634
Ca	0.685	0.690	0.825	0.825	0.842	0.833	0.836	0.840	0.829	0.824	0.840	0.833
Mn	0.002	0.002	0.002	0.001	0.000	0.002	0.000	0.001	0.000	0.000	0.001	0.001
Fe	0.107	0.111	0.089	0.083	0.095	0.096	0.091	0.093	0.079	0.079	0.077	0.084
Na	0.199	0.191	0.103	0.099	0.094	0.087	0.107	0.105	0.120	0.116	0.108	0.107
Σ	4.010	4.011	4.004	4.001	4.009	4.005	4.011	4.011	4.014	4.014	4.007	4.009
mg#	87.23	87.0	88.6	89.6	87.6	88.9	87.7	87.6	88.8	89.1	89.0	88.3
X_{jd}	0.199	0.191	0.103	0.099	0.094	0.087	0.107	0.105	0.120	0.116	0.108	0.107
X_{cats}	0.079	0.078	0.175	0.166	0.197	0.191	0.207	0.200	0.223	0.219	0.240	0.232
X_{hd+dl}	0.606	0.612	0.650	0.659	0.645	0.642	0.629	0.640	0.606	0.605	0.600	0.601
X_{en}	0.118	0.121	0.064	0.068	0.061	0.077	0.056	0.054	0.051	0.061	0.050	0.059

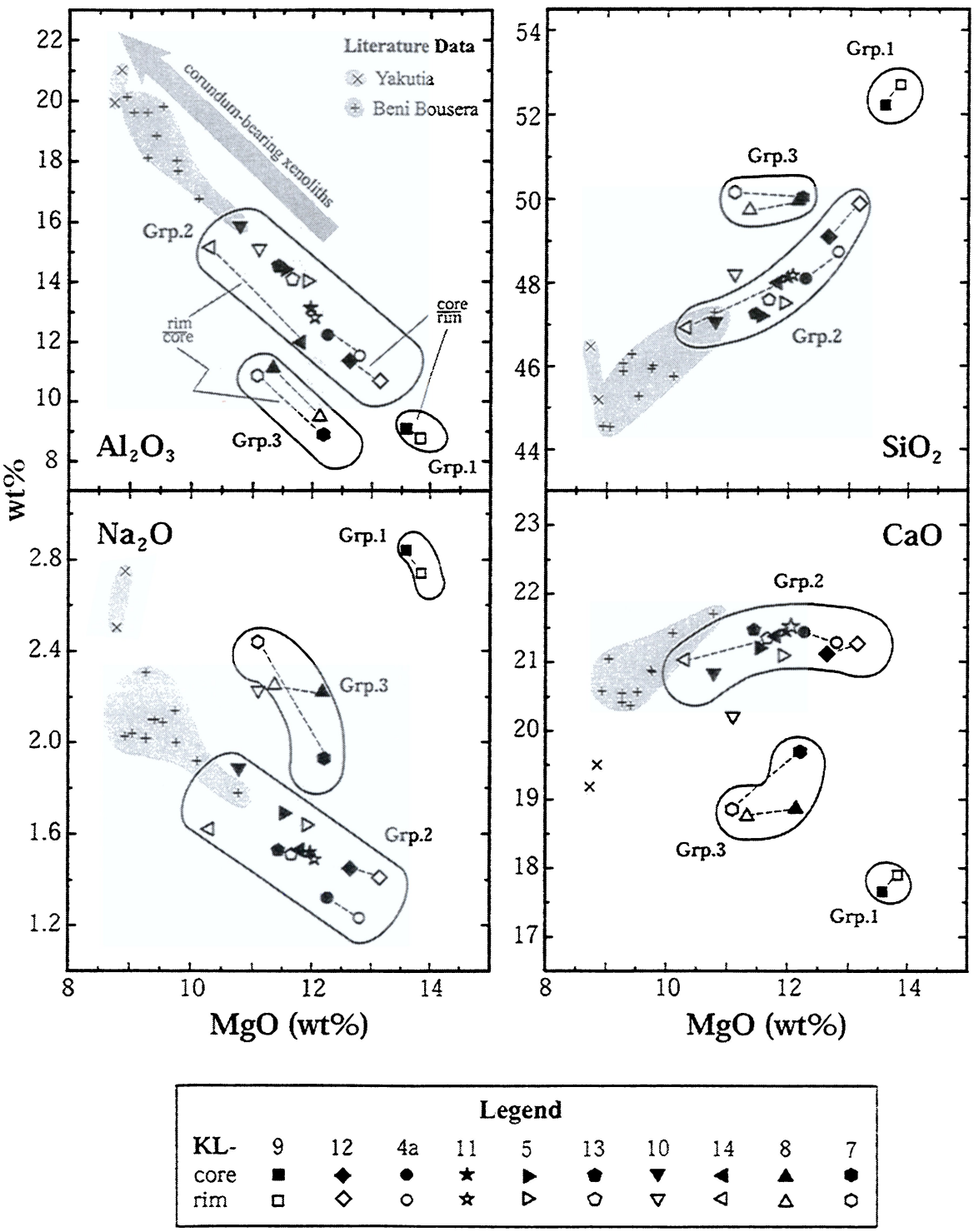
(continues)

Table 4. (continued)

Sample:	KL10		KL14		KL7		KL8	
	c	r	c	r	c	r	c	r
SiO_2	47.1	48.2	48.0	46.9	50.0	50.2	50.0	49.7
TiO_2	0.35	0.19	0.49	0.41	0.61	0.56	0.50	0.54
Al_2O_3	15.8	15.1	12.0	15.1	8.86	10.8	9.46	11.1
Cr_2O_3	0.03	<0.03	0.18	0.12	0.09	0.04	0.11	0.11
MgO	10.8	11.1	11.8	10.3	12.2	11.1	12.2	11.4
CaO	20.8	20.2	21.4	21.0	19.7	18.9	18.7	18.8
MnO	0.04	<0.03	0.04	0.04	0.08	0.07	0.09	0.06
FeO	2.78	3.03	4.01	3.96	5.86	5.52	5.79	5.83
Na_2O	1.89	2.23	1.53	1.62	1.93	2.44	2.23	2.26
Total	99.62	100.10	99.36	99.52	99.35	99.58	99.15	99.71
Cations based on 6 oxygens								
Si	1.709	1.739	1.762	1.715	1.843	1.833	1.840	1.818
Ti	0.010	0.005	0.014	0.011	0.017	0.015	0.014	0.015
Al	0.677	0.642	0.517	0.651	0.384	0.467	0.411	0.477
Cr	0.001	0.000	0.005	0.003	0.003	0.001	0.003	0.003
Mg	0.584	0.597	0.647	0.562	0.671	0.605	0.667	0.619
Ca	0.810	0.781	0.840	0.823	0.777	0.738	0.744	0.734
Mn	0.001	0.001	0.001	0.001	0.003	0.002	0.003	0.002
Fe	0.084	0.091	0.123	0.121	0.180	0.169	0.178	0.178
Na	0.133	0.156	0.109	0.115	0.138	0.173	0.159	0.160
Σ	4.009	4.012	4.018	4.002	4.016	4.003	4.019	4.006
mg#	87.4	86.8	84.0	82.3	78.9	78.2	78.9	77.7
X_{Jd}	0.133	0.156	0.109	0.115	0.138	0.173	0.159	0.160
X_{cats}	0.253	0.225	0.170	0.251	0.089	0.127	0.092	0.135
X_{hd+dl}	0.557	0.556	0.670	0.572	0.688	0.611	0.652	0.599
X_{en}	0.056	0.066	0.050	0.056	0.082	0.082	0.097	0.099

Note: c,r represent analyses at cores, rims, respectively. K_2O contents of all analyses listed are <0.03 wt%.

Figure 7. Major-element compositions of representative core and rim analyses of clinopyroxenes in olivine-garnet clinopyroxenite (grp. 1), garnet-rich granulite (grp. 2), and pyroxene-rich granulite (grp.3) xenoliths. Envelopes represent the distribution of all analyses. Notice the higher Al_2O_3 in cores for group 1 and for the majority of group 2 xenoliths; the opposite is seen for group 3 and KL4 of group 2. The shaded arrow in the Al_2O_3 plot represents the Cpx compositions that are suitable for corundum formation, based on KL13 and KL10 (this study) and corundum-bearing xenoliths from Beni Bousera (Kornprobst et al., 1990) and Yakutia (Qi et al., 1995).


Literature Data
Yakutia
Beni Bousera
corundum-bearing xenoliths
Grp.1
Grp.2
Grp.3
core
rim
rim
core
Al2O3
SiO2
Na2O
CaO
wt%
MgO (wt%)
MgO (wt%)
Legend
KL- 9 12 4a 11 5 13 10 14 8 7
core
rim

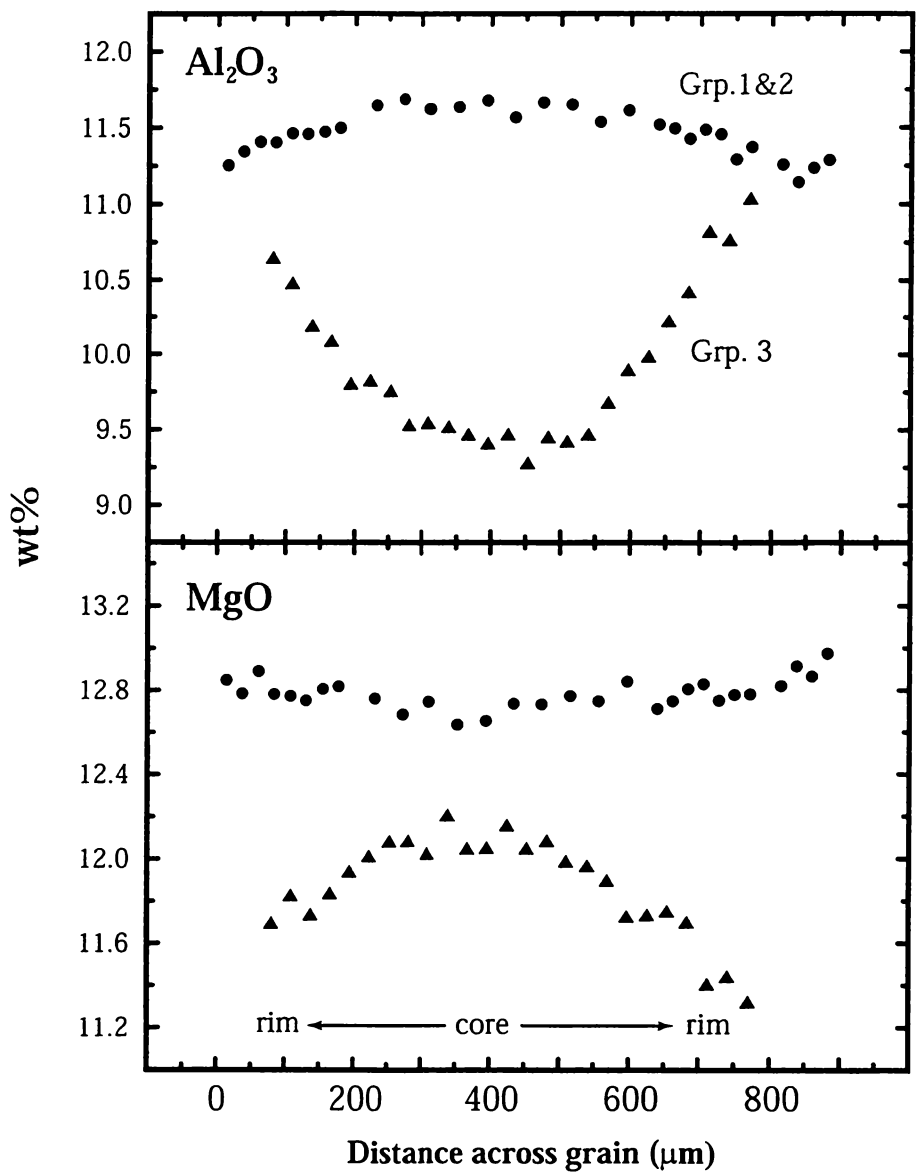


Figure 8. Characteristic zoning profiles of clinopyroxenes. Al_2O_3 contents in groups 1 and 2 clinopyroxenes decrease towards rims; the opposite trend is seen in group 3.

Table 5. Selected analyses of secondary minerals and interstitial glass.

Sample:	KL8					KL10	KL9
Phase:	Cpx†	Feld†	Feld‡	Gls*		Sp†	Sp†
SiO_2	50.70	56.2	51.4	49.7	SiO_2	0.03	0.04
TiO_2	0.91	n.a.*	n.a.	n.a	TiO_2	<0.03	<0.03
Al_2O_3	2.88	26.7	30.3	27.6	Al_2O_3	66.4	66.0
Cr_2O_3	0.10	n.a.	n.a.	n.a.	V_2O_3	<0.03	<0.03
MgO	15.17	n.a.	n.a.	n.a.	Cr_2O_3	0.04	0.41
CaO	18.74	9.29	13.3	8.30	MgO	21.2	21.3
MnO	0.21	n.a.	n.a.	n.a.	MnO	0.03	<0.03
FeO	10.03	0.52	0.39	0.19	FeO	11.6	11.4
Na_2O	0.28	5.71	3.74	0.43	NiO	0.42	0.33
K_2O	<0.03	0.50	0.21	4.30	ZnO	0.09	0.14
Total	99.02	98.94	99.41	90.48	Total	99.82	99.58
O-basis:	6	8	8			4	4
Si	1.907	2.556	2.355		Si	0.001	0.001
Ti	0.026	-	-		Ti	0.000	0.000
Al	0.128	1.433	1.634		Al	1.965	1.958
Cr	0.003	-	-		V	0.000	0.000
Mg	0.851	-	-		Cr	0.001	0.008
Ca	0.755	0.453	0.653		Mg	0.795	0.800
Mn	0.007	-	-		Mn	0.001	0.000
Fe	0.316	0.020	0.015		Fe	0.243	0.239
Na	0.020	0.503	0.332		Ni	0.009	0.007
K	0.000	0.029	0.012		Zn	0.002	0.003
Σ	4.013	4.994	5.001		Σ	3.017	3.016
An	-	46.0	65.5		mg#	76.6	77.0
Ab	-	51.1	33.3				
Or	-	2.9	1.2				

†Clinopyroxene (Cpx), feldspar (Feld), or spinel (Sp) on spongy rims of primary clinopyroxene.

‡Feldspar on partially-melted rind of plagioclase.

*Interstitial glass.

*n.a. = not analyzed.

interpreted this reduction of Al and Na in Cpx as the result of metasomatic partial melting, assisted by the host basalts or kimberlites. In KL10, clinopyroxenes have core compositions similar to those of other Gt-rich granulites, but with the rims ranging towards compositions of Cpx-rich granulites.

Plagioclase. Analyses of plagioclase (Table 6) show that they are broadly labradorite (An_{54-61}) for Gt-rich granulite xenoliths, and become andesine (An_{35-41}) for the Cpx-rich xenoliths, with orthoclase components varying slightly in most cases (Fig. 9). In KL10, plagioclases become considerably enriched in Na and K towards rims. This is associated with its highly metasomatized texture. KL7 possesses similar zoning pattern, although with little sign of metasomatic reaction, probably reflecting a magmatic differentiation trend. Plagioclases in KL8 show partially melted rinds along grain boundaries that leave "residual" plagioclase (Pl_2) with a substantial increase in anorthite contents (e.g., from An_{36} at cores to An_{66} at rims; Table 5).

Garnet and kelyphite. Compositions of relic garnet cores are broadly homogeneous, with pyrope components (Pyr) ranging from ~60 to 68 mol% (Table 7). All garnets, however, are extensively to completely overprinted by kelyphite. The extremely fine-grained nature ($\perp$ 1μm) of kelyphite hinders direct identification of individual phases with EMP. Therefore, bulk chemical compositions of kelyphitic rims were obtained using a defocused electron beam (5 or 10 μm). The analyses obtained from the kelyphite are closely similar to its garnet precursors (Table 8), but with detectable Na_2O contents. It is, therefore, likely that kelyphitization was largely isochemical, with evidence for only minor metasomatism.

Table 6. Representative compositions of plagioclase in granulite xenoliths.

Sample:	KL4a		KL13		KL5		KL11		KL12	
	c	r	c	r	c	r	c	r	c	r
SiO_2	52.5	52.3	52.9	52.3	53.2	53.0	53.6	53.2	53.8	54.7
Al_2O_3	29.6	29.3	29.1	29.4	28.9	29.1	28.7	28.7	28.7	29.1
CaO	12.4	12.6	12.0	12.3	11.5	11.7	11.6	11.7	11.2	11.3
FeO	0.07	0.16	0.03	0.08	0.07	0.12	0.05	0.16	0.05	0.13
Na_2O	4.35	4.16	4.59	4.21	4.96	4.73	5.03	4.64	5.22	4.91
K_2O	0.08	0.14	0.07	0.13	0.10	0.11	0.20	0.19	0.03	0.27
Total	98.92	98.65	98.67	98.56	98.74	98.86	99.23	98.65	98.94	100.40
Cations based on 8 oxygens										
Si	2.402	2.403	2.422	2.404	2.435	2.426	2.445	2.440	2.454	2.460
Al	1.595	1.587	1.573	1.594	1.560	1.571	1.543	1.551	1.541	1.540
Ca	0.606	0.619	0.589	0.607	0.565	0.575	0.565	0.576	0.546	0.543
Fe	0.003	0.006	0.001	0.003	0.003	0.005	0.002	0.006	0.002	0.005
Na	0.386	0.370	0.408	0.375	0.440	0.419	0.444	0.412	0.462	0.428
K	0.005	0.008	0.004	0.008	0.006	0.006	0.012	0.011	0.002	0.016
Σ	4.997	4.997	4.997	4.991	5.009	5.002	5.011	4.996	5.007	4.992
An	60.78	62.09	58.84	61.31	55.89	57.46	55.34	57.66	54.06	55.02
Ab	38.72	37.11	40.76	37.88	43.52	41.90	43.49	41.24	45.74	43.36
Or	0.50	0.80	0.40	0.81	0.59	0.64	1.18	1.10	0.20	1.62

(continues)

Table 6. (continued)

Sample:	KL14		KL10		KL7		KL8	
	c	r	c	r	c	r	c	r
SiO_2	52.7	53.7	53.7	55.9	57.4	58.2	58.8	59.2
Al_2O_3	29.3	29.3	28.8	26.9	26.4	25.4	25.7	25.4
CaO	12.2	12.0	11.2	9.44	8.53	7.84	7.33	7.43
FeO	0.07	0.37	0.08	0.31	0.09	0.16	0.12	0.24
Na_2O	4.55	4.48	5.05	5.62	6.59	6.74	7.08	6.86
K_2O	0.22	0.44	0.20	0.65	0.16	0.26	0.35	0.44
Total	99.04	100.18	99.06	98.78	99.23	98.61	99.35	99.55
Cations based on 8 oxygens								
Si	2.409	2.428	2.450	2.547	2.591	2.636	2.640	2.654
Al	1.581	1.560	1.547	1.444	1.407	1.358	1.362	1.343
Ca	0.599	0.580	0.547	0.461	0.412	0.381	0.353	0.357
Fe	0.003	0.014	0.003	0.012	0.003	0.006	0.005	0.009
Na	0.403	0.393	0.447	0.497	0.577	0.592	0.617	0.596
K	0.013	0.026	0.011	0.038	0.009	0.015	0.020	0.025
Σ	5.008	5.001	5.005	4.999	4.999	4.988	4.997	4.984
An	59.01	58.06	54.43	46.29	41.28	38.56	35.66	36.50
Ab	39.70	39.34	44.48	49.90	57.82	59.92	61.32	60.94
Or	1.28	2.60	1.09	3.81	0.90	1.52	2.02	2.56

Note: c, r represent core and rim analyses, respectively.

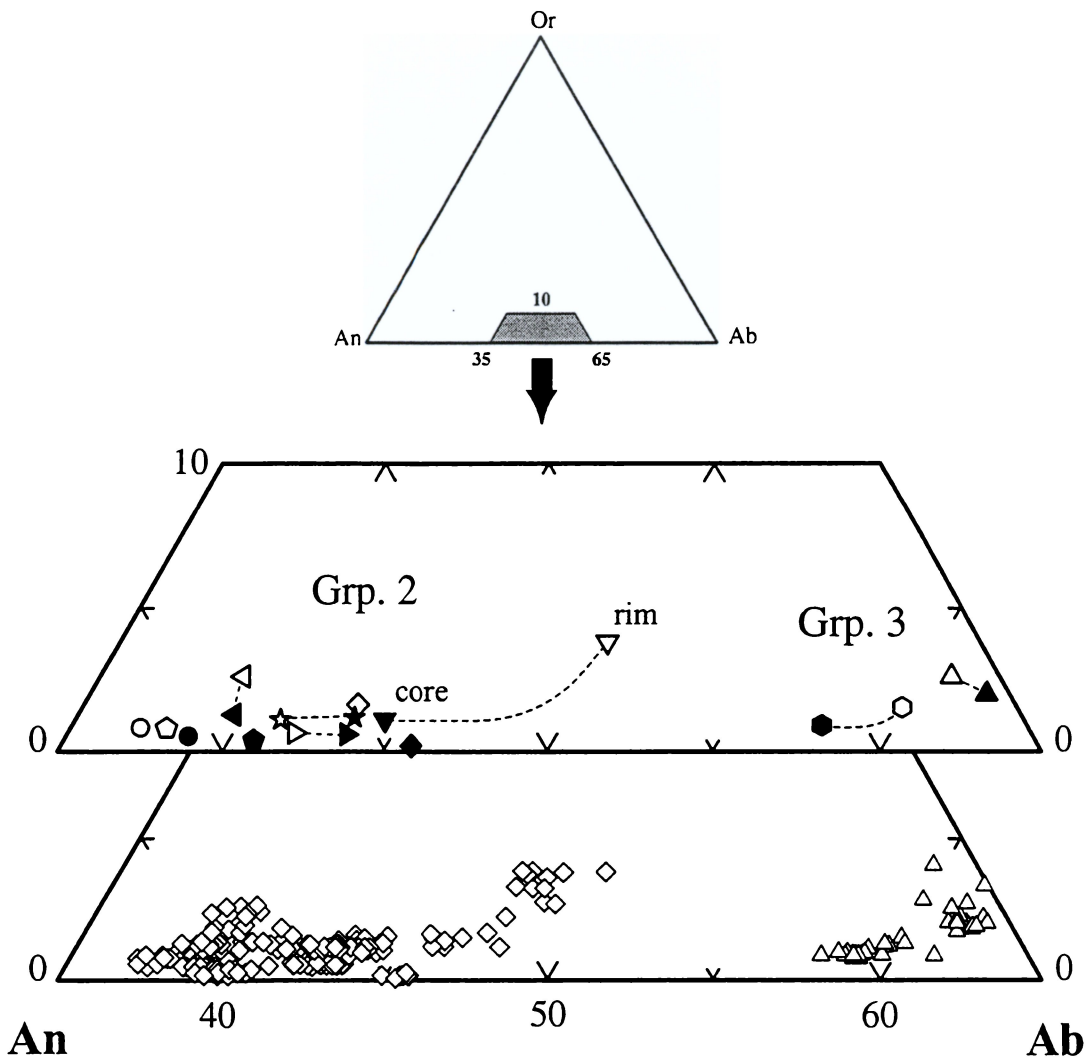


Figure 9. Representative core and rim compositions of plagioclase shown with only specific tie-lines for clarity. All analyses are also plotted below to indicate compositional variations within each group.

Table 7. Average compositions of garnet in granulite xenoliths.

Sample:	KL9	KL5	KL12	KL13	KL11
$n^{\ddagger}$:	8	11	15	10	12
SiO_2	41.5 (3)*	41.7 (1)	41.7 (1)	41.8 (1)	41.6 (3)
TiO_2	0.04 (1)	0.04 (2)	0.04 (1)	0.06 (1)	0.04 (1)
Al_2O_3	23.9 (1)	23.7 (2)	23.7 (1)	23.6 (2)	23.6 (1)
Cr_2O_3	<0.03	0.03 (2)	0.09 (4)	<0.03	<0.03
MgO	19.8 (1)	18.2 (3)	18.1 (4)	17.6 (3)	17.2 (3)
CaO	4.77 (12)	8.00 (12)	6.94 (17)	8.50 (18)	8.27 (28)
MnO	0.20 (2)	0.13 (3)	0.20 (2)	0.14 (2)	0.16 (2)
FeO	9.97 (7)	7.95 (15)	9.45 (13)	8.36 (12)	9.25 (26)
Na_2O	<0.03	<0.03	<0.03	<0.03	<0.03
Total	100.28	99.81	100.27	100.00	100.07
Cations based on 12 oxygens					
Si	2.957	2.979	2.979	2.988	2.982
Ti	0.002	0.002	0.002	0.003	0.002
Al	2.005	1.997	1.995	1.990	1.992
Cr	0.001	0.002	0.005	0.001	0.001
Mg	2.103	1.943	1.928	1.872	1.840
Ca	0.364	0.612	0.531	0.651	0.636
Mn	0.012	0.008	0.012	0.009	0.010
Fe	0.594	0.475	0.564	0.500	0.555
Na	0.001	0.001	0.001	0.001	0.001
Σ	8.038	8.020	8.019	8.014	8.019
Pyr	68.4	64.0	63.5	61.7	60.5
Alm+Sps	19.7	15.9	19.0	16.8	18.6
Grs	11.8	20.2	17.5	21.5	20.9

‡Number of analyses of relic garnet cores used in the average.

*Represent 1 σ of replicate analyses in term of last unit cited.

Table 8. Average compositions of kelyphite in granulite xenoliths[†].

Sample:	KL9	KL5	KL12	KL13	KL11	KL4a	KL7
n[‡]:	15	17	18	19	23	31	8
SiO_2	41.8 (3)*	41.7 (4)	41.8 (4)	41.8 (3)	41.7 (2)	41.5 (3)	40.5 (3)
TiO_2	0.03 (1)	0.04 (1)	0.04 (1)	0.05 (1)	0.03 (1)	0.04 (2)	0.13 (1)
Al_2O_3	23.7 (2)	23.7 (2)	23.7 (3)	23.5 (3)	23.6 (2)	23.6 (4)	22.7 (3)
Cr_2O_3	0.03 (2)	<0.03	0.13 (4)	0.04 (2)	<0.03	0.08 (4)	0.08 (2)
MgO	19.7 (2)	18.0 (5)	17.6 (4)	17.3 (4)	17.0 (3)	17.0 (8)	12.6 (3)
CaO	4.53 (25)	7.93 (26)	7.04 (27)	8.37 (27)	8.16 (31)	7.80 (61)	7.32 (41)
MnO	0.20 (3)	0.14 (3)	0.20 (3)	0.15(2)	0.16 (2)	0.16 (2)	0.40 (3)
FeO	9.87 (14)	7.91 (13)	9.37 (18)	8.31 (22)	9.14 (26)	9.09 (41)	15.3 (6)
Na_2O	0.12 (9)	0.10 (6)	0.09 (4)	0.06 (6)	0.06 (5)	0.07 (6)	0.07 (4)
K_2O	<0.03	<0.03	<0.03	<0.03	<0.03	<0.03	<0.03
Total	99.96	99.53	99.91	99.50	99.87	99.43	99.17

[†]"Bulk" kelyphite analyses were analyzed with a 5 or 10 μm defocused beam.

[‡]Number of analyses used in the average.

*Represent 1 σ of replicate analyses in term of last unit cited.

Olivines and Corundum. Olivines have Fo contents of ~86 (Table 9), similar to other basaltic cumulates observed in a previous study (Promprated et al., 1999). Corundum inclusions contain considerably higher FeO contents than Cr_2O_3 (up to 0.44 versus 0.04 wt%, respectively; Table 9) that are similar to analyses reported by Sutthirat et al. (2001).

Discussion

Cumulate protoliths and granulite-facies metamorphism

The variations in whole-rock major and trace elements as a function of MgO reflect a change of the proportions of minerals present. Although the current modes most likely indicate granulite-facies assemblages, the normative mineralogy (Table 2) can be used as a good approximation of the original mineralogy in the protoliths. It is apparent

Table 9. Average compositions of olivine and corundum.

Sample:	KL9 Ol (4)†		KL10 Cor (14)	KL13 Cor (9)
SiO_2	39.9 (3)‡	TiO_2	<0.03 (2)	0.04 (0)
MgO	46.8 (4)	Al_2O_3	99.6 (6)	99.3 (4)
CaO	0.06 (1)	Cr_2O_3	0.04 (2)	0.03 (2)
MnO	0.09 (2)	MgO	0.03 (1)	0.03 (0)
FeO	13.1 (0)	FeO	0.44 (13)	0.41 (10)
NiO	0.26 (4)			
Total	100.25	Total	100.13	99.80
O-basis:	4		3	3
Si	0.992	Ti	0.000	0.001
Mg	1.734	Al	1.992	1.993
Ca	0.002	Cr	0.001	0.000
Mn	0.002	Mg	0.001	0.001
Fe	0.273	Fe	0.006	0.005
Ni	0.005			
Σ	3.008	Σ	2.000	2.000
Fo	86.38			

Note for abbreviations: Ol = olivine; Cor = corundum.
†Number of analyses used in the average.
‡Represent 1 σ of replicate analyses in term of last unit cited.

from Table 2 that olivine, plagioclase, and diopside were present initially. Thus, the protoliths of Thai granulites are probably basaltic cumulates similar to troctolite and olivine gabbro. This interpretation is confirmed by the comparable REE patterns of the Thai granulite xenoliths with those of well-studied Oman ophiolites and Chudleigh granulite xenoliths, both of which contain textural evidence of igneous origin (Fig. 6).

Rudnick et al. (1986) also pointed to the significance of trapped melts that contribute to the overall whole-rock chemistry of the protoliths. This may be applicable to observations in KL12, which contains relatively primitive clinopyroxene (i.e., high MgO) but evolved plagioclase (high Ab contents). In this case, the plagioclase may have crystallized from "trapped" liquids, resulting in the light LREE-enriched pattern (Fig.

6b). Further support for this interpretation is the similarity of whole-rock chemistry of KL12, with that of the more evolved KL8 xenolith (Fig. 4).

The transformation of the cumulate protoliths to the garnet-bearing, granulite-facies rocks possibly occurred during the cooling process from the initial igneous temperatures. This can be described by the reaction: Pl + Ol = Cpx + Gt (Harley, 1988; Pearson et al., 1991). Perhaps, olivine was less abundant and usually consumed by the reaction, leaving almost all samples with plagioclase, clinopyroxene, and garnet (or kelyphite). Clinopyroxenite KL9 in which plagioclase was reacted out is an exception. In this case, the positive Eu anomaly in KL9 is still preserved in the whole-rock chemistry. Such an interpretation is consistent with that reached by Kornprobst et al. (1990) who observed positive Eu anomalies in plagioclase-barren garnet pyroxenites from Beni Bousera.

Effects of secondary processes: Kelyphitic and spongy rims

Kelyphitic rims are typically produced either by: (1) metasomatic reaction between garnets and kimberlite magmas, or (2) the reaction of garnets with surrounding minerals such as olivine, pyroxenes, and plagioclase (Garvie and Robinson, 1984). Evidence indicating the first mode of origin includes the formation of phlogopite, amphibole, and K-rich glass (Taylor and Neal, 1989; Sobolev et al., 1994; Snyder et al., 1997). In the latter case, the breakdown of garnet with pyroxene or plagioclase produces a variety of minerals such as orthopyroxene, spinel, olivine, plagioclase, and ilmenite (Rudnick, 1992; Obata, 1994). This mineralogical evidence is not readily seen in the Thai granulite xenoliths, due to the submicroscopic nature of kelyphite. Nevertheless, the

bulk analyses of kelyphite show compositional similarity to those of its garnet precursors (Tables 6 and 7). This may indicate that the kelyphite formation was little affected by both metasomatic fluids and surrounding minerals of garnets. As most garnets in the Thai granulite xenoliths contain microcracks, often used as the evidence for decompression (Rudnick, 1992), this kelyphitization probably occurred while the xenoliths were en route to the surface.

Spongy rims developed on clinopyroxenes have been interpreted as the consequence of metasomatic partial melting (Taylor and Neal, 1989; Snyder et al., 1997; Spetsius and Taylor, 2001). This partial-melting process involves the "leaching" of Na and Al from primary clinopyroxene (Cpx_1), and the formation of secondary phases on the spongy rims, often between grain boundaries. Based on petrographic and geochemical evidence (Table 8), a reaction applicable to the xenoliths in this study can be formulated as follows:

$$Cpx_1 + \text{K-rich fluids} \Rightarrow Cpx_2 + Sp \pm \text{K-rich glass } (Pl_2)$$

The xenolith host-basalts are the most likely sources for the K-rich fluids. The intensity of this reaction is therefore a function of the residence time of the xenolith in the host magma as concluded earlier by Snyder et al. (1997).

P-T estimates

Equilibrium attainment of the xenoliths is suggested by the homogeneity of the core compositions of coexisting phases, and the abundant triple-junction grain boundaries. All P-T calculations were carried out using several selected mineral pairs in a sample. Only core compositions of primary minerals were used to avoid secondary

products such as kelyphite and spongy rinds. The P-T estimations obtained from the cores, therefore, represent the last equilibration conditions prior to the development of these secondary textures.

Temperatures were calculated using a number of Cpx-Gt thermometers, with a reference pressure of 15 kbar (Table 10). It has been previously shown (Pearson et al., 1991, 1995) and was observed in this study that these thermometers are relatively insensitive to pressure changes. For example, calculations using 10 or 20 kbar pressure shift the calculated temperatures for only -/+ 20° C, respectively. Generally, temperatures obtained from Ellis and Green (1979) are in good agreement with those of Powell (1985), whereas the largest differences occur between those from the Ganguly (1979) and Krogh (1988) thermometers. The maximum temperature difference (± 44°C) observed in KL9 is possibly due to its low grossular contents in the garnets that affect the partitioning of Fe^{2+} and Mg of both garnet and clinopyroxene, as discussed by Krogh (1988). In most cases, however, the temperature estimates from these thermometers are consistent, with variations in a narrow range (≤ 21°C).

Table 10. P-T estimates of granulite xenoliths from Thailand.

Sample	T (°C)						P (kb)
	EG79	G79	P85	K88	Avg.	S.D.	E91
KL9	1110	1152	1093	1043	*1097*	44	-
KL12	1095	1124	1088	1085	*1098*	18	15.5
KL11	1162	1158	1161	1190	*1168*	15	18.0
KL13	1188	1174	1188	1223	*1193*	21	18.1
KL5	1193	1184	1194	1223	*1199*	17	18.3

Note: EG79 = Ellis and Green (1979); G79 = Ganguly (1979); P85 = Powell (1985); K88 = Krogh (1988); E91 = Eckert et al. (1991). Temperature estimates were calculated at pressure 15 kilobar (kb). Pressures were calculated using average temperatures.

Equilibration pressures were obtained from the barometer of Eckert et al. (1991), using the average temperatures. This barometer is calibrated from the assemblage Cpx-Gt-Pl-Qtz, and is essentially a modification of the Newton and Perkins (1982) barometer. It is obvious in this and other studies (e.g., Pearson et al., 1991) that this barometer is relatively insensitive to the temperature changes. That is, a change of ~100° C results in only a 1 kbar pressure difference, which is well within the precision of this barometer (± 1.90 kbar). Pressure calculations from the Thai granulite-xenolith suite yield a small range of ~15 to 18 kbar (Table 10). Pressure calculation cannot be obtained from the Ol-Gt clinopyroxenite KL9 because plagioclase is absent. However, the presence of olivine suggests its derivation from a lowest pressure/depth compared with other samples. This was noted earlier in the Chudleigh xenolith suite (Rudnick and Taylor, 1991).

Plot of the P-T data obtained in this study appears to follow approximately the Spitsbergen Geotherm (Fig. 10). Amundsen et al. (1987) suggested that the high-rate geotherm of Spitsbergen is typical for young rift environments, where basaltic magmatisms add heat to an already elevated temperature regime. Thus, the P-T conditions recorded by the Thai granulite xenoliths may reflect the lower crustal environments at the time of Cenozoic rifting event, as a consequence of mantle upwelling (e.g., Smith, 1998; Griffin, 1998).

Origin of corundum inclusions

The occurrence of corundum inclusions in two granulite xenoliths (KL13 and KL10) is significant in this region where gem corundum (ruby and sapphire) has been commercially mined from alluvial deposits. Various models put forth to explain the

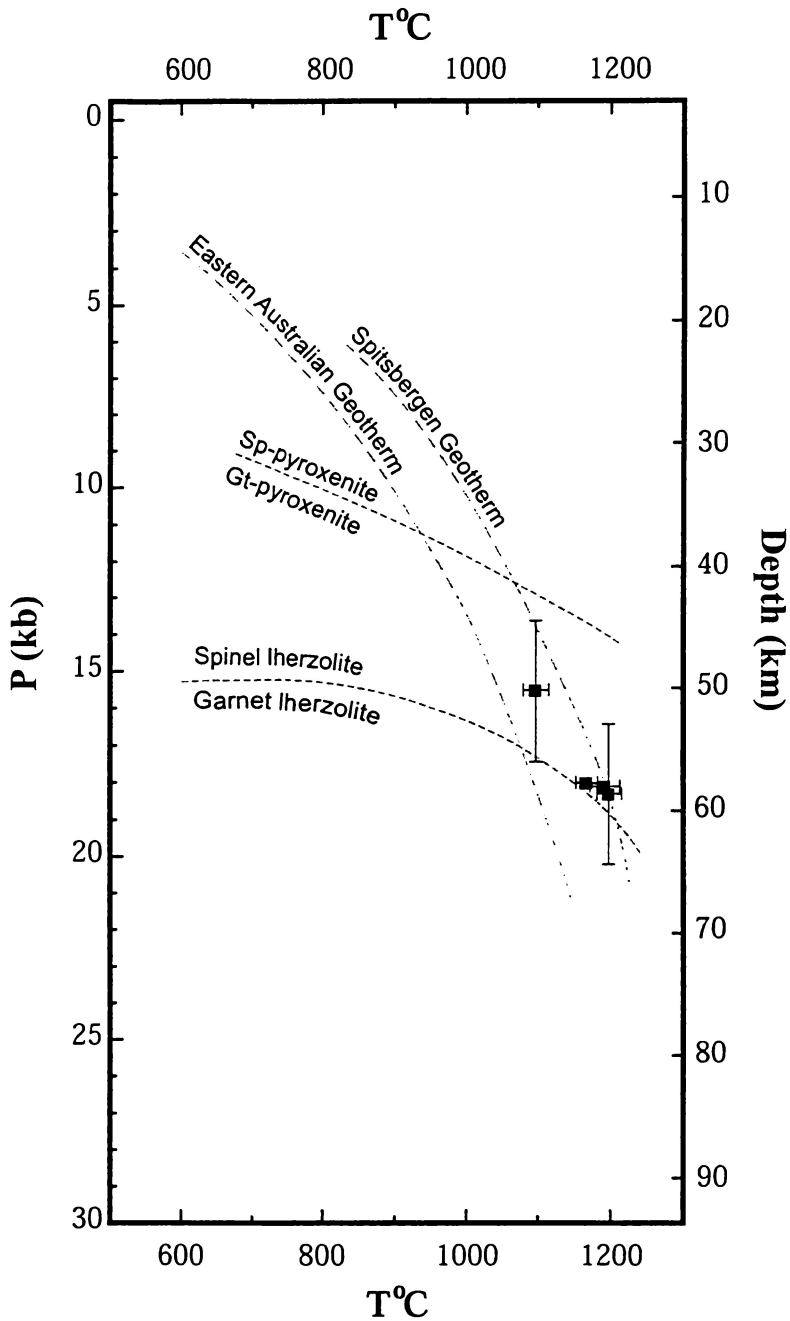


Figure 10. P-T estimates of the granulite xenoliths from Thailand. The P-T data appear to follow the spitsbergen geotherm. Phase-transition boundaries (short dashes), and the Eastern Australia and Spitsbergen geotherms (long dashes) are taken from Kopylova et al. (1995).

genesis of this gem corundum (e.g., Levinson and Cook, 1995; Coenraads et al., 1995; Sutherland et al., 1998) have apparently not taken into account the importance of corundum-bearing granulites. Therefore, our granulite samples may provide additional insights to the processes governing the formation of corundum in this, as well as other, corundum-producing regions.

The corundum inclusions observed in this study occur in large plagioclases, with a few in kelyphitic overgrowths. P-T estimations obtained from a relatively fresh corundum-bearing sample (KL13) are well constrained at ~1190° C and 18 kbar (Table 10), in agreement with that reported in a recent study by Sutthirat et al. (2001) (i.e., ~800 to 1150° C at ~10 to 25 kbar).

The absence of discrete corundum grains in mutual contact with other phases indicates that corundum probably did not occur as a cumulus phase in the protoliths of granulite xenoliths. In addition, experiments by Presnall et al. (1978) and Milholand and Presnall (1998) suggested high temperatures in excess of 1400°C (at 10 kbar) and high An-content melts (>An_{80}) for corundum-melt crystallization. No evidence exists to suggest such conditions to have occurred within the region of Thailand.

Goldsmith (1980 and references therein) observed the similarly intimate association of corundum and plagioclase in anorthite melting experiments. It was concluded from this study that corundum could be produced at elevated pressures (>9 kbar) by exsolution from solid anorthite at temperatures as low as 1200° C. The exsolution of corundum also results in non-stoichiometric anorthite, which is Al_2O_3-deficient anorthite with site vacancies. Such P-T conditions are in good agreement with that estimated from our study. Therefore, anorthite exsolution may be used to explain the

formation of corundum inclusions in some Thai granulite xenoliths. Although the anorthite analyses (Table 5) do not indicate site vacancies, this may be due to the minute amount of corundums that was actually produced. A compositional re-adjustment is an alternative explanation for this phenomenon (Goldsmith, 1980).

Based upon the data presented above, corundum was formed at high P-T granulite-facies conditions (e.g, $\geq$ 1190° C, 18 kbar) from plagioclase-rich mafic cumulates similar to troctolite and olivine gabbro. The corundum-bearing Gt-clinopyroxenite and eclogite xenoliths observed elsewhere (Kornprobst et al., 1990; Qi et al., 1997) could be envisioned as higher P-T analogues (i.e., eclogite facies) of the granulite xenoliths from Thailand.

Conclusions

Mineralogical and geochemical evidence suggests that the granulite xenoliths from the Chantaburi-Trat area of Thailand were derived from basaltic cumulates similar to troctolite and olivine gabbro. These protoliths may have formed from underplating basaltic magmas. Subsolidus reequilibration later transformed the cumulate protoliths to granulite-facies lithologies by forming garnet and clinopyroxene at the expense of plagioclase and olivine. P-T estimates indicate that the granulite xenoliths were last equilibrated at ~1100-1200° C and 15-18 kbar, consistent with the lower crustal/upper mantle depths of approximately 50 to 60 km. The resulting P-T conditions appear to follow geotherms of young rift basins. In addition, the upper limit of this P-T range (i.e., $\geq$ 1190° C, 18 kbar) marks the appearance of corundum in the garnet-rich granulite xenoliths, possibly resulting from plagioclase exsolution. The formation of granulite

xenoliths from basaltic cumulates in this area suggests prolonged periods of basaltic magmatism that eventually resulted in alkali basalt volcanism in the Cenozoic.

References

Amundsen, H.E.F., Griffin, W.L., and O'Reilly S.Y., 1987, The lower crust and upper mantle beneath northwestern Spitsbergen: Evidence from xenoliths and gephysics, Tectonophysics, v. 139, p. 169-185.

Anders, E., and Grevesse, N, 1989, Abundances of the elements: meteoritic and solar: Geochim. Cosmochim. Acta, v. 53, p. 197-214.

Barr, S.M., amd James, D.E., 1990, Trace element characteristics of upper Cenozoic basaltic rocks of Thailand, Kampuchea, and Vietnam, J. Southeast Asian Earth Sci., v. 4, p. 233-242.

Barr, S.M., and Macdonald, A.S., 1981, Geochemistry and geochronology of late Cenozoic basalts of Southeast Asia, Geol. Soc. Am. Bull., 92, p. 1069-1142.

Benoit, M., Polvé, M., and Ceulenner, G., 1996, Trace element and isotopic characterization of mafic cumulates in a fossil mantle diapir (Oman ophiolite), Chem. Geol., v. 134, p. 199-214.

Bunopas, S., and Vella, P., 1992, Geotectonic and geologic evolution of Thailand, *in* Proc. Nat. Conf. Geol. Resources of Thailand: Potential for Future Development: Bangkok, Dept. Min. Resources, Thailand, p. 209-228.

Coenraads, R.R., Vichit, P., and Sutherland, F.L., 1995, Ann unusual sapphire-aircon-magnetite xenolith from the Chanthaburi gem province, Thailand, Mineral. Mag., v. 59, p. 465-479.

Eckert, J.O., Jr., Newton, R.C., and Kleppa, O.J., 1991, The ΔH of reaction and recalibation of garnet-pyroxene-plagioclase-quartz geobarometers in the CAMS system by solution calorimetry, Amer. Mineral., v. 76, p. 148-160.

Ellis, D.J., and Green, D.H., 1979, An experimental study of the effect of Ca upon garnet-clinopyroxene Fe-Mg exchange equilibria, Contrib. Mineral. Petrol., v. 71, p. 13-22.

Ganguly, J., 1979, Garnet and clinopyroxene solid solution, and geothermometry based on Fe-Mg distribution coefficient, Geochim. Cosmochim. Acta, v. 43, p. 1021-1029.

Goldsmith, J.R., 1980, The melting and breakdown reactions of anorthite at high pressures and temperatures, Amer. Mineral., v. 65, p. 272-284.

Garvie, O.G., and Robinson, D.N., 1984, The formation of kelyphite and associated sub-kelyphitic and sculptured surfaces on pyrope from kimberlite, *in* Kornprobst, J., Kimberlites I: Kimberlites and related rocks, v. 11A, p. 371-382.

Griffin, W.L., Sutherland, F.L., Hollis, J.D., 1987, Geothermal profile and crust-mantle transition beneath east-central Queensland: volcanology, xenolith petrology, and seismic data, v. 31, p. 177-203.

Griffin, W.L., Zhang, A., O'Reilly, S.Y., and Ryan, C.G., 1998, Phanerozoic evolution of the lithosphere beneath the Sino-Korean craton, *in* Flower, M.F., Chung, S.L., Lo, C.H., and Lee, T.Y. (eds), Mantle Dynamics and Plate Interactions in East Asia, American Geophysical Union, Geodynamics Series, 27, 107-126.

Harley, S.L., 1989, The origin of granulites: A metamorphic perspective, Geol. Mag., v. 126, p. 215-331.

Jenner, G.A., Longerich, H.P., Jackson, S.E., and Fryer, B.J., 1990, ICP-MS -- A powerful tool for high precision trace-element analysis in Earth sciences: Evidence from analysis of selected U.S.G.S. reference samples: Chemical Geology, v. 83, p. 133-148.

Jezek, D.A., Sinton, J.M., Jarosewich, E., and Obermeyer, C.R., 1978, Fusion of rock mineral powders for electron microprobe analysis: Smithsonian Contributions to Earth Sciences, v. 22, p. 46-52.

Kempton, P.D., and Harmon, R.S., 1992, Oxygen isotope evidence for large-scale hybridization of the lower crust during magmatic underplating, Geochim. Cosmochim. Acta, v. 56, p. 971-986.

Kornprobst J., Piboule M., Roden M., and Tabit A., 1990, Corundum-bearing Garnet Clinopyroxenites at Beni Bousera (Morocco): Original Plagioclase-rich Gabbros Recrystallized at Depth within the Mantle. J. Petro. 31: 717-745.

Krogh, E.J., 1988, The garnet-clinopyroxene Fe-Mg geothermometer – A reinterpretation of existing experimental data, Contrib. Mineral. Petrol., v. 99., p. 44-48.

Levinson, A.A., and Cook, F.A., 1994, Gem corundum in alkali basalt: Origin and occurrence, Gems and Gemology, v. 30, p. 253-262.

Liu T-C and Presnall DC (1990) Liquidus phase relationships on the join anorthite-forsterite-quartz at 20 kbar with applications to basalts petrogenesis and igneous sapphirine

Loock, G., Stosch, H.-G., Seck, H.A., 1990, Granulite facies lower crustal xenoliths from the Eifel, West Germany: Petrological and geochemical aspects, Contrib. Mineral. Petrol., v. 105, p. 25-41.

Messiga, B., and Bettini, E., 1990, Reactions behaviour during kelyphite and symplectic formation: a case study of mafic granulites and eclogites from the Bohemian Massif, Eur. J. Mineral., v. 2, p. 125-144.

Milholland, C.S., and Presnall, D.C., 1998, Liquidus phase relations in the CaO-MgO-Al2O3-SiO2 syetem at 3.0 Gpa: The aluminous pyroxene thermal divide and high-pressure fractionation of picritic and komatiitic magmas, J. Petrol., v. 39, p. 3-27.

Mukasa, S.M., Fischer, G.M., Barr, S.M., 1996, The character of the subcontinental mantle in Southeast Asia: Evidence from isotopic and elemental compositions of extension-related Cenozoic basalts in Thailand, *in* Basu, A.R. and Hart, S.R., eds, Earth processes: Reading the isotope code, Amer. Geophys. Union, Geophys. Mono. 95, p. 233-252.

Newton, R.C., and Perkins, D., III, 1982, Thermodynamic calibration of geobarameters based on assemblages garnet-plagioclase-orthopyroxene (clinopyroxene)-quartz, Amer. Moneral., v. 67, p. 203-222.

Obata, M., 1994, Material transfer and local euilibria in a zoned kelyphite from garnet pyroxenite, Ronda, Spain, J. Petrol, v. 35, p. 271-287.

Pearson, N.J., O'Reilly, S.Y., and Griffin, W.L., 1991, The granulite to eclogite transition beneath the eastern margin of the Australian craton, Eur. J. Mineral., v. 3., p. 293-322.

Pearson, N.J., O'Reilly, S.Y., and Griffin, W.L., 1995, The crust-mantle boundary beneath cratons and craton margins: A transect across the south-west margin of the Kaapvaal craton, Lithos, v. 36, p. 257-287.

Powell, R., 1985, Regression diagnostics and robust regression in geothermometer/geobaraomter calibration: The garnet-clinopyroxene geothemometer revisited, J. Metamorphic Geol., v. 3, p. 231-243.

Presnall, D.C., Dixon, S.A., O'Donnell, T.H., Brenner, N.L., Schrock, R.L., and Dycus, D.W., 1978, Liquidus phase relations on the join diopside-forsterite-anorthite from 1 atm to 20 kbar: Their bearing on the generation and crytallization of basaltic magma, Contrib. Mineral. Petrol., v. 66, p. 203-220.

Promprated, P., Taylor, L.A., Neal, C.R., and Kurosawa, M., 2001, Trace-element characteristics of the spinel-peridotite xenoliths from Thailand: Evidence for melting and metasomatism beneath a suture zone, (in prep.).

Promprated, P., Taylor, L.A., Snyder, G.A., 1999, Petrochemistry of the mantle beneath Thailand: Evidence from peridotite xenoliths, Int. Geol. Rev., v. 41, p. 506-530.

Qi, Q., Taylor, L.A., Snyder, G.A., Clayton, R.N., Mayeda, T.K., Sobolev, N.V., 1997, Detailed petrology and geochemistry of a rare corundum eclogite xenoliths from Obnazhennaya, Yakutia, Russian Geology and Geophysics, v. 38, p. 247-260.

Rudnick, R.L., 1992, Xenoliths -- Samples of the lower continental crust, *in* Fountain, D.M, Arculus, R., and Kay, R.W., eds, Continental lower crust, Amsterdam, Elsvier, p. 269-316.

Rudnick, R.L., and Taylor, S.R., 1991, Petrology and geochemistry of lower crustal xenoliths from northern Queensland and inferences on lower crustal composition, *in* Drummond, B., ed, The Australian lithosphere, Geol. Soc. Australia, v. 17, p. 189-208.

Rudnick, R.L., McLennan, L.S., and Taylor, S.R., 1985, Large ion lithophile element in rocks from high-pressure granulite facies terrains, Geochim. Cosmochim. Acta, 49, p. 1645-1655.

Schrauf, A., 1882, Beitrage zur kenntnis des Associations kreises der Magnesiasilcate, v. 7, krist., 6: p. 321-388.

Smith, A.D., 1998, The geodynamic significance of the DUPAL anomaly in Asia, *in* Flower M.F.J., Chung S.-L., Lo C.-H., Lee T.-Y., eds.: Mantle Dynamics and Plate Interactions in East Asia, Amer. Geophys. Union, Geodynamics Series, v. 27, p. 89-105.

Snyder, G.A., Taylor, L.A., Crozaz, G., Halliday, A.N., Beard, B.L., Sobolev, V.N., Sobolev, N.V., 1997, The origins of Yakutian eclogite xenoliths, J. Petrol., v. 38, p. 85-113.

Snyder, G.A., Taylor, L.A., Jin, Y., and Taylor, D.-H., 1997, Mantle-lherzolite xenoliths from eastern China: Petrogenesis and development of secondary texture, Int. Geol. Rev., v. 39, p. 671-687.

Sobolev, V.N., Taylor, L.A., Snyder, G.A., 1994, Diamondiferous eclogites from the Udachnaya kimberlite pipe, Yakutia, Int. Geol. Rev., v. 36, p. 42-64.

Spetsius, Z.V., and Taylor, L.A., 2001, Partial melting of clinopyroxene in diamondiferous eclogite xenoliths: Int. Geol., Rev., (submitted).

Stosch, H.-G., Ionov, D.A., Puchtel, I.S., Galer, S.J.G., Sharpouri, A., 1995, Lower crustal xenoliths from Mongolia and their bearing on the nature of the deep crust beneath central Asia, Lithos, 36, 227-242.

Sutherland F.L., Hoskin, W.O., Fanning, C.M., Coenraads, R.R., 1998, Models of corundum origin from alkali basaltic terrains: A reappraisal, Contrib. Mineral. Petrol., v. 133, p. 356-372.

Sutthirat, C., Charusiri, P., Farrar, E., and Clark, A.H., 1994, New $^{40}Ar/^{39}Ar$ Geochronology and characteristic of some Cenozoic basalts in Thailand: Proc. Int. Symp. on Stratigraphic Correlation of Southeast Asia, Bangkok, Thailand, p. 306-321.

Sutthirat, C., Saminpanya, S., Droop, G.T.R., Henderson, C.M.B., and Manning, D.A.C., 2000, Fassaite-corundum assemblages from alkali basalt and alluvium, eastern Thailand: Constraints on the origin of Thai rubies, Min. Mag., v. 65, p. 265-283.

Vichit, P., 1992, Gemstones in Thailand, *in* Proc. Nat. Conf. Geol. Resources of Thailand: Potential for Future Development: Bangkok, Dept. Min. Resources, Thailand, p.124-150.

VITA

Prinya Promprated (Pin) was born in September 15, 1968, and spent most of his childhood and school years in Bangkok, Thailand. Pin began his college years in 1987, at Chulalongkorn University, located in the heart of Bangkok metropolitan. In 1991, he graduated with a Bachelor of Science degree in Geology, and soon afterward, started his career as an economic geologist in a zinc mining and exploration company, based in Chiang Mai, northern Thailand. In December of 1993, he was on his way to the U.S. for a higher education (and a chance to visit the Grand Canyon). Pin first went to the University of Southern Mississippi, and, in the summer of 1996, received a Master degree in Geology. Later that year, he moved north to Knoxville for a Ph.D. program at the University of Tennessee. Finally, in May 2001, Pin received the Degree of Doctor of Philosophy with major in Geological Sciences.